A ^{2}H-NMR STUDY OF INTERACTIONS IN MODEL MEMBRANES CONTAINING PULMONARY SURFACTANT PROTEINS SP-B AND SP-C

By

©Awel Seid Dico

B.Sc. (Hons.) (Addis Ababa University), B.Sc. (University of Bergen) 1992, M.Sc. (University of Bergen, Norway) 1994.

A THESIS SUBMITTED TO THE SCHOOL OF GRADUATE STUDIES IN PARTIAL FULFILLMENT OF THE REQUIREMENTS FOR THE DEGREE OF DOCTOR OF PHILOSOPHY

DEPARTMENT OF PHYSICS AND PHYSICAL OCEANOGRAPHY
MEMORIAL UNIVERSITY OF NEWFOUNDLAND

JANUARY 1998

ST. JOHN'S NEWFOUNDLAND

Abstract

Pulmonary surfactant is a lipid/protein mixture which reduces the work of breathing by rapidly spreading into a monolayer at the alveolar air/water interface. ^{2}H NMR was used to examine the effect of porcine pulmonary surfactant protein SP-B and SP-C on lipid phase behaviour, chain order, and dynamics in bilayers of chain-perdeuterated dipalmitoylphosphatidylglycerol (DPPG-d_{62}) or mixed bilayers containing 70 mol % dipalmitoylphosphatidylcholine (DPPC) and 30 mol % DPPG with one or the other lipid labeled. While SP-B was found to have little effect on chain order, deuteron transverse relaxation was strongly affected by the presence of the protein in both the liquid crystal and gel phases of each lipid system. Perturbation of the bilayer by SP-B was insensitive to the relative amounts of DPPC and DPPG present. There was no indication of a preferential interaction of SP-B with either lipid component. These observation may constrain possible models for SP-B/phospholipid interaction in bilayer precursors of the pulmonary surfactant monolayer. SP-C was found to have a similar effect on the chain order and phase behaviour of DPPC and DPPG in bilayers with a single lipid component. In gel phase DPPC/DPPG (70:30 w/w) bilayers with one or the other lipid component chain-perdeuterated, SP-C was found to affect the first spectral moment more strongly for DPPG than for DPPC. This may indicate that SP-C induced a non-random lateral distribution in the mixed lipid bilayer. SP-C was also found to influence motions responsible for deuteron transverse relaxation in both the gel and liquid crystalline phases. The presence of 5 mM Ca^{2+} in the aqueous phase substantially altered the effect of SP-C on the acyl chains' orientational order and transverse relaxation in the bilayer. In the

presence of Ca^{2+}, SP-C was found to have no or little effect on the transverse relaxation and chain order in the gel phase of DPPC/DPPG (70:30 w/w) mixed bilayers. This removal of the effect of SP-C on gel phase may reflect a Ca^{2+}-induced partial separation of bilayer components at the phase transition. The effect of SP-B on the DPPC head group was also studied. It was found that the effect of SP-B on the head group region is concentration dependent. Increasing SP-B concentration induced motional asymmetry in both head group and acyl chains region. This was indicated by the highly asymmetric ^{2}H-NMR spectra observed for both head group deuterated DPPC (DPPC-d_4) and chain perdeuterated DPPC (DPPC-d_{62}). The results suggest that SP-B interacts with the bilayer in two different ways. One mode of interaction is primarily at the head group region while the other affects motions of whole molecule and is seen in our experiments only at high SP-B concentration.

Table of Contents

List of Figures

Acknowledgements

I am extremely grateful to my supervisor Professor Michael Morrow for his guidance, friendly encouragement, financial support and tireless help throughout my research work. I also thank him with great pleasure for making the publications of some of the results of this work possible. I would also thank him and Professor John de Bruyn for trying to help me with my immigration problems.

This work wouldn't have been possible without the collaboration of Dr. K. M. Keough and his group from the Department of Biochemistry. Sample preparation, particularly isolating the pulmonary surfactant proteins SP-B and SP-C from a pig lung, is a complex process. I thus express my special thanks to Dr. K. M. Keough for his collaboration and for paying my air ticket to New Orleans, Louisiana, for Biophysical meeting. I would also like to express my special thanks to Dr. Svetla Taneva, June Stewart, Jennifer Hancock and Scott Harris for preparing all the samples studied in this work.

I would like to thank members of my advisory committee Professors John Whitehead, John De Bruyn and Phil Davis for their valuable advice and for keeping me on track. Understanding the theory of NMR wouldn't have been easy without the quantum mechanics and statistical mechanics knowledges I acquired from Professor John Whitehead who made these courses more interesting and fruitful.

I am grateful to School of Graduate Studies and Department of Physics and Physical Oceanography for financial support as a form of fellowship and graduate assistantship.

It is my pleasure to acknowledge the help of the departmental workshop and the university technical services; especially, I would like to thank Wayne Holly for keeping

our lab going with an excellent cryogenic facility and to William Kieley for his help in ^{2}H-NMR probe construction. Without the excellent facilities and friendly staff of the Physics Department, my work would have been extremely hard; special thanks to Daphne Corbett, Chris Stevenson, Joy Simmons, Elizabeth Crocker, Fred Perry and Brenda Burke. I acknowledge the support of all my friends and fellow graduate students who contributed in one way or another toward this work.

Finally, I wish to thank my parents, Zeneba Buli and Seid Dico, who taught me how to appreciate life and whose love and encouragement have been a driving force for me to face problems not as problems but as challenges.

This work is dedicated to

- my parents, Zeneba Buli and Seid Dico, and
- all human beings deprived of their basic rights.

Chapter 1

Introduction

1.1 Pulmonary Surfactant System

Pulmonary surfactant is a complex mixture of lipids and proteins produced by type II cells in the lung [1]. This material lines the surface of the lung alveoli and respiratory bronchioles and its function is related to lung mechanics and alveolar stability. Deficiency of this material can lead to the development of respiratory distress syndrome (RDS) in premature infants and adults [2]. Surfactant material, produced in type II cells, undergoes several transformations before it adsorbs at the air/water interface as a monolayer film. The primary function of this film is to reduce the surface tension at the air-water interface and hence avoid alveolar collapse [3]. These transformation processes are reviewed below in order to get a clear understanding of the system and questions addressed in this work.

1.1.1 Pulmonary Surfactant secretion and transport

Pulmonary surfactant is produced and stored in type II cells as lamellar bodies, organelles that are released by exocytosis into the alveolar lumen [4]. These lamellar bodies contain almost all of the surfactant components and hence the release of lamellar bodies is generally considered as surfactant secretion.

To function physiologically, the surfactant material contained in the lamellar bodies

must first transform to tubular myelin [5]. The designation of this phase of the surfactant as "tubular" is based on the observation, by electron micrography, of tightly packed tubules arranged in a square lattice [5]. Direct evidence of the conversion of lamellar body contents into tubular myelin has been observed *in vivo* [6, 7].

The square lattice of the tubular myelin is presumed to transform into the surfactant film. On the basis of theoretical and experimental studies, it has been concluded that surfactant film should be a molecular monolayer, be able to achieve reduced surface tension, be stable at low respiratory lung volume, and adsorb quickly at an air/water interface, and be able to re-expand at decompression (inspiration). In the pulmonary surfactant system, several components work together to generate these properties. These components are discussed in the following subsections.

1.1.2 Surfactant Lipids

Pulmonary surfactant is composed of approximately 90% lipid and 10% protein [8, 3]. Of the surfactant lipids, 80%-90% are phospholipids. The other lipids, in decreasing order, are cholesterol, triacylglycerol and free fatty acids. Of the phospholipids, 70%-80% are phosphatidylcholine (PC) of which about 60% - 80% is saturated. The saturated PC is predominantly dipalmitoylphosphatidylcholine (DPPC), which accounts for about 50% of the total surfactant lipid. Various studies have pointed out that DPPC is an important component because of its surface tension lowering activity [3]. Figure 1.1 shows the molecular structure of DPPC. Phosphatidylglycerol (PG) is the major acidic phospholipid of pulmonary surfactant (about 10% of the total lipid), while phosphatidylinositol (PI) is only a minor component. The molecular structure of saturated PG, dipalmitoylphosphatidylglycerol (DPPG), is also shown in figure 1.1.

Some biophysical studies have demonstrated that a film of pure phospholipid fails to

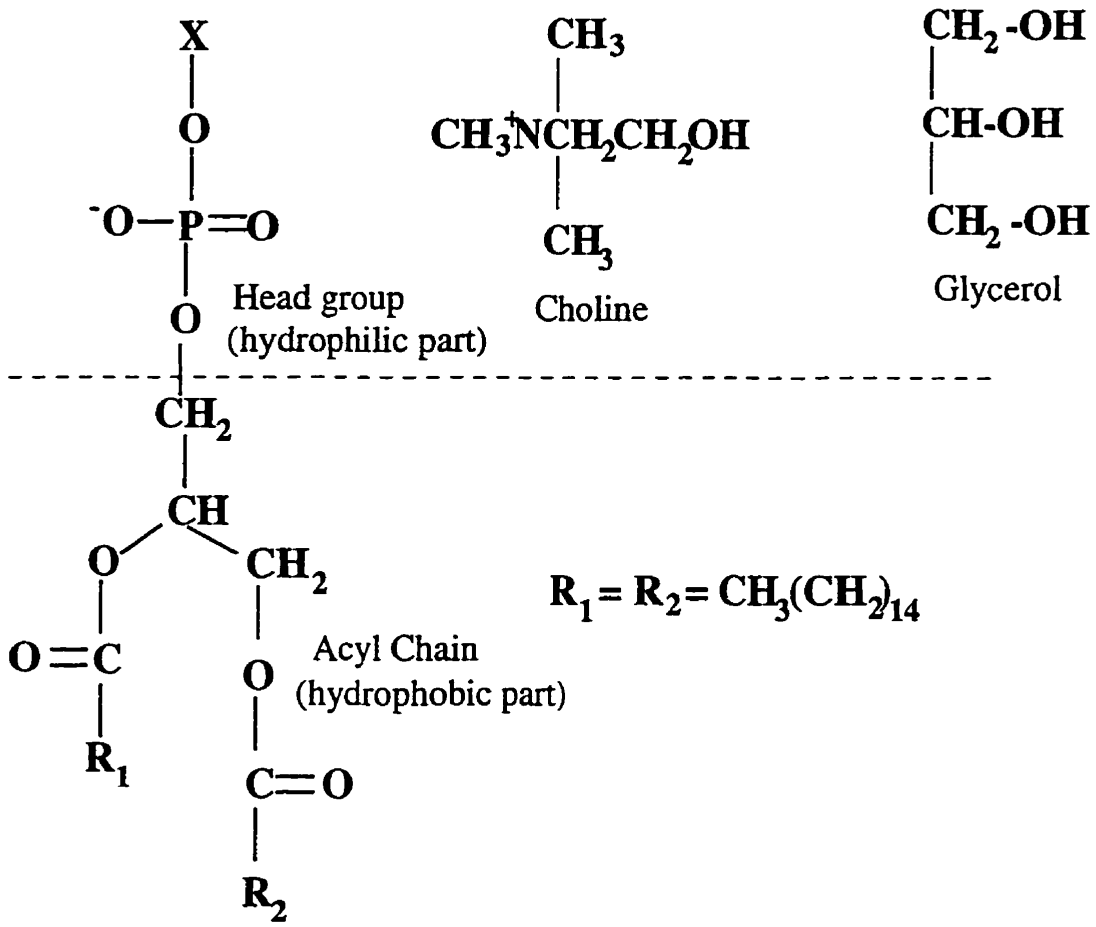

Figure 1.1: Molecular structure of DPPC (when **X** is choline) and DPPG (when **X** is glycerol). The hydrocarbon chains R_1 and R_2 are equal, and they are same for both DPPC and DPPG. DPPC and DPPG differ in head group.

adsorb quickly at the air/water interface. This implies that the surfactant system cannot be a simple lipid mixture and that other surfactant components, such as specific proteins and cations, must play a major role in the conversion of the densely packed material contained in the lamellar bodies into active surface films. These specific proteins, called surfactant proteins, are introduced below.

1.1.3 Pulmonary surfactant proteins

The surfactant specific proteins are designated by SP (surfactant protein) followed by a letter reflecting their order of discovery [9]. There are four pulmonary surfactant associated proteins identified to date [3, 10, 11, 12]. These are surfactant proteins A, B, C and D. SP-A, with a mass of 35 kD, is the most abundant hydrophilic surfactant protein in the alveoli. It constitutes about 50% of the total surfactant protein. Structurally, the SP-A polypeptide chain consists of two different sections. The N-terminal portion has a collagen-like amino acid sequence. The C-terminal domain contains two intra-chain disulphide bridges. In its native state, SP-A is arranged as a hexamer, with subunits consisting of trimers of polypeptide chains [11, 13].

The hydrophilic surfactant protein, SP-D, is probably made up of four subunits, each of them composed of three apparently identical disulphide-linked glycosylated polypeptides of about 43 kD in molecular mass [11, 12, 14]. The lamellar bodies do not contain SP-D [15].

SP-B and SP-C, which are the main subjects of this work, are highly hydrophobic proteins constituting about 1% of the total surfactant mass. Possible secondary structures of SP-B and SP-C are shown in figures 1.2 and 1.3, respectively. SP-B consists of a dimer with an apparent molecular weight of 17.4 kDa [15, 16]. The monomer contains 79 amino acids including 7 cysteines, which form 3 intra-chain and one inter-chain disulphide bonds, and several positively charged residues [17]. SP-B has no extremely hydrophobic segment except for short stretches of hydrophobic residues at positions 37-42 and 54-58. However, due to the three intra-chain disulphide bridges that connect distant parts of the polypeptide chain, the monomer is probably tightly folded and there is an over all excess of aliphatic residues in SP-B [17].

SP-C is a small peptide of 35 amino acids with an apparent molecular weight of

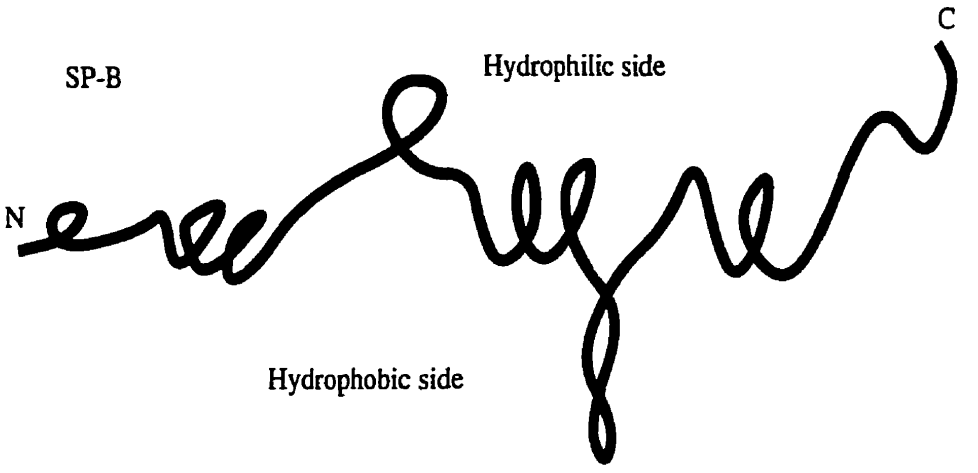

Figure 1.2: The probable folding of SP-B molecule showing hydrophilic and hydrophobic parts. See references [12,15] for the detail discussion of the amino acid sequence and structure of this protein.

4.2 kDa [15]. It has a C-terminal region of 23 hydrophobic, branched residues. The N-terminal, which has a cationic character, is increased in hydrophobicity by palmitoylation of the two cysteines in this region of the molecule [15, 18]. The SP-C polypeptide sequence is highly unusual, lacking at least 8 of the 20 common types of amino acid residues. Between positions 13 and 28, it contains only aliphatic branched chain residues (valine, leucine or isoleucine) and up to seven consecutive valines.

The secondary structures of SP-B and SP-C, in phospholipid bilayers containing DPPC and/or DPPG, have been determined using Fourier transform infra-red spectroscopy [19, 20, 21, 22]. SP-B contains about 27-45% α-helical structures [21, 22] and about 22% β-sheet [21]. SP-C is predominantly α-helical. In the phospholipid bilayers, the α-helical region of SP-C is oriented parallel to the lipid acyl chains [19, 20] suggesting that the hydrophobic part of SP-C spans the bilayer. Removal of the palmitoyl groups of SP-C reduces the α-helical content significantly when SP-C is incorporated into phospholipid bilayers [20].

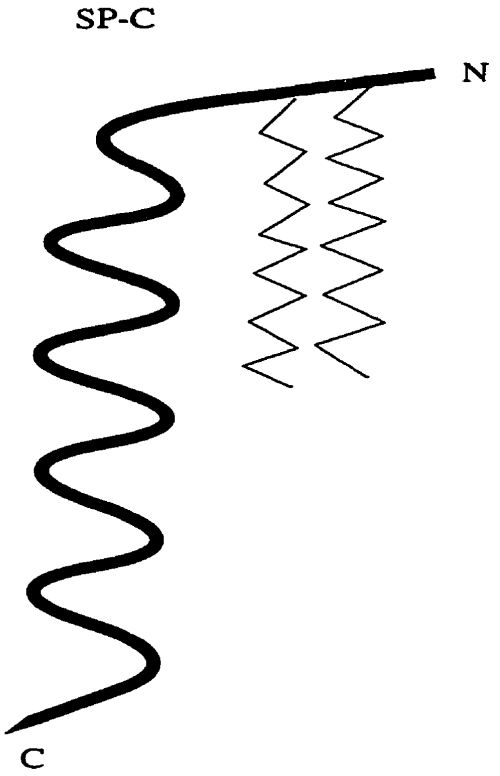

Figure 1.3: The probable α-helical structure of SP-C. See references [12,15] for the detail discussion of the amino acid sequence and structure of this protein.

1.1.4 Surfactant protein-lipid interaction

As pointed out above, the major constituents of pulmonary surfactant are a mixture of lipids and surfactant proteins. These components must interact in a very specific way for the proper functioning of our lung. It is known that the interaction of surfactant proteins with the lipid mixtures in the lung surfactant has an important role in forming the monolayer which decreases the surface tension of the material lining the alveoli and thus prevents both the collapse of the lung and edema during expiration [23]. The functions of the individual components of pulmonary surfactant have been proposed based on many experimental results [3, 12, 10, 24, 25, 26].

The proposed functions of SP-A [10] are to facilitate formation of tubular myelin,

to enhance phospholipid uptake and to activate alveolar macrophage. SP-D is the most recently discovered pulmonary surfactant protein, and its functional property in the surfactant system is not yet clear. There is a suggestion that it may play a role in the host defense system of the lung [24].

Some functions of the hydrophobic proteins SP-B and SP-C have been proposed [25, 26]. It is suggested that in addition to playing a role in formation of tubular myelin, both proteins enhance the surface properties and uptake of phospholipids (recycling). The mechanism by which these surfactant proteins interact with the lipid mixtures to give such a function is, however, not well understood. It is interesting to note that even with limited knowledge about these interactions, the abilities of SP-B and SP-C to promote the adsorption of surfactant lipids from the hypophase to the interface are already being used to prepare an exogenous surfactant material for treating neonatal respiratory distress syndrome (RDS). This indicates the importance of the interaction of these hydrophobic proteins in the pulmonary surfactant complex.

Various studies have pointed out that DPPC is an important component of the pulmonary surfactant system because of its surface tension lowering activity [3, 8]. However, physiologically useful surfactant must be effective in the dynamic environment of the lung. Since alveoli expand and contract during the respiratory cycle, an efficient surfactant must adsorb rapidly to the surface and respread quickly after compression [27]. In addition, the surfactant monolayer must withstand high compression forces in order to generate the required low surface tension. Although DPPC withstands high compression at physiologically relevant temperature, it cannot respread easily after compression. At physiological temperature DPPC is rigid. In order to respread quickly, DPPC has to be above its gel-to-liquid crystalline transition temperature. It is interesting to ask how the opposing requirements, namely, respreading quickly and rigidity, are both met. It is clear that the interactions between the various components of pulmonary surfactant are

important in changing the state of DPPC in the dynamical situation of the lung.

In order to understand how this system works, it is important to investigate systematically how the various components of lung surfactant interact with each other. Since the pulmonary surfactant system seems to operate by interconversion of bilayer to monolayer, many studies are aimed at probing these interactions in both lipid monolayer and bilayer models. The various experimental approaches used to study interaction of the pulmonary surfactant components in monolayers include surface pressure-area measurements[28, 29, 30, 31, 32, 33, 34], fluorescence studies [35, 36, 37], and infrared spectroscopy [22, 38, 39]. In bilayers, methods used include fluorescence studies [40, 41, 42, 43, 44, 45, 46], Raman and infrared spectroscopy [19, 20, 21, 47, 48], differential scanning calorimetry (DSC) [49, 50], electron microscopy [51], electron spin resonance [52, 53] and NMR [50, 54, 55, 56]. All of these studies indicate the importance of the interaction of the hydrophobic surfactant proteins with phospholipid mixtures in order to form an active monolayer film and result in the observed surface activity.

The monolayer studies show that, although SP-B is more effective than SP-C, both proteins enhance phospholipid monolayer formation from vesicles. These proteins participate in the adsorption of surfactant lipid from the hypophase to the air-water interface and formation of a stable, functionally active monolayer film. Both SP-B and SP-C are found to be effective in promoting selective squeezing-out of acidic phospholipids from the interface on compression and in respreading phospholipids after compression. The selective squeeze-out of phospholipids by hydrophobic surfactant proteins results in a DPPC-enriched monolayer that can reach very low surface tension under compression. The influence of these proteins on the surface activity of phospholipids is concentration dependent [49].

Although it is not yet clear how SP-B and SP-C participate in the transformation of lamellar body material into an effective surfactant monolayer, some studies show that

hydrophobic proteins and Ca^{2+} are extremely important in the formation of tubular myelin which is believed to be a monolayer precursor [43, 51].

Bilayer studies show that SP-B and SP-C, when added to multilamellar vesicles of DPPC or DPPG, influence the lipid acyl chain motions and broaden the main phase transition of the phospholipids. NMR studies indicate that SP-C, in dimyristoylphosphatidylcholine (DMPC-d_{54}), has no effect on lipid chain order in the liquid crystal phase but reduces the orientational order in the gel phase [50]. A fluorescence study of DPPC/DPPG model membrane shows that SP-C orders the bilayer surface and disrupts acyl chain packing. When incorporated into a DPPC/DPPG bilayer, SP-B induces bilayer surface order [41], without any significant effect on acyl chain order [54, 41]. Although the precise way in which SP-B and SP-C interact with surfactant phospholipids is not yet well understood, these studies show that the effects of these two hydrophobic proteins on the physical properties of the lipid bilayers are not identical. In spite of their overall hydrophobicity, SP-B and SP-C are different in structure and amino acid sequences. Due to these differences, these proteins seems to interact with phospholipids differently and play distinct roles in the pulmonary surfactant system.

1.2 Objective of this work

The protein-lipid complex, introduced above, reduces the work associated with breathing by forming a DPPC-enriched film which modifies the surface properties of the air-water interface in the lung. It has been suggested that enrichment of the film in DPPC may result from a process of selective exclusion of other surfactant components facilitated by hydrophobic surfactant proteins SP-B and SP-C [18, 30, 49, 52]. Though SP-A, SP-B and SP-C are all present in alveolar surfactant, only SP-B and SP-C appear to be essential components in surfactant preparation for replacement therapy ([15] and references

therein), indicating that they have unique functional roles in the formation of the surface active monolayer. It has also been suggested that these proteins may be required both for the transition between lamellar bodies and tubular myelin, and for the spreading of tubular myelin components into the surface film [31, 43, 51]. Some results from various laboratories also indicate that the calcium ions may be essential for this transition between lamellar bodies and tubular myelin [31, 43, 51]. However the mechanisms by which these components interact to give such functions are not fully understood. In order to gain a better understanding of how the components of lung surfactant contribute to this transformation process, it is important to learn how these components, particularly the hydrophobic proteins and calcium ions, interact with lamellar bilayer structures from which the surfactant monolayer or its precursor tubular myelin may be derived. Thus with this in mind, the present work addresses the following questions:

- How do the hydrophobic proteins SP-B and SP-C perturb bilayer order, phase behaviour and dynamics?
- How does this effect depend on the bilayer composition?
- How is this effect modified by the presence of calcium ions?
- Is there any selective interaction between these proteins and DPPC or DPPG?

In order to get some insight into these questions and further information about these systems, ^{2}H-NMR is used to investigate the interaction of SP-B and SP-C with the two major surfactant lipids, DPPC and DPPG. The effect of the interaction is probed by means of observable ^{2}H-NMR parameters which are sensitive to molecular motions and reorientations. These ^{2}H-NMR parameters are presented in the next chapter.

The systems studied in this work are both pure and mixed DPPC and DPPG bilayers. To investigate the above questions, this work approaches the problem in two ways. First,

we look at how SP-B and SP-C, with or without Ca^{2+} ion, affect the orientational order, phase behaviour and dynamics of the acyl chains of the phospholipids making up the bilayer. Second, we look at how these proteins interact with the bilayer head group region. Based on the results, we ask how and where these proteins pack in the bilayer. The results are compared to expectations based on the models proposed by some investigators [12, 51] regarding positions of these proteins relative to the bilayer surface.

Chapter 2

^{2}H NMR Theory and Experiment

In the pulmonary surfactant system, the complex transformation from bilayer to monolayer structures is a crucial process. The study of interactions between different components in a bilayer structure is expected to give valuable information towards understanding the transformation process from tubular myelin to monolayer film at the air-water interface of the lung. The pulmonary surfactant system, being a complex mixture of lipids and proteins, is grouped under partially ordered systems. In such systems, the molecular motions are generally anisotropic. In partially ordered systems, unlike isotropic systems, the orientation dependent interactions are not averaged out completely. Instead, they are modulated by molecular motions. These interactions include anisotropic chemical shift, dipole-dipole and quadrupole interactions. Since the amplitude of these interactions is dependent on the molecular orientations, any external effect, such as temperature or the addition of other components to the system, which may induce a change in molecular motions can be detected by probing the relevant interactions by means of solid state NMR methods. ^{2}H-NMR is one of these methods which has proved suitable for studying partially ordered systems or liquid crystals. This chapter presents a brief description of ^{2}H-NMR theory and experiment as applied to these systems.

2.1 Quadrupole interaction and quadrupole splitting

One of the advantages of ^{2}H-NMR is that ^{2}H can be substituted for hydrogen in a number of organic molecules without changing the relevant properties of the compounds. ^{2}H nucleus has spin angular momentum $I = 1$ and magnetic moment $\mu_{^2H} = 0.8574376$. Compared to the magnetic moment of hydrogen (μ_H), for which it is substituted, $\mu_{^2H}$ is a factor of 3.25 smaller than μ_H.

The total Hamiltonian for the spin-1 system can be written in general as [57]

$$H = H_Z + H_Q + H_D + H_C \tag{2.1}$$

where H_Z is the Zeeman interaction, H_Q is the quadrupolar interaction, H_D is the dipolar interaction, and H_C is the chemical shift. The magnitude of the electric quadrupole interaction in C-^{2}H bonds is large relative to the strength of the magnetic dipole-dipole and chemical shift interactions [58]. The maximum ^{2}H quadrupolar splitting for a C-^{2}H bond is about 250 kHz, while the ^{2}H-^{2}H dipolar splitting is about a few kHz. The dipolar splitting of a ^{2}H-^{1}H pair of similar geometry is of the order of 10 kHz. The chemical shift, in a magnetic field of 7.1 T, is about 1 kHz [59]. It is thus possible to neglect the chemical shift and the dipolar interactions and treat ^{2}H as an isolated spin-1 nucleus. Moreover, the electric quadrupole moment of ^{2}H is small enough to permit us to treat the quadrupolar interaction as a first order perturbation on the Zeeman interaction in the magnetic field (3.6 T in our lab).

The Hamiltonian of Equation (2.1) then becomes

$$H = H_Z + H_Q. \tag{2.2}$$

Consider first the effect of Zeeman interactions. Suppose that an ensemble of N deuterons is placed in a strong magnetic field ($\mathbf{H}_o \parallel \mathbf{z}$), and allowed to come to thermal equilibrium with the lattice. The Zeeman Hamiltonian for this case is

$$\mathbf{H}_Z = -\mu.\mathbf{H}_o = -\gamma\hbar\omega_o\mathbf{I}_Z \tag{2.3}$$

where γ is a gyromagnetic ratio, ω_o is a Larmor frequency and $\mathbf{I}_Z$ is the Z-component of spin angular momentum. The energy levels corresponding to this Hamiltonian are

$$E_m = -m\hbar\omega_o \tag{2.4}$$

where m= (-1,0,1), the quantum mechanically allowed energy levels. The degenerate ^{2}H energy levels in the absence of a magnetic field are now split into three energy levels as shown in figure 2.1(a).

We will now consider the effect of quadrupole interaction on these energy levels. The quadrupole interaction arises from the interaction of the nuclear electric quadrupole moment eQ with the electric field gradient at the site of the nucleus due to the electronic charge distributions of the atom or molecule containing the nucleus. If $V(\vec{r})$ is the electric potential due to this charge distribution and $\rho(\vec{r})$ is the nuclear charge distribution, then the energy E of interaction of the nucleus with its surrounding electric charges is:

$$E = \int \rho(\vec{r})V(\vec{r})d^3\vec{r} \tag{2.5}$$

where the integral is over the nuclear volume. Expanding $V(\vec{r})$ in a Taylor series about $\vec{r} = 0$, gives

$$V(\vec{r}) = V(0) + \sum_i x_i \frac{\partial V}{\partial x_i}\Big|_{\vec{r}=0} + \frac{1}{2}\sum_{i,j} x_i x_j \frac{\partial^2 V}{\partial x_i \partial x_j}\Big|_{\vec{r}=0} + ... \tag{2.6}$$

When substituted in Equation (2.5), the first term gives the energy of a point charge in the electric potential $V(0)$, and the second term which involves odd powers of x_i all vanish for nuclear states with definite parity. The third term is due to the electric quadrupole interaction. With this, Equation (2.5) becomes

$$E^Q = \frac{1}{2}\sum_{i,j} V_{ij} \int x_i x_j d^3\vec{r} \tag{2.7}$$

where the superscript Q is used to indicate that the energy is quadrupole energy, and

$$V_{ij} = \left.\frac{\partial^2 V}{\partial x_i \partial x_j}\right|_{\vec{r}=0} \tag{2.8}$$

is the electric field gradient tensor at the nucleus ($\vec{r} = 0$). V_{ij} is symmetric in that $V_{ij} = V_{ji}$. If there is no electron density at the nucleus, V_{ij} must satisfy the Laplace's equation [58],

$$\nabla^2 V = 0. \tag{2.9}$$

When this equation is evaluated at the origin ($\vec{r} = 0$), it yields

$$\sum_i V_{ii} = 0. \tag{2.10}$$

V_{ij} is thus traceless and symmetric.

The nuclear quadrupole moment is defined by [60, 58]

$$Q_{ij}^N = \int \left(3x_i x_j - \delta_{ij} r^2\right) \rho(\vec{r}) d^3\vec{r} \tag{2.11}$$

where the integral is over the nuclear volume. The electric quadrupole interaction energy is then given by

$$E^Q = \frac{1}{2}\sum_{i,j} V_{ij} Q_{ij}^N. \tag{2.12}$$

The electric quadrupole Hamiltonian can be obtained, using the Wigner-Eckart theorem [60], as

$$H_Q = \frac{eQ}{6I(2I-1)}\sum_{i,j} V_{ij}\left[\frac{3}{2}(I_i I_j + I_j I_i) - \delta_{ij} I^2\right]. \tag{2.13}$$

This Hamiltonian applies for any arbitrary orientation of the rectangular coordinate frame. Using rotations through the three Euler angles (α, β, γ) [61], this Hamiltonian is transformed to the principal axis system of the electric field gradient tensor where $V_{ij} = 0$ for $i \neq j$, to get [58]

$$H_Q = \frac{eQ}{4I(2I-1)}\left[V_{zz}(3I_z^2 - I^2) + (V_{xx} - V_{yy})(I_x^2 - I_y^2)\right]. \tag{2.14}$$

By defining the electric field gradient

$$eq = V_{zz} \tag{2.15}$$

and asymmetry parameter

$$\eta = \frac{V_{xx} - V_{yy}}{V_{zz}} \tag{2.16}$$

this Hamiltonian is usually written as

$$H_Q = \frac{e^2qQ}{4I(2I-1)}\left[(3I_z^2 - I^2) + \eta(I_x^2 - I_y^2)\right]. \tag{2.17}$$

This is the Hamiltonian in the principal axis system of the electric field gradient. In order to see the effect of this Hamiltonian on the Zeeman energy levels, we need to transform it back to laboratory frame of reference. This is normally done in a spherical coordinate system by making use of the irreducible spherical tensors formalism, to get the Hamiltonian in laboratory frame as [62]

$$H_Q = \frac{e^2qQ}{8}\left[3I_z^2 - I(I+1)\right]\left[(3\cos^2\beta - 1) + \eta\sin^2\beta\cos 2\alpha\right]. \tag{2.18}$$

The eigenvalues of this Hamiltonian are thus given by

$$E_m^Q = \frac{e^2qQ}{8}(3m^2 - 2)\left[(3\cos^2\beta - 1) + \eta\sin^2\beta\cos 2\alpha\right] \tag{2.19}$$

This means, to first order in H_Q, the nuclear Zeeman energy levels of Equation (2.4) are shifted by an amount E_m^Q. As a result, the energy levels corresponding to $m = \pm 1$ are

shifted upwards by an amount

$$\Delta = \frac{e^2qQ}{8}\left[(3\cos^2\beta - 1) + \eta\sin^2\beta\cos 2\alpha\right] \tag{2.20}$$

and the energy level with $m = 0$ is shifted down by the amount 2Δ as shown in figure 2.1(a). Due to the perturbation by quadrupole interaction, the energy levels are shifted and we observe a doublet spectrum which is symmetrically displaced about ω_o with a quadrupole splitting of

$$\Delta\nu_Q = \frac{3e^2qQ}{4h}\left[(3\cos^2\beta - 1) + \eta\sin^2\beta\cos 2\alpha\right] \tag{2.21}$$

as shown in figure 2.1(b) and (c).

This splitting is for a localized deuteron. In the presence of molecular motion, however, the quadrupole splitting is modulated by the motion. To obtain the expression for this case, two coordinate transformations are required. We first transform from the principal axes frame to the bilayer fixed frame and then from the bilayer fixed frame to the laboratory frame. In phospholipid bilayers, the bilayer normal is an axis of symmetry for molecular motion. The bilayer fixed frame is thus introduced such that the effect of molecular motion can be taken into account. Let (α, β, γ) be the Euler angles which transform from the principal axis frame to the bilayer fixed frame, and $(\alpha', \beta', \gamma')$ be the Euler angles for the transformation from the bilayer fixed frame to the laboratory frame. Due to the symmetry of laboratory and bilayer fixed frames, a simplification can be made by choosing α', γ' and γ equal to zero. Making use of this, it can be shown [58] that the quadrupole splitting in the presence of molecular motion is

$$\Delta\nu_Q = \frac{3e^2qQ}{8h}\left[(3\cos^2\beta' - 1)\langle(3\cos^2\beta - 1) + \eta\sin^2\beta\cos 2\alpha\rangle\right] \tag{2.22}$$

where $\langle ... \rangle$ indicates a time average. The time average is taken because the molecular reorientation may cause the angles α and β to change with time. The angle β', defining

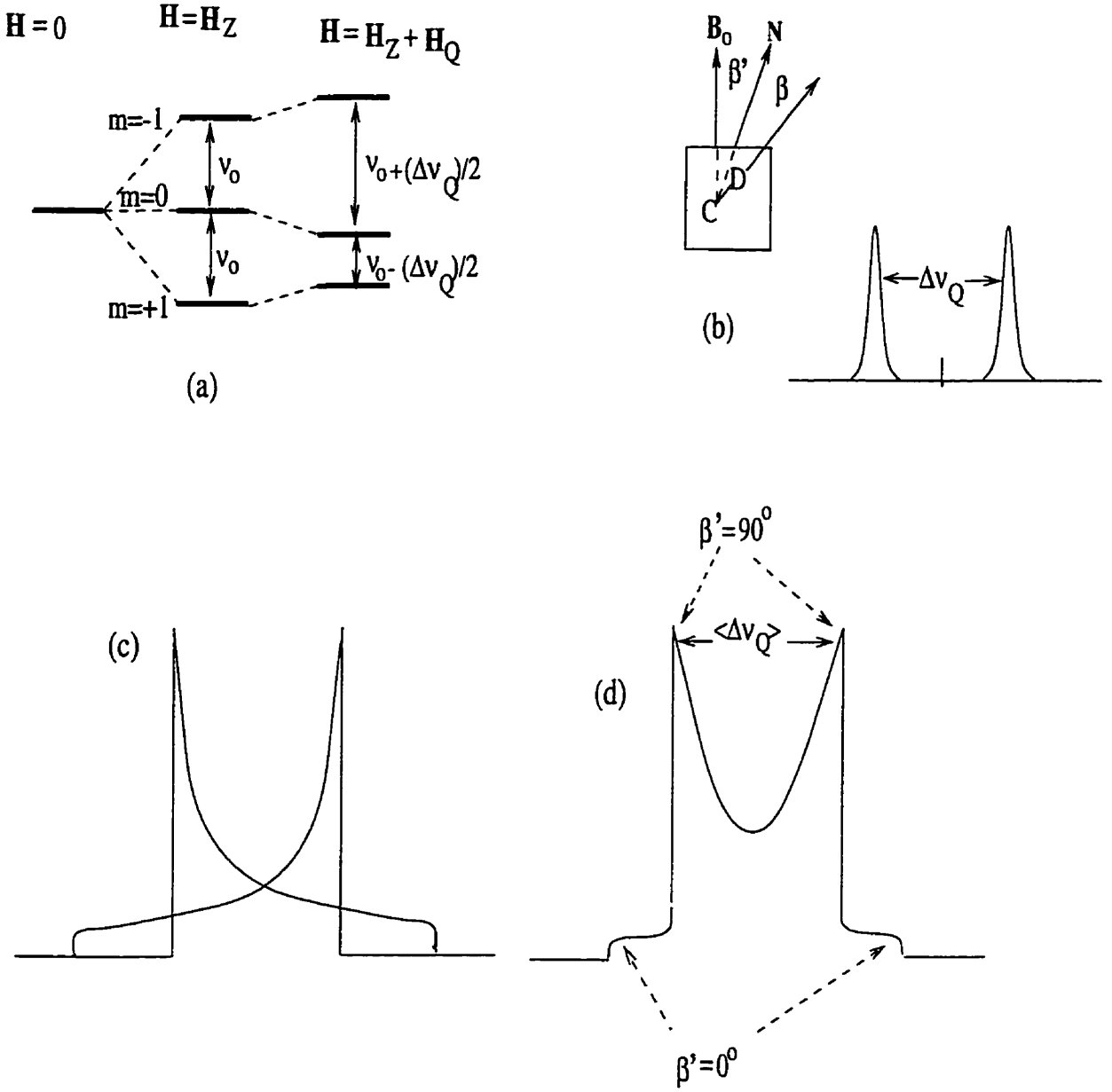

Figure 2.1: (a) Zeeman energy levels for spin 1, (b) C-^{2}H bond orientation and splitting for single deuteron, (c) line shapes of the two NMR transitions, and (d) the powder pattern.

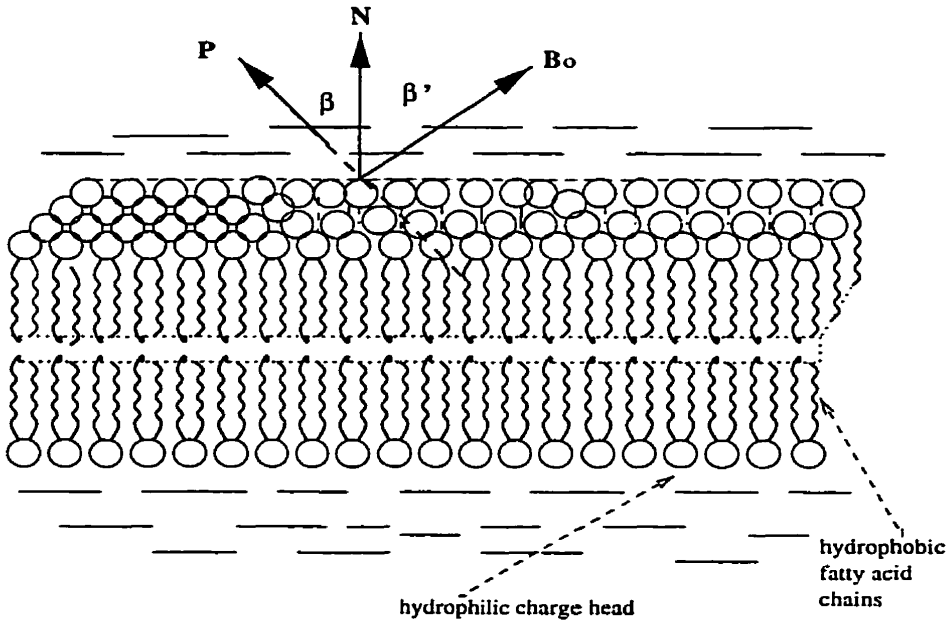

Figure 2.2: Angles β and β'. p is the principal axis (or C-^{2}H bond vector), N is the bilayer normal and $\mathbf{B}_o$ is the magnetic field (or laboratory frame).

the orientation of the bilayer fixed frame with respect to the laboratory frame of reference, may often be taken as fixed.

Equation (2.22) is only valid for a homogeneously oriented sample where all deuteron sites have the same orientation with respect to the magnetic field (laboratory frame). Figure 2.2 defines the orientations of the principal axis and bilayer fixed frames with respect to a static magnetic field (or laboratory frame). In practical situations, the orientation of the bilayer fixed frame relative to the laboratory frame is not the same for all deuterons in a given sample. That is, the C-^{2}H bond vectors are not aligned parallel to each other and the orientation of the electric field gradient (EFG) principal axis system is random. Such a sample is normally referred to as "powder" sample. In this case, β' is not fixed, but takes all values. As a result, a superposition of quadrupole split doublets is observed. This superposition of doublets leads to the characteristic spin-1 powder pattern lineshape similar to that shown in figure 2.1(d).

For C-^{2}H bonds, the asymmetry parameter (η) is small ($\eta \leq 0.05$) and can often be neglected [63]. For this case, the quadrupole splitting is

$$\Delta\nu_Q = \frac{3e^2qQ}{8h}[(3\cos^2\beta' - 1)\langle 3\cos^2\beta - 1\rangle]. \tag{2.23}$$

This is often written in terms of the orientational order parameter (S_{CD}, where D is for ^{2}H) as

$$\Delta\nu_Q = \frac{3e^2qQ}{4h}(3\cos^2\beta' - 1)S_{CD} \tag{2.24}$$

where S_{CD} is defined by

$$S_{CD} = \frac{1}{2}\langle 3\cos^2\beta - 1\rangle. \tag{2.25}$$

In ^{2}H-NMR experiments, we normally measure the splitting between the two spectral edges corresponding to $\beta' = \pi/2$ as shown in figure 2.1(d). For $\beta' = \pi/2$, from Equation (2.23) or (2.24), the splitting is

$$\Delta\nu_Q = \frac{3e^2qQ}{8h}\langle 3\cos^2\beta - 1\rangle = \frac{3e^2qQ}{4h}S_{CD}. \tag{2.26}$$

One can thus obtain information about orientational order from measurements of quadrupole splitting.

2.2 Order and Phase Transitions

Information about the orientational order of any segment of a given organic molecule can be obtained by replacing deuterium for hydrogen and measuring the quadrupole splitting from the ^{2}H-NMR spectrum [64]. The orientational order parameter, S_{CD}, is obtained from the splitting according to Equation (2.26). If many sites in a molecule are deuterated, as is the case for a perdeuterated chain lipid, the average order parameter over all sites ($\langle S_{CD}\rangle$) is sensitive to the phase of the sample.

In dealing with perdeuterated samples, the method of moments is often used to extract information from the ^{2}H-NMR spectrum. Assuming axial symmetry of ^{2}H-NMR spectrum, which is usually the case, the nth moment of the half spectrum with lineshape $f(\omega)$ is defined by [62],

$$M_n = \frac{\int_0^\infty f(\omega)\omega^n d\omega}{\int_0^\infty f(\omega)d\omega} \tag{2.27}$$

The first spectral moment (M_1) is directly related to the mean quadrupole splitting (or equivalently the mean orientational order) by [62]

$$M_1 = (4\pi/3\sqrt{3})\langle\Delta\nu_Q\rangle = \frac{\pi}{\sqrt{3}}\frac{e^2qQ}{h}\langle S_{CD}\rangle \tag{2.28}$$

The second spectral moment (M_2) is also related to the splitting by [62]

$$M_2 = \frac{4\pi^2}{5}\langle(\Delta\nu_Q)^2\rangle \tag{2.29}$$

By obtaining M_1 directly from the ^{2}H-NMR spectrum, the mean quadrupole splitting can easily be obtained. M_2 gives the mean square quadrupole splitting.

Since M_1 is directly proportional to $\langle S_{CD}\rangle$, it is useful in studying the orientational order and phase transitions which may affect this order parameter. M_2 gives information about molecular motion as will be discussed in subsection 2.3.2. In the present work, the quadrupole echo technique, described below, is used to obtain the above mentioned parameters.

2.3 Quadrupole echo experiment

The quadrupole echo pulse sequence [65] consists of two 90° pulses separated by a time τ and 90° out of phase with each other as illustrated in figure 2.3. NMR is possible because nuclei of many atoms possess magnetic moments and angular momenta [66]. When a given sample is placed in a high static magnetic field, the magnetic moments of each

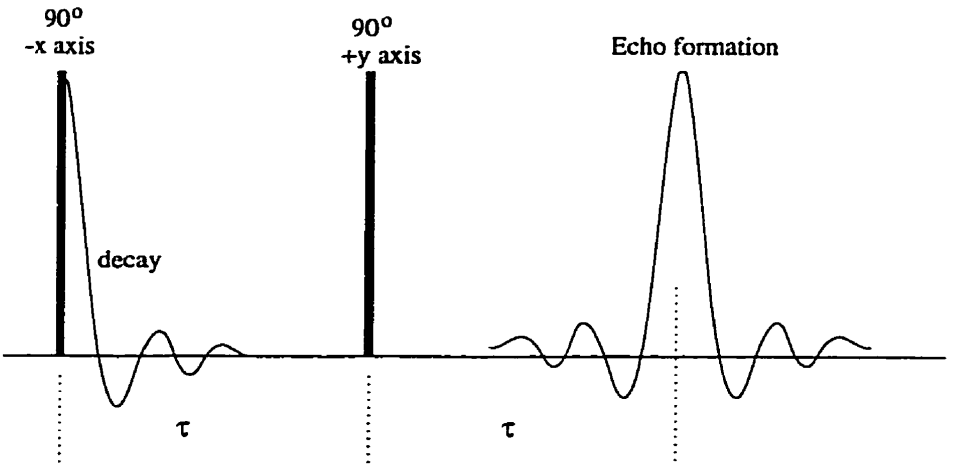

Figure 2.3: Quadrupole echo pulse sequence and the echo formation.

nucleus interact with the magnetic field. The total magnetic moment per unit volume of the sample is known as magnetization. At thermal equilibrium, the net magnetization (**M**) is parallel to the static magnetic field $\mathbf{H}_o \parallel z$. The effect of the first 90° pulse is thus to tip this magnetization by 90° away from its equilibrium z-axis. At the end of the pulse, the sample induces in the receiver coil an oscillating voltage which can be observed as the free induction decay (FID).

The observation of the FID just after the first pulse results in a distorted spectrum for the following practical reasons. The ^{2}H-NMR signal is generally weak and the ^{2}H-NMR experiments usually require the use of a high Q coil to enhance the sensitivity. This results in a long receiver "dead time" following the RF pulse. During this time the ring-down signal dominates and the initial part of the ^{2}H-NMR signal, which contains valuable information about the line shape, is lost. In order to overcome this problem, the second pulse, applied after time τ, is required. Between the two pulses, the spin system dephases and evolves freely for time $t = \tau$. At time $t = \tau$ after the second pulse, the refocusing of all nuclear spins occurs and an echo is formed at time 2τ after the first pulse as illustrated in figure 2.3. If the pulse separation τ is chosen such that the echo will

occur after the receiver dead time, undistorted ^{2}H-NMR spectrum can be obtained. The amplitude of the echo observed at time 2τ is dependent on molecular motions present during this time. These motions can modulate the quadrupole interaction and induce relaxation in the spin system (i.e. the loss of magnetization due to phase memory loss induced by slow molecular reorientations). As a result the echo amplitude decreases with increasing pulse separation. The characteristic time for the echo decay is labeled T_{2e}, the effective transverse relaxation time. This can be used to advantage, as will be discussed in subsection 2.3.2, to study the effect of external factors, such as temperature and/or addition of protein, which influence molecular motions of the sample.

2.3.1 Quadrupole echo formation

In this section, quadrupole echo formation in the absence of relaxation is discussed. First the density matrix representing the initial spin system at thermal equilibrium is determined. The standard density operator formalism is then used to follow the evolution of the density matrix under the influence of the radio frequency and quadrupole Hamiltonians and to study the general dynamical properties of the spin system. In this formalism the time-dependent density matrix is expressed in terms of an orthogonal basis set of nine ($(2I+1)^2$) 3×3 matrices in an operator space [58, 59, 67]. A representation in which these matrices are Hermitian is chosen so that the spin states represented by these matrices have real physical significance, and the matrices obey convenient commutation relations with the operators in the Hamiltonian of interest. The choice of this complete basis set is not unique and varies according to the nature of the problem to be solved.

The two relevant interactions are quadrupole interaction and the interaction of the spin system with the radio frequency pulses. Since the quadrupole interaction (maximum 250 kHz) is very small compared to the RF interaction (tens of MHz), the former is

neglected during the application of the RF pulse. When the RF pulse is off, the effective Hamiltonian is the quadrupole interaction, H_Q, given by Equation (2.18). For a spin-1 system subjected to these interactions, following Bloom *et al.* [67] and Dong [59], the nine basis operators consist of a unit matrix, three components of spin polarization and five components of quadrupolar polarization as given below:

$$\begin{aligned} &\mathbf{O}_0 = \mathbf{1} \qquad \mathbf{O}_1 = \mathbf{I}_x \qquad \mathbf{O}_2 = \mathbf{I}_y \qquad \mathbf{O}_3 = \mathbf{I}_z \\ &\mathbf{O}_4 = \frac{1}{3}(3\mathbf{I}_z^2 - 2) \quad \mathbf{O}_5 = (\mathbf{I}_x\mathbf{I}_z + \mathbf{I}_z\mathbf{I}_x) \quad \mathbf{O}_6 = (\mathbf{I}_y\mathbf{I}_z + \mathbf{I}_z\mathbf{I}_y) \\ &\mathbf{O}_7 = (\mathbf{I}_z^2 - \mathbf{I}_x^2) \quad \mathbf{O}_8 = (\mathbf{I}_x\mathbf{I}_y + \mathbf{I}_y\mathbf{I}_x) \end{aligned} \tag{2.30}$$

Any time-dependent density operator $\rho(t)$ can then be expressed as a linear combination of these basis operators as

$$\rho(t) = C_0\mathbf{1} + \sum_i a_i(t)\mathbf{O}_i \tag{2.31}$$

Because of the Hermitian property of ρ(t), the time-dependent coefficients a_i are real. Using the Schroedinger equation, the equation of motion of density matrix can easily be obtained as [61]:

$$\frac{d\rho(t)}{dt} = i\,[\rho(t), \mathbf{H}] \tag{2.32}$$

The basis operators $\mathbf{O}_i$ obey the following commutator relations:

$$[\mathbf{O}_\alpha, \mathbf{O}_\beta] = i\epsilon\mathbf{O}_\gamma \tag{2.33}$$

and its cyclic permutation

$$[\mathbf{O}_\alpha, \mathbf{O}_\gamma] = -i\epsilon\mathbf{O}_\beta \tag{2.34}$$

where, depending on the commutator, ϵ can either be ± 1 or ± 2. For commuting operators, $\epsilon = 0$.

By using the above basis operators, we can now demonstrate formation of the echo when the quadrupole pulse sequence shown in figure 2.3 is applied to a deuteron spin

system. The initial state of a spin system considered here is that of an ensemble of N deuteron nuclei allowed to come to thermal equilibrium with the lattice at temperature T in a strong magnetic field, $\mathbf{H}_o$, oriented parallel to z-axis. From Equation (2.31), this initial state is described by a density matrix at thermal equilibrium given by

$$\rho_{eq} = \mathbf{1} + a_3(0)\mathbf{O}_3 \tag{2.35}$$

where $a_3(0)$ is the only non-zero coefficient of the density matrix at time $t = 0$. One can also obtain Equation (2.35) and get $a_3(0) = \hbar\omega_o/3k_BT$ by using the Boltzmann distribution at thermal equilibrium and high temperature approximation [59]. The spins, initially in the $\mathbf{O}_3$ state, are then subjected to a 90°_{-x} pulse (where subscript $-x$ indicates that the pulse is applied in $-x$-axis direction). During this pulse, the rotating frame Hamiltonian, in frequency units, is

$$H_{1x} = -\omega_1\mathbf{O}_1. \tag{2.36}$$

Under this Hamiltonian, the equilibrium density operator evolves according to Equation (2.32). Since the Hamiltonian is time independent, the solution of Equation (2.32) is

$$\rho(t) = \exp(-i\mathbf{H}_{1x}t)\rho_{eq}\exp(i\mathbf{H}_{1x}t) \tag{2.37}$$

where ρ_{eq} is given by Equation (2.35). Using Equations (2:35) and (2:36), Equation (2.37) becomes

$$\rho(t) = \mathbf{1} + a_3(0)\exp(-i\omega_1\mathbf{O}_1t)\mathbf{O}_3\exp(i\omega_1\mathbf{O}_1t). \tag{2.38}$$

This can also be written as

$$\rho(t) = \mathbf{1} + a_3(0)\left[\mathbf{O}_3\cos(\epsilon\omega_1t) + \mathbf{O}_2\sin(\epsilon\omega_1t)\right]. \tag{2.39}$$

Using Equation (2.33), $\epsilon = 1$, since $[\mathbf{O}_3, \mathbf{O}_1] = i\mathbf{O}_2$. This gives,

$$\rho(t) = \mathbf{1} + a_3(0)\left[\mathbf{O}_3\cos(\omega_1t) + \mathbf{O}_2\sin(\omega_1t)\right]. \tag{2.40}$$

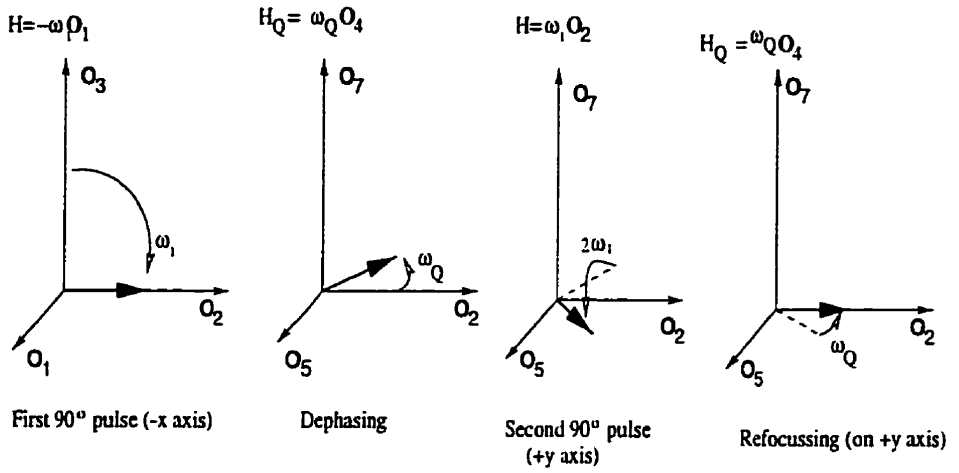

Figure 2.4: The precession diagram for the evolution of the density matrix under quadrupole pulse sequence

Just after the first pulse, $(\omega_1 t = 90^o_x)$,

$$\rho(t) = \mathbf{1} + \mathbf{O}_2. \tag{2.41}$$

That is, the magnetization is rotated onto the y-axis by the pulse as shown in figure 2.4. In general, for the system under a Hamiltonian $\omega_\alpha \mathbf{O}_\alpha$, the operator $\mathbf{O}_\beta$ will be transformed according to

$$\exp(-i\omega_\alpha \mathbf{O}_\alpha t)\mathbf{O}_\beta \exp(i\omega_\alpha \mathbf{O}_\alpha t) = \mathbf{O}_\beta \cos \epsilon\omega_\alpha t + \mathbf{O}_\gamma \sin \epsilon\omega_\alpha t \tag{2.42}$$

where, again, $\epsilon = \pm 1$ or ± 2, depending on the commutator. Dong [59] describes this as a precession of $\mathbf{O}_\beta$ in the "$\mathbf{O}_\beta$ - $\mathbf{O}_\gamma$ plane".

Right after the first pulse, the spin system evolves under the quadrupolar interaction given by Equation (2.18). For the sake of simplicity, setting $\beta = 0$ and $\eta = 0$ in Equation (2.18), we get

$$H_Q = \omega_Q \mathbf{O}_4 \tag{2.43}$$

where $\omega_Q = 3e^2qQ/4\hbar$. Interaction with H_Q causes the precession of $\mathbf{O}_2$ in the "$\mathbf{O}_2$ - $\mathbf{O}_5$

plane" as shown in figure 2.4, so that, just before the second pulse, the density matrix is

$$\rho(\tau^-) = \mathbf{1} + a_2(\tau)\mathbf{O}_2 + a_5(\tau)\mathbf{O}_5 \tag{2.44}$$

where τ^- denotes the time just before the second pulse is applied,

$$a_2(\tau) = a_3(0)\cos(\omega_Q \tau) \tag{2.45}$$

and

$$a_5(\tau) = a_3(0)\sin(\omega_Q \tau) \tag{2.46}$$

are the only non-zero coefficients of the density matrix just before the second pulse. Since $\mathbf{O}_2$ commutes with the second 90^o_y pulse Hamiltonian, $\mathbf{O}_2$ is not affected by the 90^o_y pulse, while $\mathbf{O}_5$ precesses in "$\mathbf{O}_5$ - $\mathbf{O}_7$ plane" at a frequency of $-2\omega_1$ as shown in figure 2.4. As a result the density matrix, at a time τ^+ just after the second 90^o_y pulse, is

$$\rho(\tau^+) = \mathbf{1} + a_2(\tau)\mathbf{O}_2 - a_5(\tau)\mathbf{O}_5 \tag{2.47}$$

Further evolution of the density matrix under the quadrupole interaction leaves it in the "$\mathbf{O}_2$ - $\mathbf{O}_5$ plane" and the density matrix at time t after the second 90^o_y pulse is

$$\rho(\tau + t) = \mathbf{1} + a_2(t + \tau)\mathbf{O}_2 + a_5(t + \tau)\mathbf{O}_5 \tag{2.48}$$

where

$$a_2(t + \tau) = a_3(0)\cos(\omega_Q(t - \tau)) \tag{2.49}$$

and

$$a_5(t + \tau) = a_3(0)\sin(\omega_Q(t - \tau)). \tag{2.50}$$

The coefficients a_1 and a_2 correspond to transverse components of magnetization which induce an oscillating voltage in the RF coil, and hence they are the only coefficients accessible in NMR to direct experimental observation. Therefore, the expression for

$a_2(t+\tau)$ gives us the quadrupole echo signal. The observable signal can be obtained by evaluating the trace of $\mathbf{I}_y$ $(= \mathbf{O}_2)$ as

$$\langle \mathbf{I}_y(t+\tau) \rangle = Tr\{\mathbf{O}_2 \rho(\tau + t)\} = a_2(t+\tau) \tag{2.51}$$

This signal has a maximum at time $t = \tau$ after the second pulse (or at $t = 2\tau$ after the first pulse) and is symmetric about that point. At exactly $t = \tau$ after the second pulse,

$$\langle \mathbf{I}_y(2\tau) \rangle = a_3(0) \tag{2.52}$$

which shows that the refocusing of all spins occurs at $t = 2\tau$ after the first pulse as shown in figure 2.3. and the magnitude of the magnetization is not changed during this time. In obtaining the result in Equation (2.52) , it is assumed that the quadrupole frequency (ω_Q) remains constant during the time 2τ. As mentioned earlier, however, the quadrupole interaction is modulated by molecular motions. This may cause transverse relaxation (i.e. all the spins do not refocus at time $t = 2\tau$). As a result, the echo amplitude decreases with increasing τ as discussed in more detail in the following subsection.

2.3.2 Transverse relaxation and quadrupole echo decay

The quadrupole-echo sequence consists of two $\pi/2$ radio frequency pulses separated by an interval τ. The echo is formed at time 2τ following the start of the sequence. Motions which alter the orientation-dependent quadrupole interaction during the interval 2τ cause the echo amplitude to decrease with increasing pulse separation, τ. Decay of the echo amplitude with increasing τ is characterized by the effective transverse relaxation time, T_{2e}, which is the inverse of the transverse relaxation rate averaged over all deuterons in a given sample.

A variety of motions may cause the echo to decay. Some of these motions include inter- and intra-molecular motions (such as lipid acyl chain rotations, chain fluctuations,

and *trans-gauche* isomerizations), lipid bilayer surface undulation and lateral diffusion of lipid molecules [68, 69, 70, 71, 72, 73, 74, 75]. A given motion, i, is characterized by a correlation time, τ_{ci}, and the second moment, ΔM_{2i}, of that part of the quadrupole Hamiltonian modulated by the motion. Motions which satisfy $\tau_{ci} \ll (\Delta M_{2i})^{-1/2}$ contribute to motional narrowing of the NMR spectrum. For such motions, ΔM_{2i} corresponds to the reduction in spectral second moment resulting from motion, i.e.

$$\Delta M_2 = M_2 - M_{2r} \tag{2.53}$$

where M_2 is a full second moment of the interaction and M_{2r} is the residual second moment (that is, the second moment of the motionally narrowed spectrum). Motions with long correlation times ($\tau_{ci} \gg (\Delta M_{2i})^{-1/2}$) are too slow to contribute to motional averaging, and they are only capable of gradually modulating the quadrupole splittings, which we measure in the ^{2}H-NMR spectrum. In this case, ΔM_{2i} corresponds to the residual second moment (M_{2r}) [68, 76].

In order to separate the contributions of the different motions to transverse relaxation, a multi-pulse form of quadrupole echo pulse sequence known as Q-CPMG (quadrupole Carr-Purcell-Meiboom-Gill) pulse sequence is used [68]. This pulse sequence is $90_x - \tau - (90_y - 2\tau)_N$. When $N = 1$, it is same as the two pulse quadrupole echo sequence described above. An approximate expression has been developed for the amplitude of the quadrupole echo or subsequent echoes in Q-CPMG experiment. The reduced echo amplitude at time 2τ is approximated by a single exponential decay as [68].

$$A(2n\tau) = A(0) \exp\left(\frac{-2n\tau}{T^{\text{q-cpmg}}}\right). \tag{2.54}$$

where τ is a pulse separation and

$$\frac{1}{T^{\text{q-cpmg}}} = \sum_i \left[\Delta M_{2i}\tau_{ci}\left[1 - \frac{\tau_{ci}}{\tau}\tanh\left(\frac{\tau}{\tau_{ci}}\right)\right]\right] \tag{2.55}$$

The first echo in Q-CPMG experiment is the same as the echo from quadrupole echo pulse sequence. The echo amplitude from the quadrupole echo pulse sequence can thus be approximated as

$$A(2\tau) = A(0)\exp\left(-2\tau\sum_i\left[\Delta M_{2i}\tau_{ci}\left[1-\frac{\tau_{ci}}{\tau}\tanh\left(\frac{\tau}{\tau_{ci}}\right)\right]\right]\right). \tag{2.56}$$

The contribution to the quadrupole echo decay rate ($1/T_{2e}$) from each motion is

$$\frac{1}{(T_{2e})_i} = \Delta M_{2i}\tau_{ci}\left[1-\frac{\tau_{ci}}{\tau}\tanh\left(\frac{\tau}{\tau_{ci}}\right)\right] \tag{2.57}$$

where τ is the pulse separation time in the quadrupole echo pulse sequence. For the case when $\tau_{ci} \ll \tau$ (fast motions), Equation (2.57) reduces to

$$\frac{1}{(T_{2e})_i} = \Delta M_{2i}\tau_{ci}. \tag{2.58}$$

For motions which satisfy $\tau_{ci} \gg \tau$ (slow motions), Equation (2.57) reduces to

$$\frac{1}{(T_{2e})_i} = \frac{\Delta M_{2i}\tau^2}{3\tau_{ci}}. \tag{2.59}$$

In this case, the transverse relaxation rate is τ dependent.

The above expressions for $1/T_{2e}$ are valid provided that $(\Delta M_{2i})^{-1/2}$ is at least greater than τ_{ci} or τ [77]. For the case when $(\Delta M_{2i})^{-1/2} \ll \tau_{ci} \ll \tau$, the decay time is much shorter than pulse spacing and no echo can be observed. If, however, $(\Delta M_{2i})^{-1/2} \ll \tau \ll \tau_{ci}$, the relaxation time becomes comparable to the correlation time and the spins relax non-uniformly [77]. As a result, the quadrupole echo decay is dependent on the detail of the motional process. The transverse relaxation rate for this case is proportional to τ_{ci} and it is independent of the pulse separation τ. That is

$$T_{2ei} \approx \tau_{ci}. \tag{2.60}$$

Some external factors, such as a change in sample temperature, can cause a jump in correlation time τ_{ci} of a given motion, i, resulting in a transition from the $\tau_{ci} \ll \tau$

case to the $\tau_{ci} \gg \tau$ case. As a result, the contribution to the echo decay rate will pass through a maximum. As presented in the following chapters, the transverse relaxation rate obtained for all samples studied in this work passes through a maximum at or just below the main phase transition.

As an example, figure 2.5 shows experimental data collected for a pure DPPG-d_{62} bilayer at 43°C. Figure 2.5(a) shows the echo for a series of pulse spacings, τ. Echo decay resulting from the modulation of the quadrupole interaction by bilayer motions is evident from this data. The characteristic time T_{2e} of the echo decay is obtained from the initial slope of the log-amplitude plot versus 2τ as shown in figure 2.5(c). The corresponding spectra are shown in figure 2.5(b).

Figure 2.5(b) implicitly shows the orientation (β') dependence of transverse relaxation time T_{2e}. β' is defined earlier in figure 2.2. The transverse relaxation rate is smallest at the $\pi/2$ edge of the spectrum and increases towards the center of the spectrum. This can be seen from the expanded spectrum shown in figure 2.5(d). A theoretical expression, which shows this orientation dependence of T_{2e}, has been developed based on relaxation models for collective order fluctuations [70] and surface undulations [69]. It was predicted that

$$\frac{1}{T_{2e}} \propto \sin^2 \beta' \cos^2 \beta' \tag{2.61}$$

where β', defined in subsection 2.1, is the angle between the external magnetic field (laboratory frame) and the surface normal (molecular fixed frame). These authors have attributed this dependence to the effect of thermally excited undulations of the membranes [69] and order director fluctuations of the acyl chains [70]. This orientation dependence of T_{2e} has also been observed experimentally for specifically deuterated acyl chains [70].

Chapters 3, 4, and 5 show that addition of the surfactant proteins and/or Ca^{2+} to

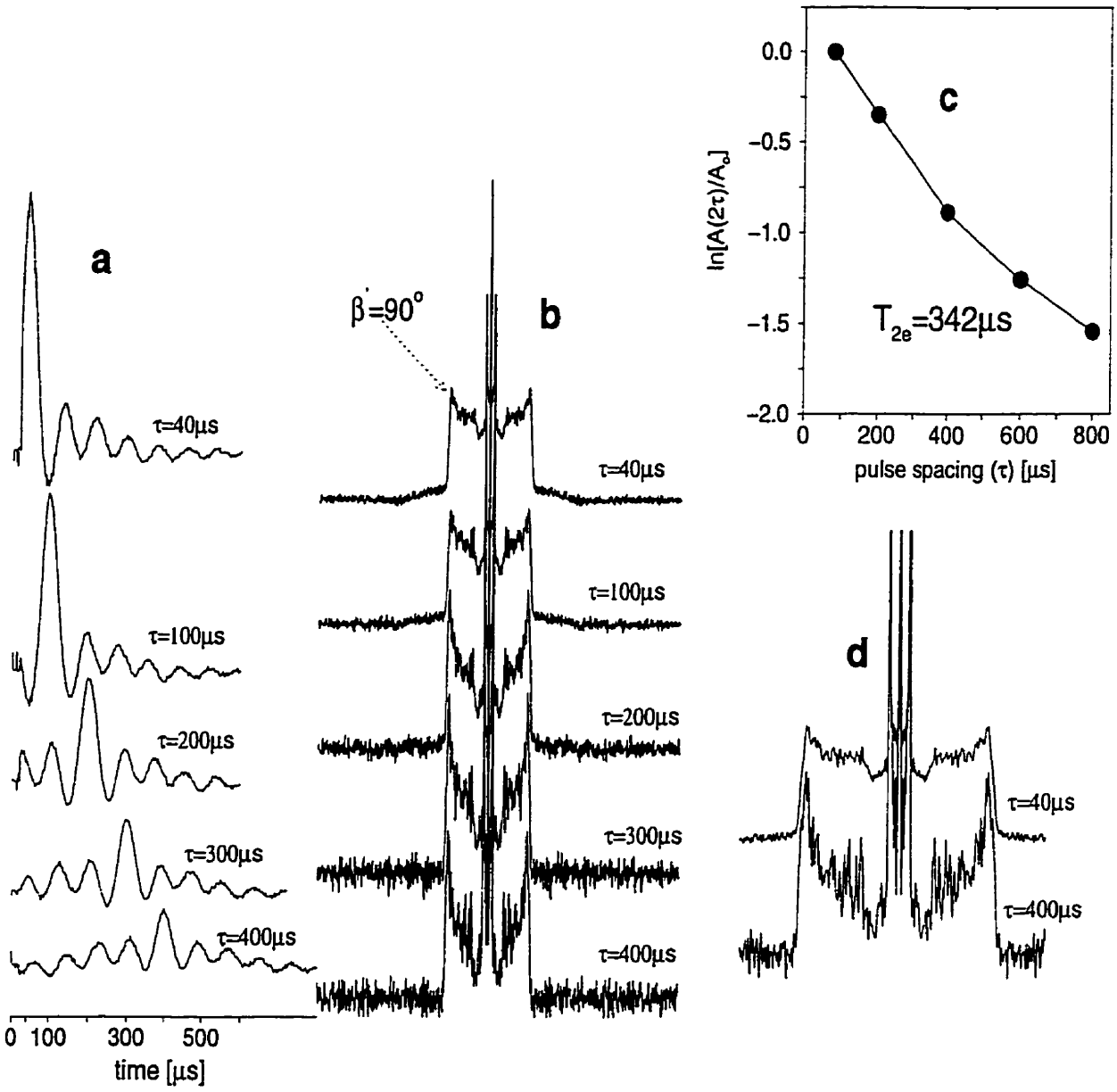

Figure 2.5: The quadrupole echo decay at 43°C for a pure DPPG-d_{62} bilayer. (a) free-induction decay as a function of pulse spacing (τ), (b) the corresponding spectra, (c) its log-amplitude whose slope is equal to the transverse relaxation rate, and (d) expanded spectra.

lipid bilayer induces changes in the correlation times of the motions of the bilayer which we can detect by ^{2}H transverse relaxation time T_{2e} measurements and thereby obtain information about the interactions.

2.3.3 The ^{2}H-NMR experimental setup

All the experiments in this work were performed using a locally constructed solid state ^{2}H-NMR spectrometer in a 3.6 T superconducting magnet (Nalorac, Cryogenics, Martinez, CA). Figure 2.6 shows the setup of this spectrometer in some detail. The various components function as described below. The frequency synthesizer generates signals with frequencies of 33.2 MHz and 10 MHz. The 10 MHz signal is fed into a phase splitter which sends this signal to the phase detector and pulse generator. The 33.2 MHz signal is sent to both the single side-band generator and the receiver. The 10 MHz signal is edited into pulses with phases of 0°, 90°, 180°, and 270° in the pulse generator and sent to mixers contained in the single side-band generator. The output and the duration of these pulses are controlled by a pulse programmer. The single side-band system mixes the 33.2 MHz and 10 MHz signals to generate pulses at the ^{2}H resonance frequency (23.2 MHz). These pulses are then sent to a transmitter via a pulse amplifier. The pulse amplifier transmits pulses at the resonance frequency with an amplitude of about 300 Volts into the probe via crossed diodes which provide a passage for the AC current. The r.f. coil and the sample are contained in a temperature controlled copper oven in the probe which is inserted into the room temperature bore of a superconducting magnet.

The response of the spin system to a pair of high power pulses induces a weak voltage signal in the coil. This weak signal is amplified in the preamplifier and then fed into the receiver system. The receiver system contains a mixer, a 10 MHz amplifier, and a quadrature detector. The mixer mixes the 33.2 MHz signal from the frequency synthesizer

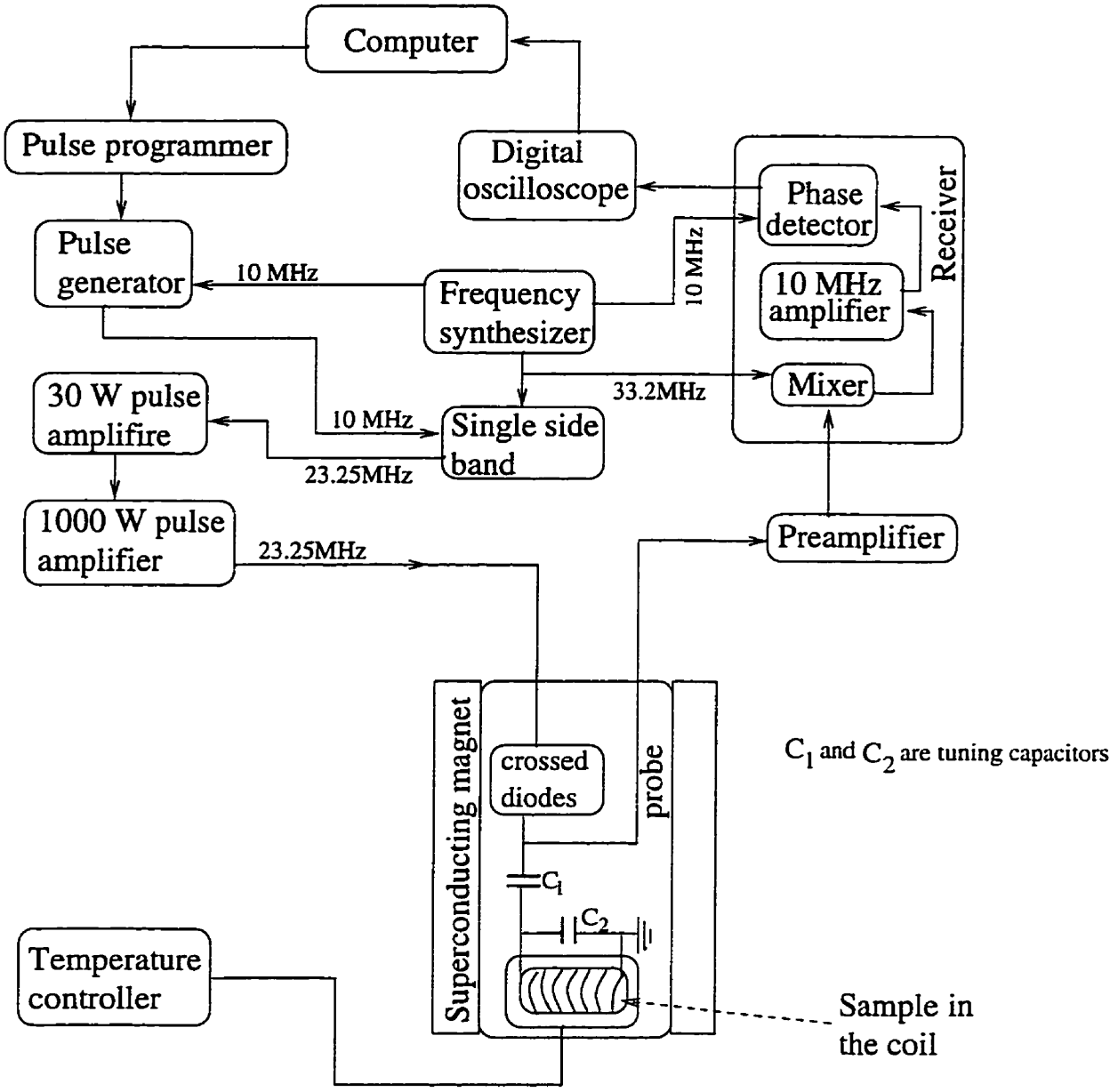

Figure 2.6: The solid state NMR experimental setup used in this work.

with the 23.2 MHz carrier wave modulated by FID signal from the preamplifier and generates a 10 MHz carrier wave modulated by the FID signal. This 10 MHz wave carrying the FID signal is sent to the quadrature detector, which detects both the real and the imaginary parts of the FID signal separately by comparing the FID signal with the reference signal coming from the frequency synthesizer. Then the FID signals are digitized by a digital oscilloscope with sampling times of 1 μs (gel phase) and 2 μs (liquid crystalline phase) for results in chapters 3 and 4. For results in chapter 5, sampling times of 2 μs and 5 μs are used for samples in gel and liquid crystalline phases, respectively. The pulse parameters of the quadrupole echo sequence (figure 2.3) are determined depending on the experimental situations and these are given in the corresponding chapters where the results are presented.

Chapter 3

Results and Discussion I: SP-B Effect on DPPC/DPPG Acyl Chains

3.1 Introduction

SP-B is among the four surfactant proteins that play a major role in the pulmonary surfactant system. The influence of this protein on phosphatidylcholine (PC) and/or phosphatidylglycerol (PG) monolayers and bilayers has been studied by many investigators using several techniques [28, 33, 41, 47, 54, 78]. These studies indicate that SP-B is not a transmembrane protein. Fluorescence anisotropy measurements of interior-selective fluorescent probes show that the order of the lipid acyl chains was not altered by the presence of SP-B [41, 42]. A Fourier transform infrared spectroscopy study [78] of this protein in DPPC/DPPG bilayers showed no modification of the conformation or orientation of the lipids in the presence of SP-B in the bilayer. SP-B is a highly hydrophobic protein and an absence of any effect on molecular order in the interior of the bilayer raises a question as to how this protein might be incorporated into a bilayer. Models as to how this protein might be accommodated in the bilayer have been proposed [51, 12, 78]. Results

presented below may provide some insight into how these models might be distinguished.

SP-B has net positive charge at physiological pH. DPPG has one negative charge while DPPC is neutral. Recent work has shown that synthetic SP-B does not affect chain order in bilayers of DPPC [54]. Since DPPC and DPPG differ in head group charge, the interest in this part of my project is to investigate the extent to which the interaction of SP-B with bilayers is sensitive to lipid charge. This is done by probing the effects of SP-B on the chain order, phase behaviour and dynamics in bilayers of DPPG and mixed DPPC/DPPG using ^{2}H-NMR.

3.2 Sample and experimental conditions

3.2.1 Sample preparation

All the samples used in this work were prepared in Dr. K. M. W. Keough's laboratory (Biochemistry, Memorial University of Newfoundland) by Dr. S. Taneva, J. Hancock, J. Stewart and S. Harris according to the following protocol.

DPPC-d_{62} and DPPG-d_{62} were purchased from Avanti Polar Lipids (Pelham, AL). Unlabeled DPPC and DPPG were purchased from Sigma Chemical Co. (St. Louis, Mo). The lipids ran as single spots on thin layer chromatography and were used without further purification.

Pulmonary surfactant proteins SP-B and SP-C were obtained from extracts of porcine lung lavage as described previously [28]. Isolation and purification of the surfactant proteins SP-B and SP-C from the lipid extract were performed by gel exclusion chromatography on Sephadex LH-60 (Pharmacia, Uppsala, Sweden) in 1:1 (v/v) chloroform/methanol containing 0.1 M HCl (2%). SDS-polyacrylamide gel electrophoresis (16% gels) [79, 28] of the SP-B and SP-C under nonreducing conditions yielded bands at about 18 kD and

5 kD, respectively.

Lipids were weighed and dissolved in $CHCl_3$/MeOH (1:1) to give a concentration of 2 mg/ml. The protein concentration in the column eluent was determined by fluorescamine assay [80]. Solvents were removed by rotary evaporation under N_2 followed by overnight evacuation. Samples were suspended by adding buffer (135 mM NaCl and 15 mM Hepes at pH 7.0) to the flask containing the dried sample film and then rotating the flask in a water bath at 45-50 °C for about 1h. Films containing the protein were scraped from the walls of the flask to ensure complete suspension in the buffer. The amount of buffer added was chosen to yield a suspension of about 2 mg/ml which was then centrifuged at 14,000 rpm for 10 min. Most of the supernatent was removed. The resulting pellet was scraped into an 8 mm NMR tube with a volume of about 400 μl.

In all the mixed lipid samples discussed in this and the following chapters, the DPPC:DPPG concentration ratio of 70:30 w/w is used. While this is not the physiological concentration, 30% w/w DPPG was chosen to yield a measurable signal from DPPG in DPPC/DPPG mixture and to amplify the effects of any selective interactions with DPPG.

3.2.2 Experimental details

^{2}H-NMR measurements at 23.215 MHz were carried out in a superconducting solenoid (Nalorac, Martinez, CA), using a locally constructed spectrometer, introduced in chapter 2. Quadrupole echo pulse sequences (see chapter 2) with $\pi/2$ pulse lengths of 2.3-2.75 μs were used. For spectra from which first spectral moments were taken, the pulse separation (τ) was 40 μs. For transverse relaxation time measurements, pulse separations were varied from 40 μs to 400 μs. Typical spectra were obtained by averaging 24,000 transients obtained with phase cycling, using a repetition time of 0.5 s. The sample

tube and probe coil were enclosed within a copper oven, the temperature of which was maintained by a microprocessor-based temperature controller. Experiments were carried out for a series of temperatures beginning at 55°C and descending in steps of 2°C (1°C near the phase transition). Samples were allowed to reach thermal equilibrium, before starting each experiment, by waiting for at least 20 minutes after each cooling step.

3.3 Interaction of SP-B with DPPG bilayer

Effects of SP-B on the physical properties of the DPPG bilayer were studied by observing ^{2}H-NMR spectra and quadrupole echo decay rates as presented below.

3.3.1 ^{2}H-NMR spectra and first moment

In general, effects of proteins on the bilayer phase behaviour and chain order are reflected in ^{2}H-NMR spectra. To study effects due to the presence of SP-B in the DPPG bilayer, ^{2}H-NMR spectra were collected at selected temperatures. Figure 3.1 shows ^{2}H NMR spectra for DPPG-d_{62} and DPPG-d_{62} plus 11% (w/w) SP-B (about 174 DPPG molecules per SP-B molecule). In the absence of SP-B, the spectra above 36°C are superpositions of sharp doublets characteristic of axially symmetric chain reorientation in the liquid crystalline phase. Below 36°C, the spectra show the wider, more continuous intensity distribution characteristic of the gel phase in which chain motions are not axially symmetric. A relatively sharp transition from liquid crystal to gel phase occurs at 36°C where spectra characteristic of the two coexisting phases are superimposed. For the DPPG-d_{62} sample containing SP-B, the spectra display a more continuous change from liquid crystal to gel characteristics. The most abrupt change in spectral shape occurs between 37°C and 36°C. Comparison of the spectra for DPPG-d_{62} with and without SP-B

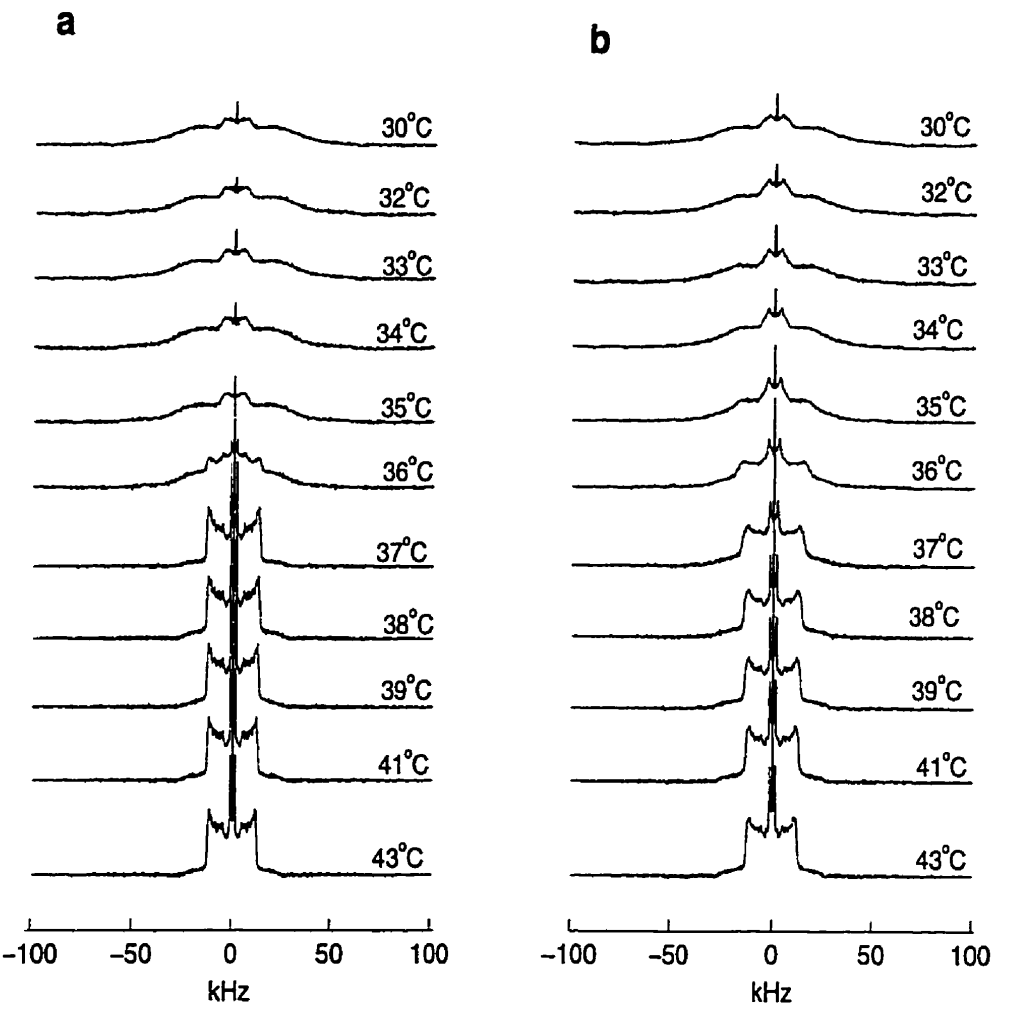

Figure 3.1: ^{2}H NMR spectra for (a) DPPG-d_{62} and (b) DPPG-d_{62} plus 11% (w/w) SP-B.

show a slight increase in transition temperature and broadening of the main phase transition. This slight increase in transition temperature may be due to the increased head group constraints as a result of electrostatic interaction between positive charges on SP-B and negative charges on DPPG. The increase in transition temperature of DPPC/DPPG bilayer by SP-B was also observed previously [41]. In an earlier ^{2}H-NMR study [54] of the effect of SP-B on the physical properties of DPPC, although the protein induced broadening of the transition, an increase in transition temperature was not observed. This might show that the interaction between the charged lipid head group and the charges on SP-B may affect the transition temperature slightly.

The powder pattern spectra can be transformed to yield the spectrum which would be seen for an oriented sample by using a process known as de-Paking [81, 82]. Figure 3.2 shows dePaked spectra, corresponding to 0° orientation of the bilayer normal, for DPPG-d_{62} without and with 11% (w/w) SP-B at 45 °C. The distribution of resolved doublet splittings is typical of the dependence of orientational order on position along the chain for a range of saturated diacylphosphatidylcholines [83]. SP-B has no appreciable effect on either the mean orientational order or the dependence of deuteron orientational order on positions along the DPPG-d_{62} chains.

As introduced in chapter 2, the ^{2}H first spectral moment (M_1) gives the mean quadrupole splitting or the mean orientational order parameter. M_1 was measured in order to study the effect of SP-B on the mean orientational order of acyl chains of DPPG. Figure 3.3 shows first spectral moments (M_1) derived from the ^{2}H-NMR spectra of DPPG-d_{62} with and without 11% SP-B. As was reported for synthetic SP-B in bilayers of DPPC-d_{62} [54], the protein has little effect on chain order in the liquid crystalline phase at temperatures away from the transition. The effect, if any, in the gel phase is small. This is also in agreement with the result from a fluorescence anisotropy study [42] which showed that insertion of SP-B into a model membrane did not alter the fluorescence

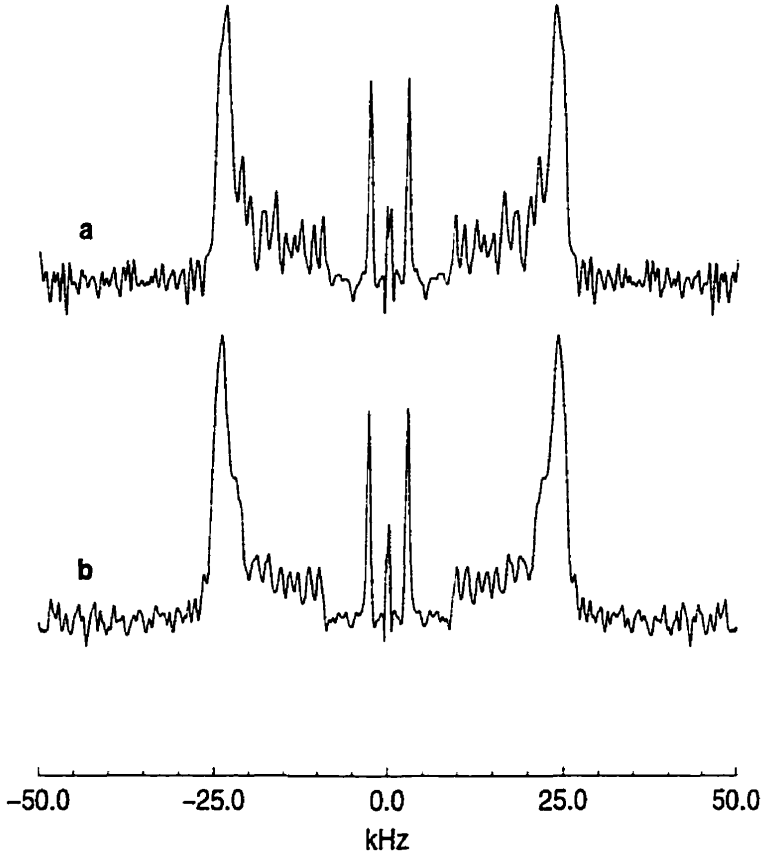

Figure 3.2: DePaked ^{2}H-NMR spectra for (a) DPPG-d_{62} and (b) DPPG-d_{62} plus 11% (w/w) SP-B at 45 °C.

anisotropy of the membrane-probes at both fluid and gel phase temperatures.

3.3.2 Deuteron transverse relaxation

Additional information about the lipid-protein interaction can be obtained from an examination of deuteron transverse relaxation times which can indicate how slow molecular reorientation is perturbed by the presence of the protein. It was discussed in chapter 2 that motions which affect the orientation-dependent quadrupole interaction can cause the quadrupole echo amplitude to decay with time. Figures 3.4(a) and 3.4(b) show the

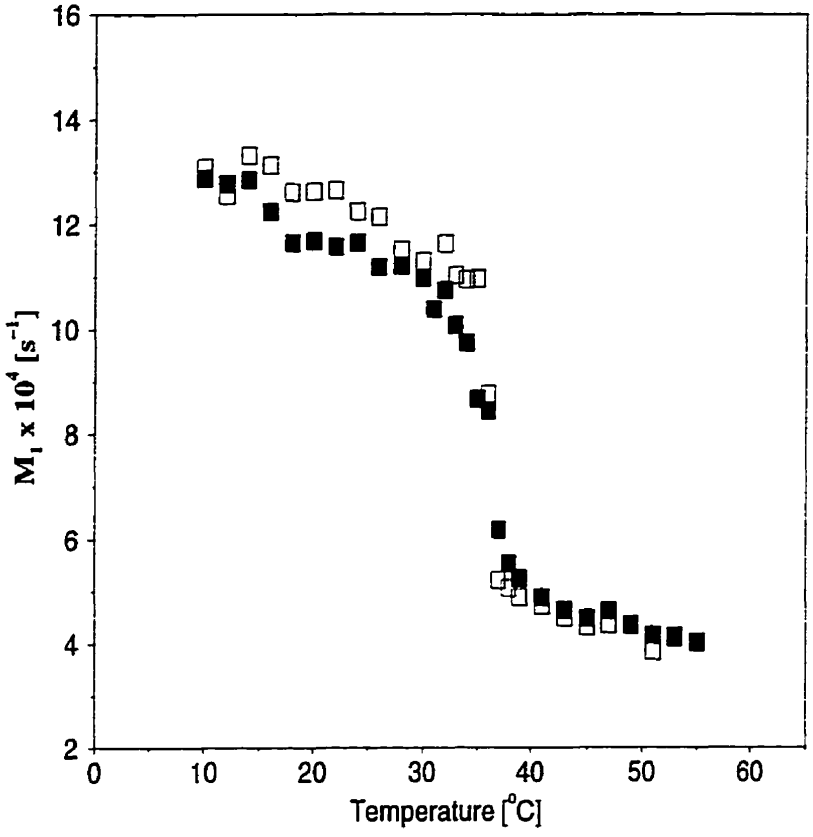

Figure 3.3: Temperature dependence of ^{2}H-NMR first spectral moments for (□) DPPG-d_{62} and (■) DPPG-d_{62} plus 11% (w/w) SP-B.

quadrupole echo amplitude decay as a function of pulse spacing, 2τ, for DPPG-d_{62} with and without 11% (w/w) SP-B, respectively. The effective transverse relaxation time (T_{2e}) is obtained from the initial slopes of these log-amplitude plots. Comparing figures 3.4(a) and 3.4(b), the echo amplitude decay is approximately exponential for the sample without protein except possibly at 35°C where non-exponential dependence on 2τ is seen. This is also the temperature at which T_{2e} is a minimum near the phase transition as can be seen from figure 3.4(c). This might be explained as follows. In the liquid crystalline and gel phases of the pure DPPG-d_{62}, deuterons in almost all parts of the sample are,

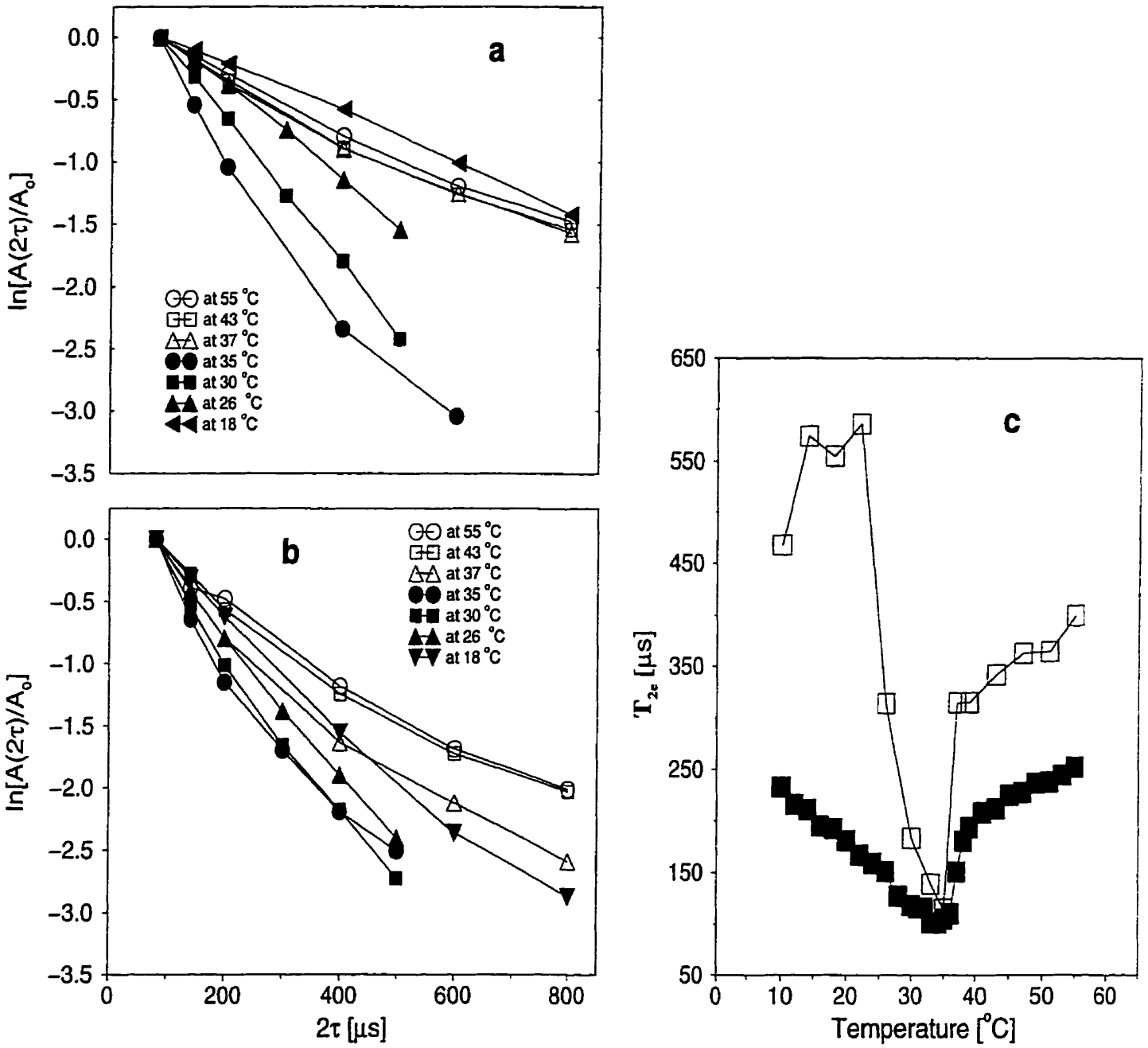

Figure 3.4: (a) Quadrupole echo decay for pure DPPG-d_{62}, (b) Quadrupole echo decay for DPPG-d_{62} plus 11% (w/w) SP-B, and (c) temperature dependence of T_{2e} for (□) pure DPPG-d_{62} and (■) DPPG-d_{62} plus 11% (w/w) SP-B.

approximately, subjected to the same fast and slow motional modes. The signal from deuterons at different sites presumably decays with a single average relaxation rate and thus we observe nearly exponential decay in the liquid crystalline phase. At the phase transition, however, a two phase coexistence was observed as discussed above. This means that some deuterons are in the gel phase domain and some are in the liquid crystal phase domain. Due to this, the signals from the deuterons in different environments decay with different relaxation rates. As the result, the echo decay becomes a sum of exponentials, which explains the non-exponential data observed at the phase transition.

In the presence of SP-B, the quadrupole echo decay displays non-exponential behaviour as shown in figure 3.4(b). The above reasoning for the pure lipid case may not be applicable here, because the decay is non-exponential even in the liquid crystalline phase. In the presence of SP-B, signals from deuterons on different segments along the acyl chains decay with different relaxation rates and the echo amplitude is described by the sum of exponentials resulting in the observed non-exponential decay.

Figure 3.4(c) shows that, in the liquid crystalline phase, T_{2e} decreases as the temperature is decreased and reaches a minimum at or just below the main phase transition. In the gel phase, as the temperature is decreased, T_{2e} increases and passes through a maximum (for the sample without SP-B). This variation of T_{2e} with temperature may, in general, be explained as follows.

Both fast and slow motions exist in the liquid crystalline phase. Fast and slow motions are defined in chapter 2. If the correlation time of a given motion is much greater than the quadrupole echo pulse spacing, the motion is said to be slow relative to the experimental time, which is the duration of the quadrupole echo pulse sequence. The motion is fast otherwise. Depending on the order of magnitude of their correlation time, these motions contribute to the transverse relaxation rate according to Equations (2.58) and (2.59) of chapter 2. The contribution of the fast motions to the decay rate is *proportional* to the

correlation time and thus the relaxation rate increases with increasing correlation time.

As the sample is cooled and the main phase transition is approached, some fast motions slow down. At the main transition or just below it, the correlation time of these motions become long enough to exceed the quadrupole echo pulse separation. They become slow motions and their contribution to transverse relaxation rate becomes *inversely proportional* to correlation time. The relaxation rate (time) decreases (increases) with correlation time. As the result the transverse relaxation rate (time) passes through a maximum (minimum) near the main transition. Motions which were slow in the liquid crystalline phase, get even slower as the main transition is approached and probably die out in the gel phase. As the correlation times of motions increase in the gel phase, the transverse relaxation time increases, reaches a maximum and then decreases. This maximum in the gel phase indicates the presence of fast motion in the gel phase. Some of the gel phase slow motions probably freeze-out at the temperature of this maximum and the contribution of the fast motions remains and the transverse relaxation time decreases.

3.3.3 Motions affecting T_{2e}

Some of the motions which affect the transverse relaxation rate in both gel and liquid crystalline phases include bilayer surface undulation [69], diffusion along curved surfaces [68], collective bilayer modes [70], intermolecular motions (such as chain fluctuation and molecular rotations) and intra-molecular motions (such as *trans-gauche* isomerization) [71]. The order of magnitude of the correlation times of these motions in the liquid crystalline phase have been determined. The correlation time of bilayer undulation is of the order of 100 μs [69, 67], while that of lateral diffusion is of the order of 100 ms [69]. The correlation time of the collective bilayer mode is also probably of the order of tens of microseconds [70]. The correlation times of chain rotation and chain fluctuation

motions are of the order of $10^{-8}s$ [71]. *Trans-gauche* isomerization occurs at a faster rate and its correlation time is of the order of $10^{-10}s$ [71]. In the liquid crystalline phase, away from the main transition, bilayer surface undulation, lateral diffusion and collective lipid motions are the main contributors to relaxation. As discussed above, for these slow motions, T_{2e} is proportional to their correlation time. The chain fluctuations and molecular rotations are fast and their contribution to T_{2e} is inversely proportional to their correlation times. As temperature decreases, the correlation times of chain fluctuation, molecular rotation and *trans-gauche* isomerization motions increases and T_{2e} decreases. At the phase transition, the correlation time of these three motions is of the order of $10^{-6}s$ to $10^{-5}s$ [71]. Bilayer undulation, lateral diffusion and collective mode motions freeze out on the time scale of quadrupole echo pulse sequence and they do not affect T_{2e}. When the correlation times of the remaining motions becomes comparable to the quadrupole echo pulse separation just below the main phase transition, T_{2e} assumes a minimum. Further increase in the correlation times, results in an increase in T_{2e} in the gel phase. Far down in the gel phase, the intermolecular motions may die-out on the experimental time scale and fast intra-molecular motions remain (with correlation time of the order of microseconds [71]) as the main contributer to the decay, resulting in the observed T_{2e} maximum.

3.3.4 Effect of SP-B on bilayer motions

The temperature dependence of T_{2e} for DPPG-d_{62} with 11% (w/w) SP-B is shown in figure 3.4(c). SP-B increased (decreased) transverse relaxation rate (time) in both liquid crystalline and gel phases. The decrease in T_{2e} in the liquid crystalline phase indicates that either the correlation times of fast motions became longer or the correlation times of slow motions became shorter due to presence of SP-B. The former is unlikely because

no change in spectral shape or quadrupole splittings is observed. As discussed in chapter 2, fast motions cause motional narrowing of spectrum. If there were changes in motional narrowing in the presence of SP-B, the first spectral moments, which are proportional to quadrupole splittings, would likely have been affected. Since this is not observed, as can be seen from figure 3.3 and the dePaked spectra of figure 3.2, SP-B presumably affects mainly the slow motions. Therefore, protein seems to decrease the correlation times of the slow bilayer motions. This is possible if the protein shortened the wave length of the surface undulation and increased the bilayer curvature. In the gel phase, the protein interferes with the slowing down of the motions so that the motions persist to lower temperatures without freezing-out.

3.4 SP-B in a mixed DPPC/DPPG bilayer

In the above section we saw some of the effects that SP-B has on the pure DPPG bilayer. The actual pulmonary surfactant system, however, is composed of mixtures of phospholipids, including anionic phospholipids such as PG (see chapter 1). In order to get additional insights into how SP-B might interact in the pulmonary surfactant system, it is important to investigate how this protein interacts with the bilayer formed by the mixture of neutral and anionic lipids. For this reason, ^{2}H-NMR spectra, ^{2}H first spectral moment (M_1) values and ^{2}H-NMR transverse relaxation times (T_{2e}) were also obtained for mixed DPPC/DPPG bilayers without and with SP-B present.

Figure 3.5 shows spectra at selected temperatures for DPPC/DPPG-d_{62} (70:30 w/w) and for this lipid mixture plus 11% (w/w) SP-B and 15% (w/w) SP-B. Concentrations of 11% and 15% SP-B (w/w) correspond, respectively, to about 176 and 123 lipid molecules per SP-B molecule in the mixture. The sample with no protein shows a relatively sharp transition from liquid crystal to gel at 40 °C where a superposition of gel and liquid

crystal phase features can be seen. The increase in the transition temperature relative to that of the DPPG-d_{62} sample is an isotope effect and reflects the reduced degree of deuteration in the mixed lipid sample. It is interesting that, despite the difference in transition temperature of DPPC (41 °C) and DPPG-d_{62} (36 °C), the transition remains relatively narrow. The mixed lipid samples containing SP-B show a continuous change of spectral character from liquid crystal to gel.

While SP-B promotes a more continuous transition in both DPPG-d_{62} and the mixed lipid bilayers, close inspection of the gel phase spectra suggests that the perturbation of the bilayer may not be identical in the two cases. Figure 3.6 shows enlarged gel phase spectra for DPPG-d_{62} and DPPC/DPPG-d_{62} with and without SP-B. Because of rotation about the methyl group symmetry axis, methyl group deuterons in the gel phase give rise to significantly narrower spectral components than the rest of the acyl chain deuterons. As illustrated in figure 3.6, gel phase spectra for both of the DPPC/DPPG-d_{62} samples with SP-B present display methyl features which are somewhat narrower and more prominent than those seen for DPPG-d_{62} plus 11% (w/w) SP-B. This indicates that there is a population of molecules in an environment where reorientation is less restricted than in more typical gel phases. This difference between the effects of SP-B on the mixture and single component bilayers is not yet fully understood. As presented below, however, the mean transverse relaxation rates in the gel phases for the protein-containing samples with different lipid compositions are not substantially different.

In order to consider the possibility of a specific interaction between SP-B and either DPPC or DPPG in the mixture, ^{2}H-NMR spectra were also collected for DPPC-d_{62}/DPPG (70:30) and for this lipid mixture plus 11% (w/w) SP-B. Figure 3.7 shows spectra for these two samples at selected temperatures. The difference in the transition temperatures observed for the two mixed lipid samples in the absence of SP-B (figures

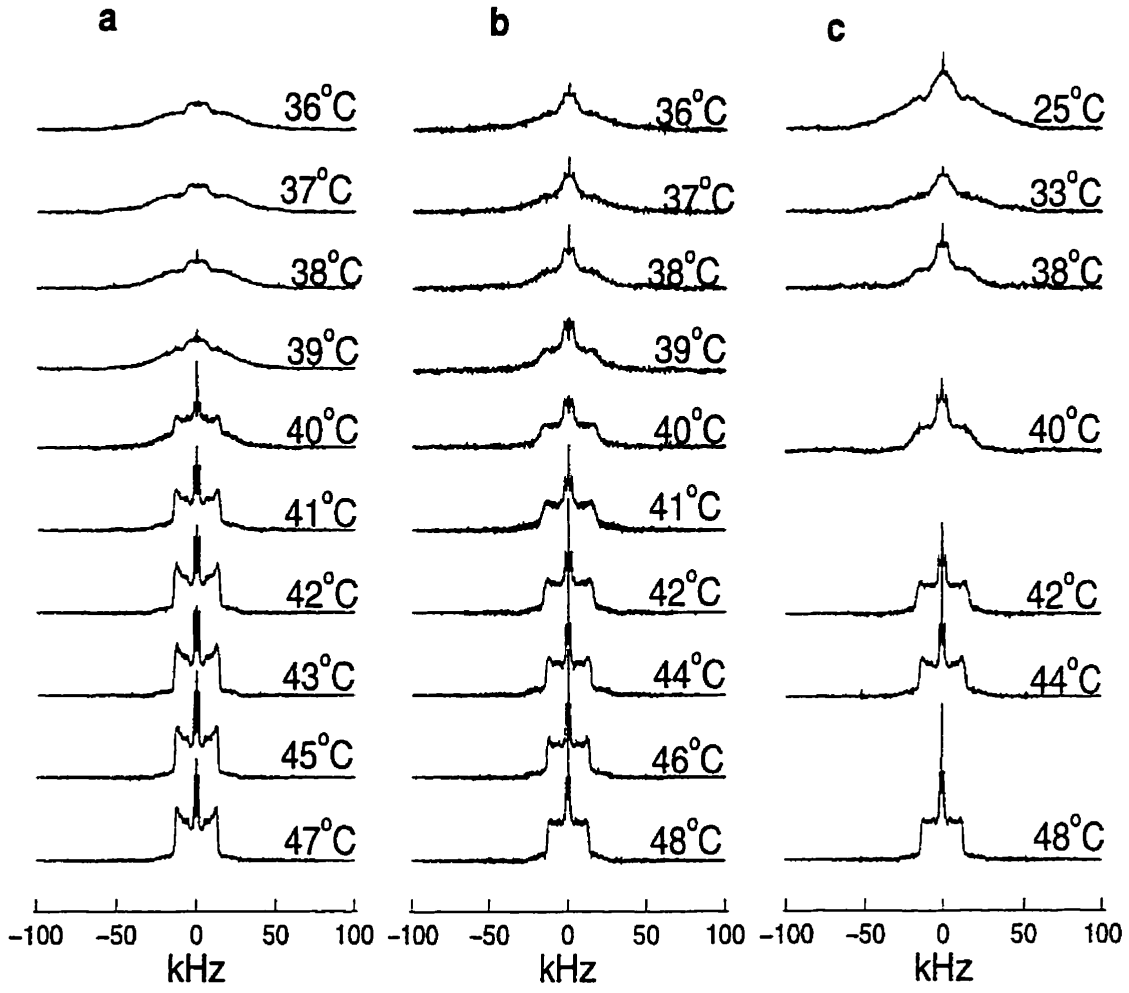

Figure 3.5: ^{2}H NMR spectra for (a) DPPC/DPPG-d_{62} (70:30), (b) DPPC/DPPG-d_{62} (70:30) plus 11% (w/w) SP-B, (c) DPPC/DPPG-d_{62} (70:30) plus 15% (w/w) SP-B at selected temperatures.

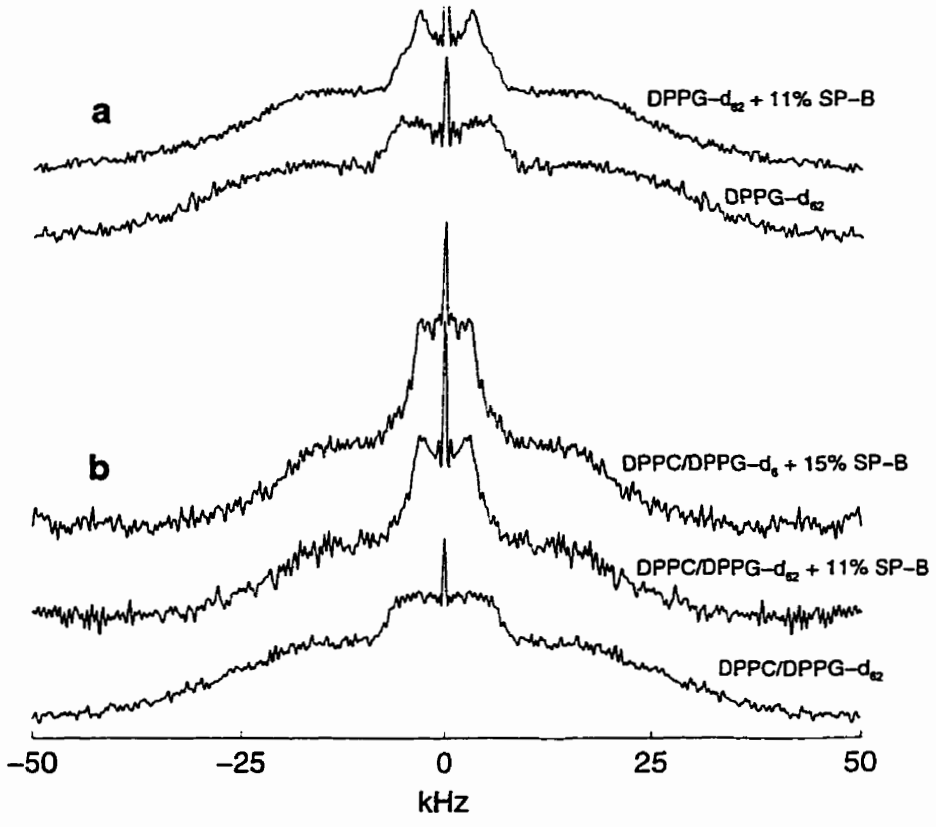

Figure 3.6: (a) Gel phase spectra at 34 °C for DPPG-d_{62} and DPPG-d_{62} plus 11% SP-B (w/w). (b) Gel phase spectra at 38 °C for DPPC/DPPG-d_{62} and DPPC/DPPG-d_{62} plus 11% SP-B (w/w) and 15% SP-B (w/w).

3.5(a) and 3.7(a)) reflects the higher degree of deuteration in the DPPC-d_{62}/DPPG sample compared to that in the DPPC/DPPG-d_{62} mixture. When this is taken into account, the sequences of spectra observed for the mixed lipid samples in the presence of SP-B (figures 3.5(b) and 3.7(b)) are nearly independent of which lipid is deuterated. There is no indication of a significant specific interaction of SP-B with one or the other lipid components of the mixture.

First spectral moment, M_1, values for DPPC/DPPG-d_{62} (70:30) with and without

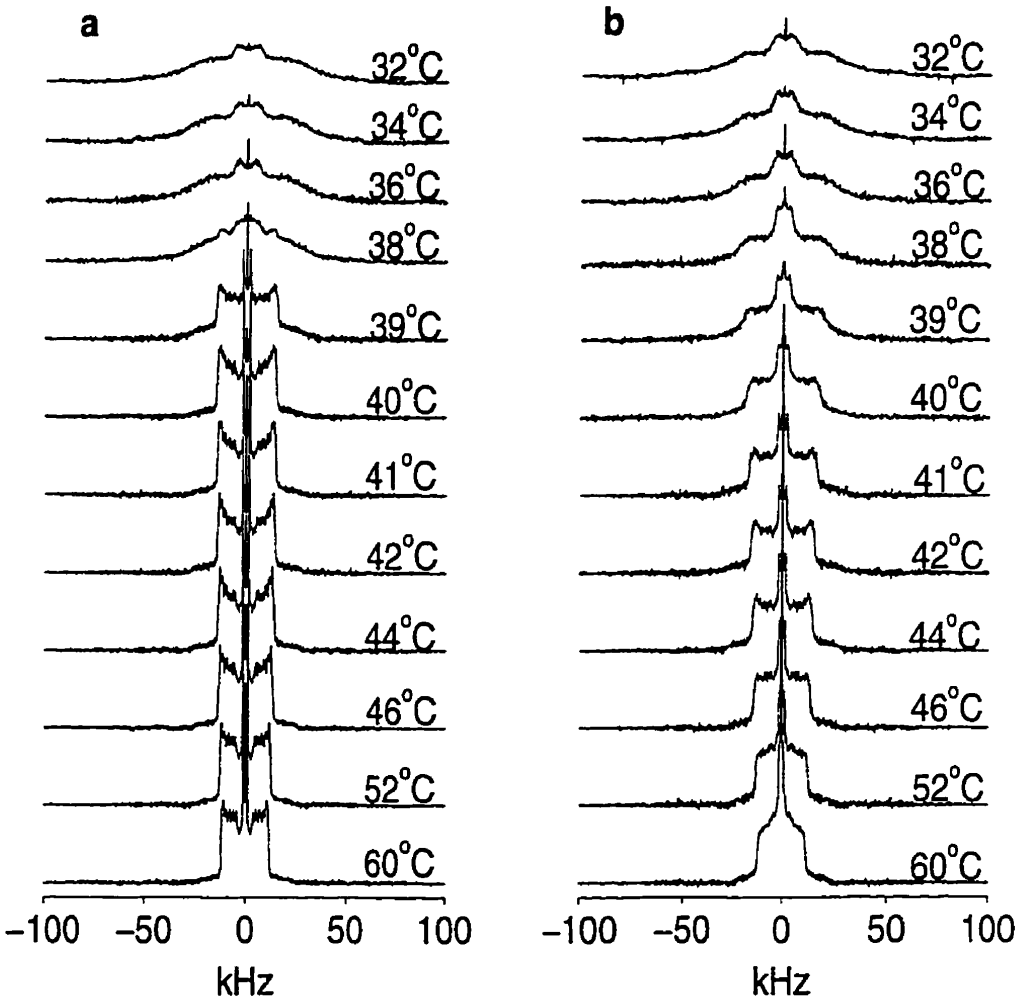

Figure 3.7: ^{2}H NMR spectra for (a) DPPC-d_{62}/DPPG (70:30), (b) DPPC-d_{62}/DPPG (70:30) plus 11% (w/w) SP-B for selected temperatures.

11% (w/w) SP-B and 15% (w/w) SP-B are shown in figure 3.8(a). M_1 values for DPPC-d_{62}/DPPG (70:30) with and without 11% (w/w) SP-B are shown in figure 3.8(b). From figure 3.8(a), the protein has little effect on chain order in the liquid crystalline phase and the effect on chain order in the gel phase is small. Figure 3.8(a) also shows M_1 values for DPPC/DPPG-d_{62} plus 15% (w/w) SP-B. The increased protein concentration has some effect on the gel phase but little effect on liquid crystal phase chain order. From comparison of figures 3.8(a) and 3.8(b), there is again no indication of a specific interaction of SP-B with one of the lipid components in the DPPC/DPPG bilayer. However, a fluorescence anisotropy study of interaction of bovine SP-B with DPPC/DPPG (7:1) bilayer indicated that SP-B interacts selectively with phosphatidylglycerol [41]. This same study discussed that the bilayer surface was ordered by SP-B. The difference between these fluorescence results and the observations of this work may be due to the difference between the time scales of the experiments and/or the sample preparation protocol used in these studies.

Figure 3.9(a) shows the temperature dependence of T_{2e} for DPPC/DPPG-d_{62} (70:30) in the absence of SP-B and with 11% (w/w) and 15% (w/w) SP-B added. Figure 3.9(b) shows the temperature dependence of T_{2e} for DPPC-d_{62}/DPPG (70:30) with and without 11% (w/w) SP-B. In the absence of SP-B, comparing figures 3.4(c), 3.9(a), and 3.9(b), the T_{2e} data for DPPG-d_{62}, DPPC/DPPG-d_{62} and DPPC-d_{62}/DPPG qualitatively show similar variation with temperature except for the difference in temperature at which the minimum occurs. The T_{2e} values for these samples in both liquid crystal and gel phases are of the same order of magnitude. The minimum values of T_{2e} are also of the same order, approximately equal to the quadrupole echo pulse spacing ($2\tau = 80\mu s$) used in these experiments, implying that the correlation times of effective motions at the temperature of the T_{2e} minimum may be less than the quadrupole pulse spacing. For these samples with no SP-B, T_{2e} goes to the minimum abruptly and rises quickly just

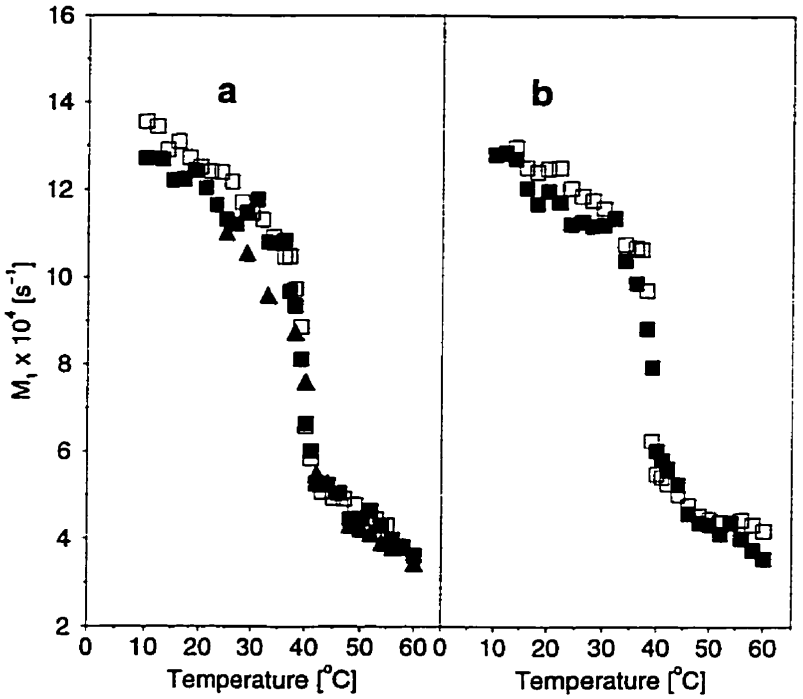

Figure 3.8: (a) Temperature dependence of ^{2}H-NMR first spectral moments for (□) DPPC/DPPG-d_{62} (70:30), (■) DPPC/DPPG-d_{62} (70:30) (70:30) plus 11% SP-B and (▲) DPPC/DPPG-d_{62} (70:30) plus 15% SP-B. (b) Temperature dependence of ^{2}H-NMR first spectral moments for (□) DPPC-d_{62}/DPPG (70:30) and (■) DPPC-d_{62}/DPPG (70:30) plus 11% SP-B.

below the transition indicating that the correlation time of these motions is very sensitive to slight changes in temperature near the main transition.

In the presence of SP-B, T_{2e} displays similar variations with temperature for DPPC/DPPG-d_{62} and DPPC-d_{62}/DPPG bilayers. The striking similarity of the behaviour of T_{2e} for pure DPPG and for mixed DPPC/DPPG bilayers, in the presence of SP-B, is unexpected. This suggests that the effects of SP-B on the motions influencing transverse relaxation rates are common for these lipid bilayers.

Figure 3.9(a) shows T_{2e} data for two protein concentrations. Concentrations of 11% and 15% (w/w) SP-B in bilayers of DPPC/DPPG-d_{62} have similar effects on transverse

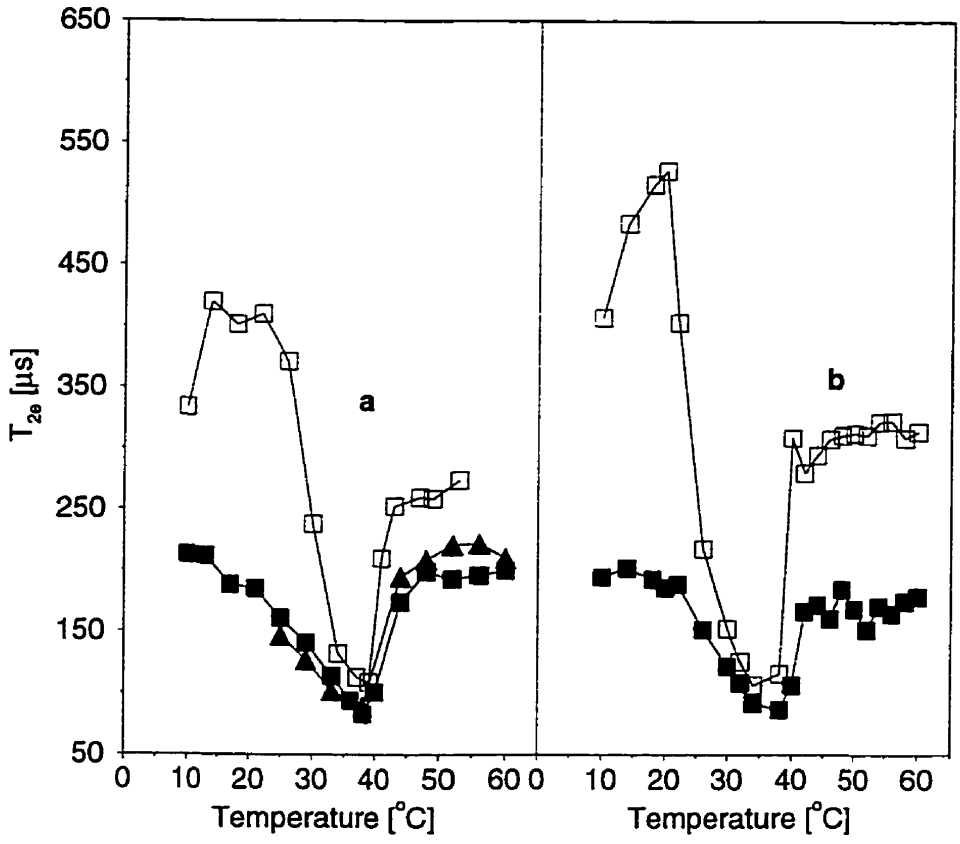

Figure 3.9: (a) Temperature dependence of T_{2e} for (□) DPPC/DPPG-d_{62} (70:30), (■) DPPC/DPPG-d_{62} (70:30) plus 11% SP-B and (▲) DPPC/DPPG-d_{62} (70:30) plus 15% SP-B. (b) Temperature dependence of T_{2e} for (□) DPPC-d_{62}/DPPG (70:30) and (■) DPPC-d_{62}/DPPG (70:30) plus 11% SP-B.

relaxation rates. This suggests that there may be a threshold SP-B concentration beyond which the response of T_{2e} to SP-B concentration saturates. This may also suggest that small SP-B concentrations are enough to have a significant influence on bilayer motions and that the increase in the amount of SP-B has only a slight additional effect on the bilayer motions. It is important to note here that although SP-B and SP-C are essential components of pulmonary surfactant system, together they comprise only 1% of the whole surfactant material.

3.5 Summary and Discussion

A recent study of synthetic SP-B in DPPC-d_{62} showed that, while the protein broadened the main phase transition, it had little effect on acyl chain order in the bilayer [54]. This work has extended these observations to natural SP-B in bilayers of DPPG-d_{62} and in DPPC/DPPG-d_{62} or DPPC-d_{62}/DPPG mixed bilayers. These observations suggest that SP-B interacts with the bilayer in a way which has little effect on the amplitude of the fast chain conformational fluctuations which determine the mean orientational order for the perdeuterated chain in the liquid crystalline phase. This would mean that SP-B does not alter interactions between neighboring lipid molecules in a way which would significantly modify the chain packing. In particular, it would be difficult to reconcile these observations with the model [12] in which the amphipathic helical segments intercalate substantially into the bilayer head group region as shown in figure 3.10. If SP-B is to be accommodated into lipid bilayers according to this model, the acyl chains packing would have been disrupted and this would be reflected in first spectral moments data.

On the other hand, SP-B is found to affect deuteron transverse relaxation rate in both the liquid crystal and gel phases of these bilayer systems, showing that the protein has substantial influence on the slow bilayer motions. This would mean that this protein is strongly associated with the bilayer. One possibility which might be consistent with these observations is that the distribution of SP-B is uniform for larger length scales but displays some degree of self-association at shorter length scales. This would be the case, for example, if the SP-B associated to form boundaries around discs of relatively unperturbed lipid which then aggregate to form large sheets as illustrated in figure 3.11. An electron microscopy study showed that SP-B generated discoidal particles and structures that appeared to be sheets of lipid bilayer bounded by associated particles [51]. This is also in agreement with a study done on apolipoprotein [84], which indicates the

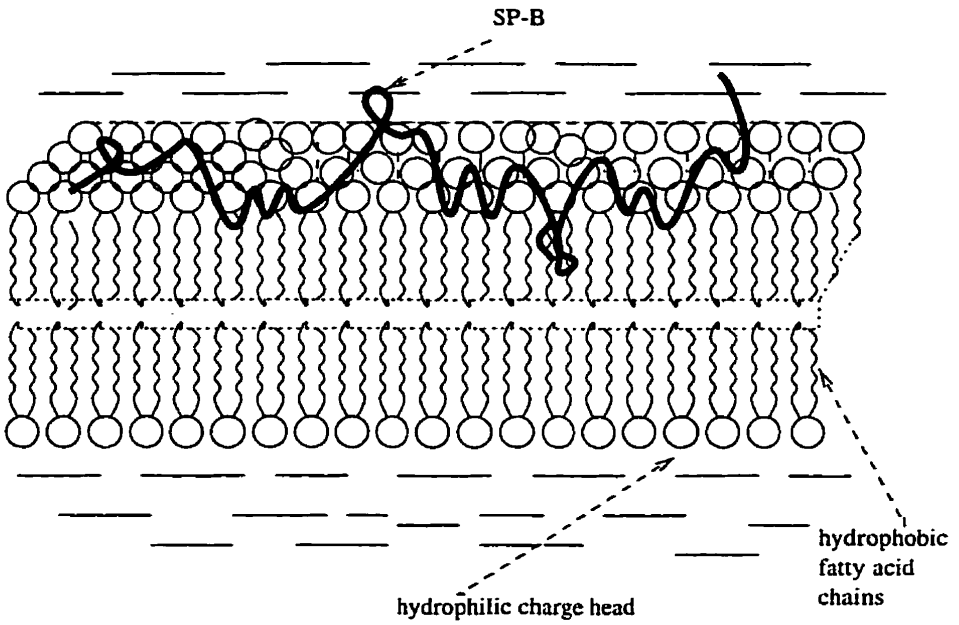

Figure 3.10: One of the proposed models for the secondary structure of SP-B in a lipid bilayer, where SP-B interacts by intercalating into the bilayer head groups. The observations in this work do not provide evidence for such a model.

formation of a ring of protein about the circumference of the single bilayer disc. These observations may give some clue of why SP-B is so important in the formation of square lattices of lipids (tubular myelin) in the pulmonary surfactant system.

For samples prepared using the formulation employed in this work, the effect of SP-B on bilayer lipid properties is found to be largely insensitive to the relative amounts of DPPC and DPPG. Furthermore, the effect of SP-B on DPPC/DPPG mixed bilayers, as indicated by above results, shows no evidence of specific interaction of SP-B with one or the other lipid components in the mixed lipid bilayer.

While SP-B has only a limited effect on mean chain order in the liquid crystal and gel phases, it does have some effect on the details of the ^{2}H-NMR spectral shape, particularly in the gel phase of the mixed lipid samples. The effect of SP-B on the width of the gel phase methyl deuteron spectral component is weaker in both DPPG-d_{62} and in

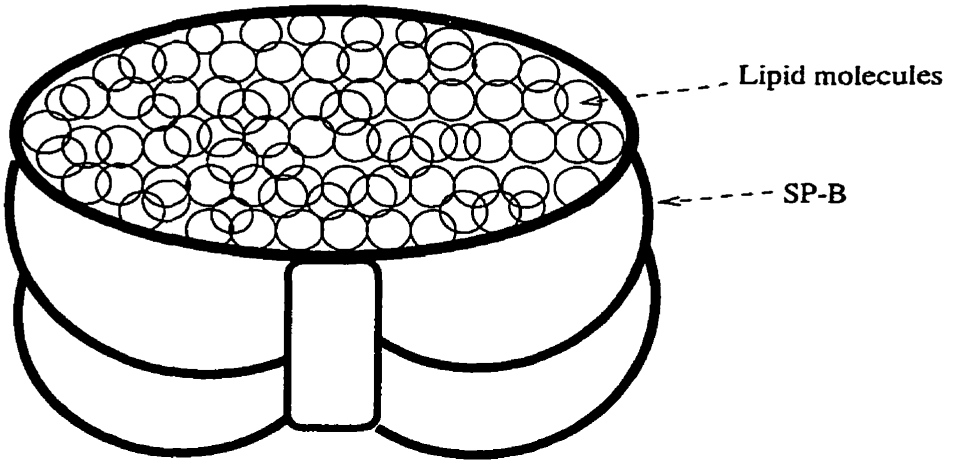

Figure 3.11: Proposed model for association of SP-B in lipid bilayer, where SP-B aggregates to form boundaries around lipid bilayer discs.

DPPC-d_{62} [54] than in the mixed lipid. This can be seen from figure 3.6, which shows gel phase spectra for pure and mixed bilayers with and without SP-B. The spectra close to and above the transition, for the mixed lipid bilayers with SP-B present, also show a narrow component which suggests that a small fraction of the sample may be reorienting isotropically. One intriguing possibility, suggested by the earlier observation of disc-like structures in bilayers containing SP-B, is that this enhanced intensity close to zero quadrupole splitting might indicate a small population of more freely reorienting bilayer fragments or disks as outlined above. Alternatively, if SP-B could associate into boundaries surrounding regions of lipid, this arrangement might provide a means for the amphipathic protein to slightly intercalate into the bilayer center, thus reducing methyl group ordering.

Chapter 4

Results and Discussion II: SP-C Effect on DPPC/DPPG Acyl Chains

4.1 Introduction

In the previous chapter, we saw the effects of hydrophobic pulmonary surfactant protein, SP-B, on the physical properties of pure DPPG and mixed DPPC/DPPG bilayers. In the work described in this chapter, effects of the other hydrophobic protein, SP-C, on these bilayer systems are investigated. The question of whether there is selectivity in the interaction between SP-C and DPPC or DPPG in the mixed lipid bilayers is also addressed. The effect of the ionic environment on this interaction is also examined. This is important because natural pulmonary surfactant contains a mixture of charged and neutral lipids in an aqueous environment containing Ca^{2+}. The Ca^{2+} level in the extracellular aqueous lining layer of lung alveoli is about 1.6 mM [85]. Monolayer studies show that the interaction of hydrophobic surfactant proteins with DPPG in spread monolayers is Ca^{2+} dependent [33, 86]. It is thus interesting to know if Ca^{2+} alters the way in which SP-C interacts with mixed lipid bilayers. In order to study these systematically and to

get some information of how this protein might function in the presence of Ca^{2+}, the interaction of SP-C with bilayers of mixed DPPC/DPPG with and without Ca^{2+} in the aqueous phase is studied. The sample preparation and the experimental conditions were as described in section 3.2 of the previous chapter. For the studies done with Ca^{2+}, the aqueous phase contained 5 mM $CaCl_2$. The choice of this concentration of Ca^{2+}, which is a bit higher than the Ca^{2+} level reported for the extracellular aqueous lining layer of lung alveoli [85], is to make sure that there is enough Ca^{2+} in the aqueous phase to bind to the lipid molecules.

4.2 Interaction of SP-C with pure DPPG and DPPC bilayers

The influence of SP-C on the orientational order and phase behaviour of pure DPPC and DPPG bilayers was examined. Figures 4.1 and 4.2 show, respectively, ^{2}H-NMR spectra for DPPG-d_{62} and DPPC-d_{62} with and without 10% (w/w) SP-C (approximately 47 lipid molecules per SP-C molecule). In the absence of SP-C, the DPPG-d_{62} main transition is lower than the DPPC-d_{62} transition by approximately 2°C. The phase transition of DPPG-d_{62} is between 35°C and 36°C while that of DPPC-d_{62} is between 37°C and 38°C. In both cases, the presence of SP-C has little effect on chain deuteron quadrupole splittings in the liquid crystalline phase. For both systems, SP-C induces coexistence of the liquid crystal and gel phases over a narrow temperature range just below the pure lipid main transition temperature.

Figure 4.3 shows first spectral moment (M_1) corresponding to the spectra shown in figures 4.1 and 4.2. These results illustrate, more quantitatively, the small broadening of the main transition by SP-C and the lack of any substantial perturbation of chain

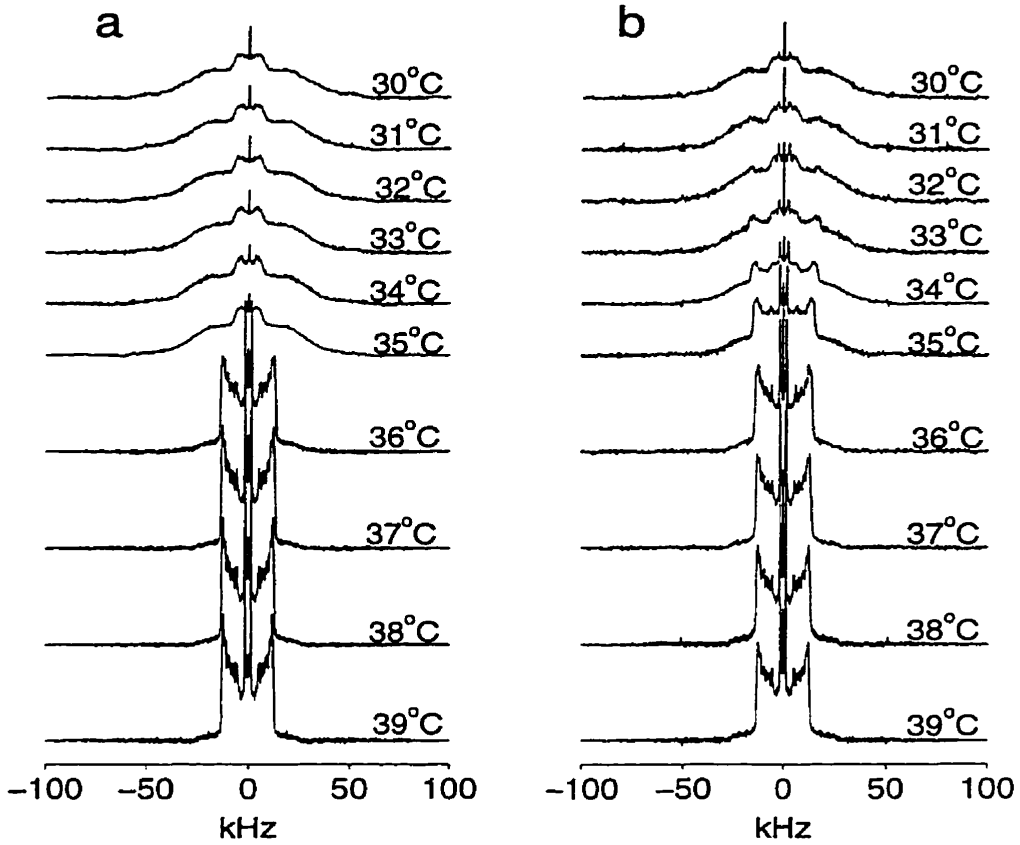

Figure 4.1: ^{2}H-NMR spectra at selected temperatures for (a) DPPG-d_{62} and (b) DPPG-d_{62} containing 10% porcine SP-C (w/w).

order in both DPPC and DPPG bilayers by SP-C. An earlier study also showed no perturbation of chain order in liquid crystalline DMPC-d_{54} by up to 8% (w/w) SP-C [50]. In the gel phase of DMPC-d_{54}, however, 8% (w/w) SP-C was found to reduce M_1. This difference may indicate that the interaction in the gel phase is more sensitive to the relative size of the protein and lipid components in the mixed bilayer or to the mismatch in hydrophobic regions of the components [87]. The absence of a significant effect of SP-C in the gel phases of DPPC and DPPG may indicate that there is little or no mismatch in hydrophobic parts of SP-C and DPPC or DPPG in the bilayer. Indeed,

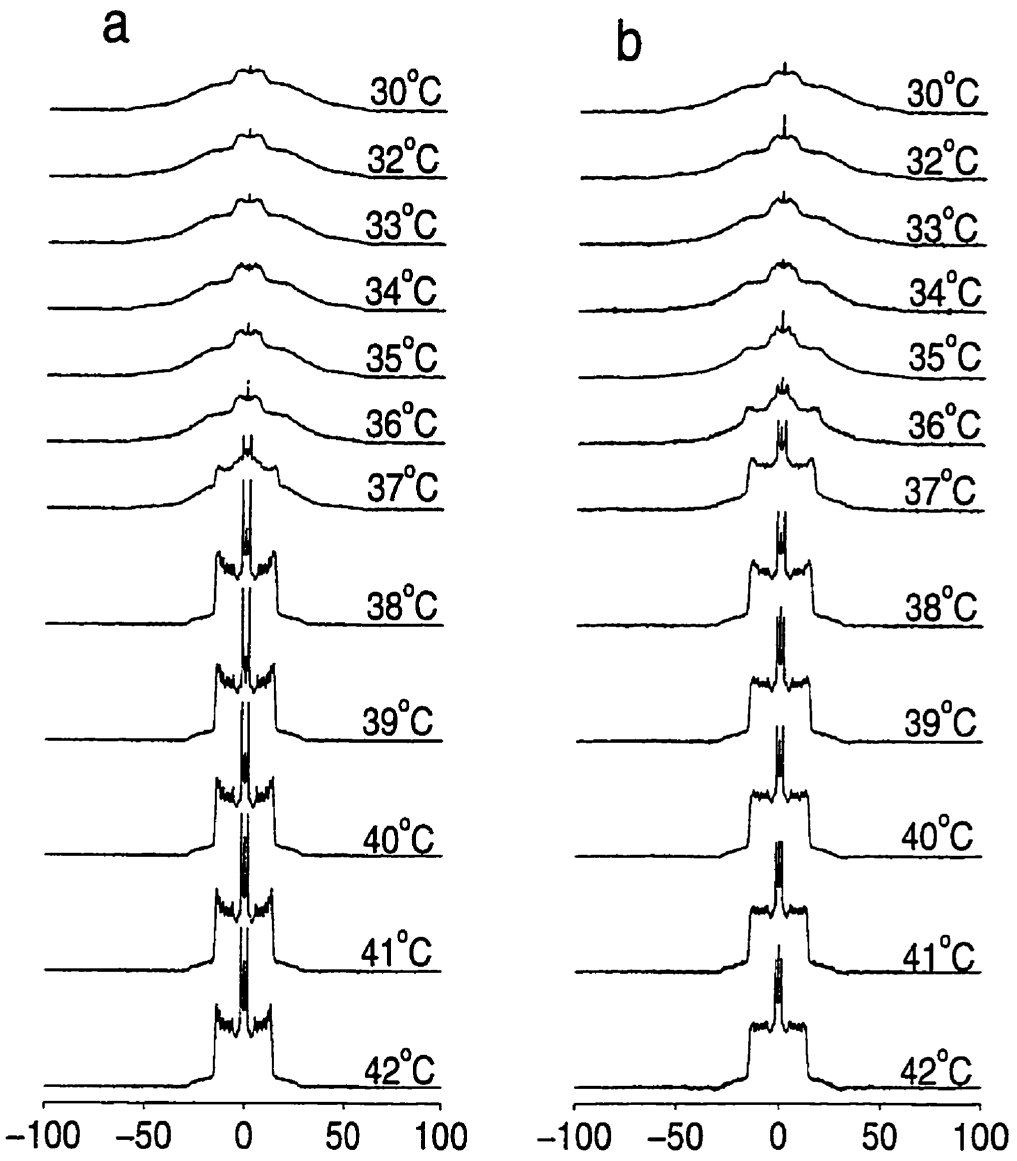

Figure 4.2: ^{2}H-NMR spectra at selected temperatures for (a) DPPC-d_{62} and (b) DPPC-d_{62} containing 10% porcine SP-C (w/w).

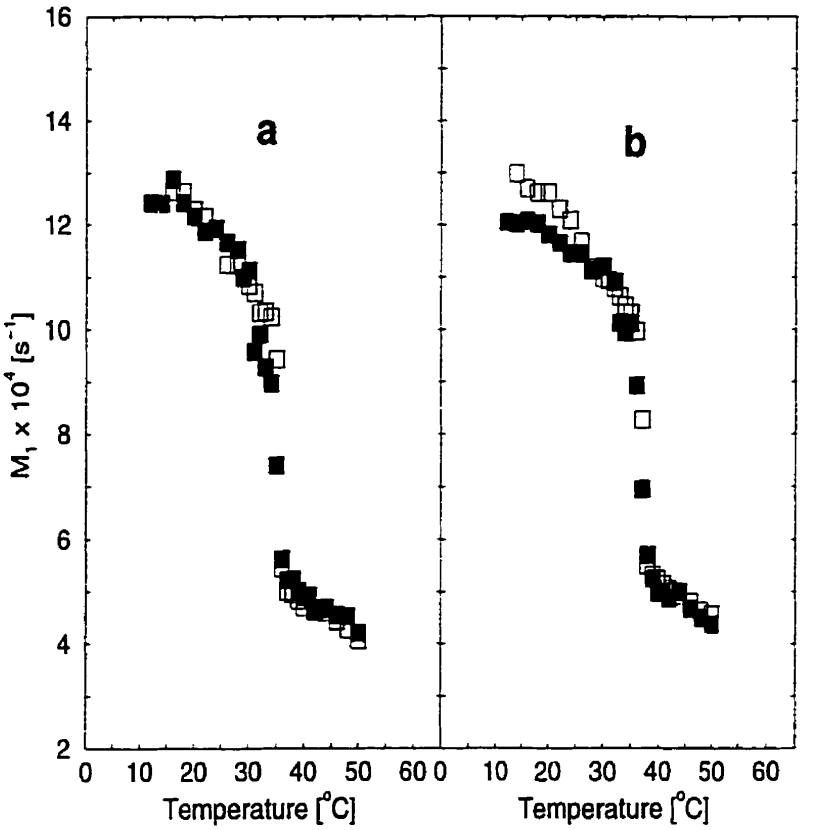

Figure 4.3: Temperature dependence of ^{2}H-NMR first spectral moments for (a) (□) DPPG-d_{62} and (■) DPPG-d_{62} plus 10% SP-C (w/w). (b) (□) DPPC-d_{62} and (■) DPPC-d_{62} plus 10% SP-C (w/w).

the length of the α-helix of SP-C is about 37 $\AA$ [56], while the width of the acyl chain region of PC bilayer is between 35 $\AA$ (in the liquid crystalline phase) and 45 $\AA$ (in the gel phase) [88]. Considering the similarity of the acyl chains of DPPC and DPPG, the observation that SP-C has a small but similar effect on the acyl chains of DPPC and DPPG in pure lipid bilayers is not surprising. Since we are looking at the acyl chains of these systems and since SP-C is a hydrophobic transbilayer protein, the interaction of this protein with DPPC or DPPG bilayer may be mostly hydrophobic in nature. The head group interaction might not be large enough to have significant influence on the

orientational order of the acyl chains and hence we observe a similar effect for both pure lipid bilayers. As presented below, however, the head group difference between these lipids may be enough to result in observable changes in orientational order of the acyl chains in mixed DPPC/DPPG bilayers.

4.3 SP-C in a mixed DPPC/DPPG bilayer

The M_1 results shown in figure 4.3 and discussed in the previous section suggest that the differences between the interactions of SP-C with DPPC-d_{62} and DPPG-d_{62} are not large enough to be apparent in the chain order of bilayers containing a single lipid species. In a bilayer containing a mixture of lipid species, however, it is conceivable that a small difference in the interactions might lead to a nonrandom distribution of bilayer components. To test this possibility, bilayers containing SP-C in a mixture of DPPC and DPPG, with one or the other lipid components deuterated, were examined.

Figure 4.4 shows ^{2}H-NMR spectra at selected temperatures for DPPC/DPPG-d_{62} (70:30) without SP-C and with 10% (w/w) and 15% (w/w) SP-C present. Concentrations of 10% and 15% SP-C (w/w) correspond, respectively, to about 47 and 30 lipid molecules per SP-C molecule in the mixture. Figure 4.5 shows ^{2}H-NMR spectra for analogous samples containing DPPC-d_{62}/DPPG (70:30). For both lipid mixtures, 10% (w/w) SP-C induces two phase coexistence over a narrow temperature range. With 15% (w/w) SP-C, the phase transition is less abrupt.

The observation that the superposition of liquid crystal and gel spectra, which would be characteristic of two-phase coexistence, is less apparent at high SP-C concentration may indicate a trend toward a more continuous phase transition. The effect of protein concentration on the phase behaviour of DPPC-d_{62} has been discussed by Morrow and Whitehead [89]. These authors used a Landau expansion of free energy in terms

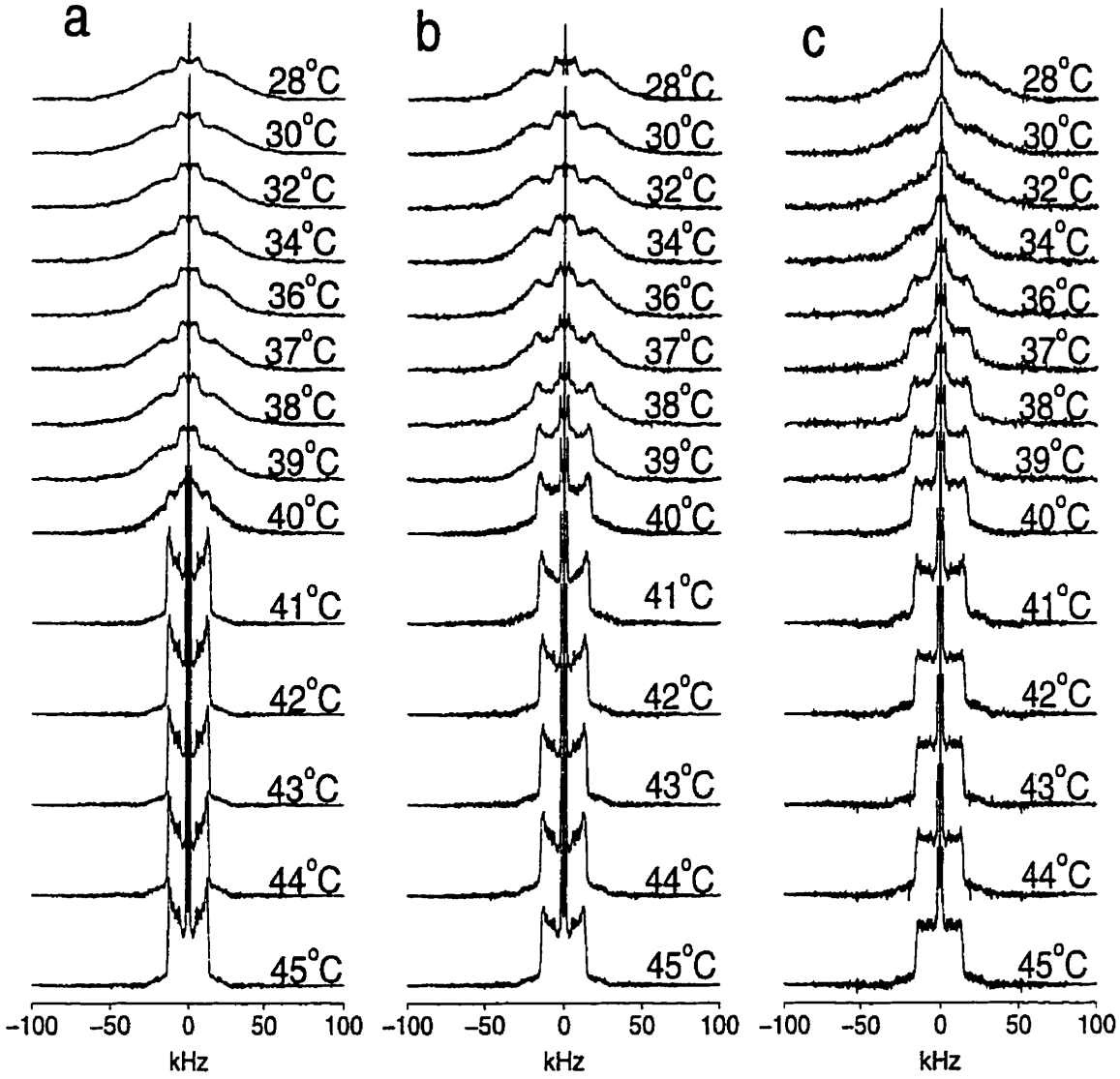

Figure 4.4: ^{2}H-NMR spectra at selected temperatures for (a) DPPC/DPPG-d_{62} , (b) DPPC/DPPG-d_{62} with 10% SP-C (w/w) and (c) DPPC/DPPG-d_{62} with 15% SP-C (w/w).

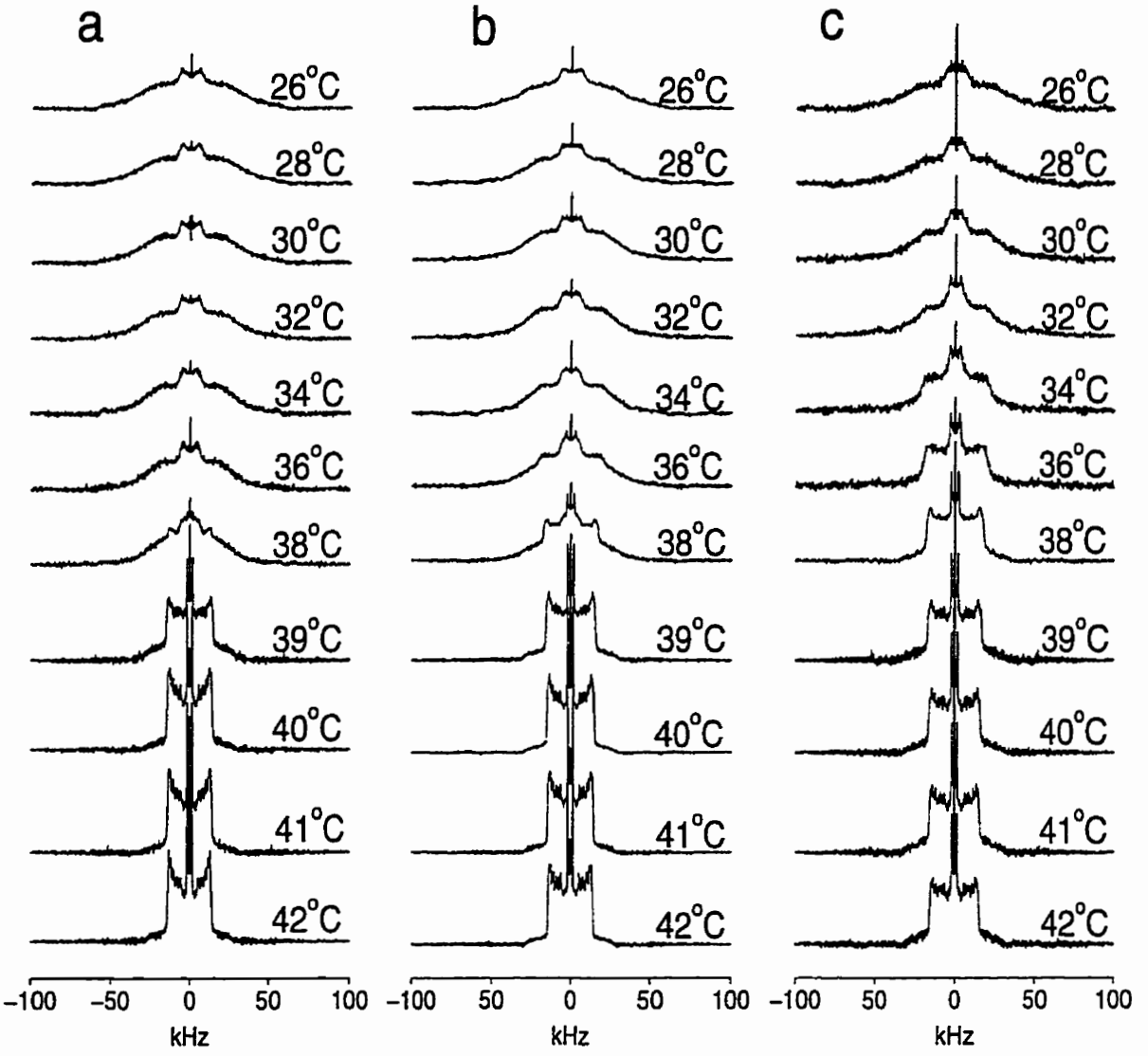

Figure 4.5: ^{2}H-NMR spectra at selected temperatures for (a) DPPC-d_{62}/DPPG (70:30), (b) DPPC-d_{62}/DPPG (70:30) with 10% SP-C (w/w) and (c) DPPC-d_{62}/DPPG (70:30) with 15% SP-C (w/w).

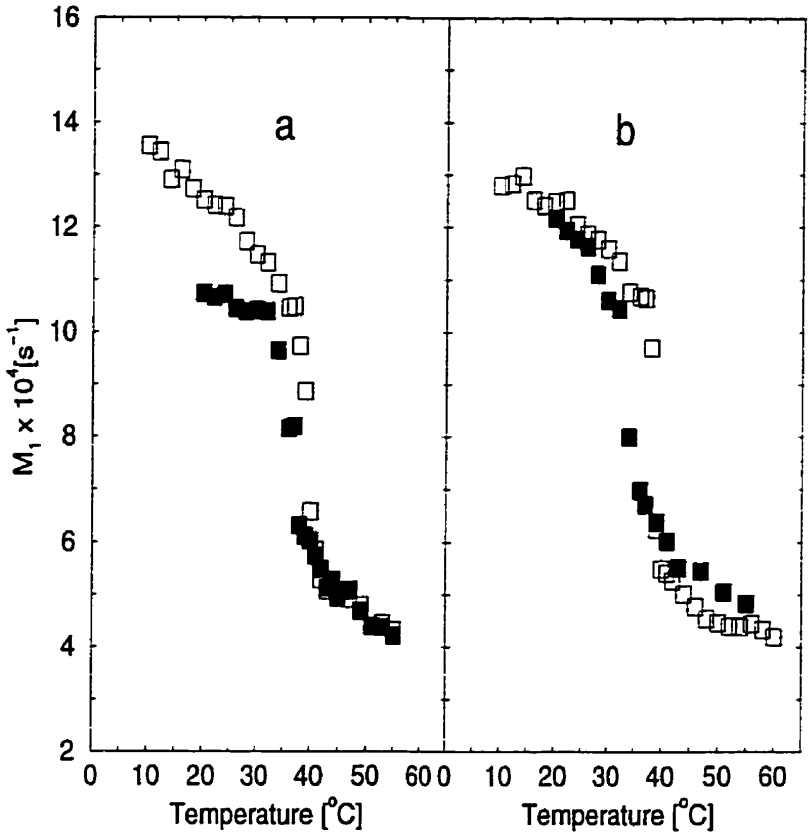

Figure 4.6: Temperature dependence of ^{2}H-NMR first spectral moments for (a) (□) DPPC/DPPG-d_{62} (70:30) and (■) DPPC/ DPPG-d_{62} (70:30) with 15% (w/w) SP-C, (b) (□) DPPC-d_{62}/DPPG (70:30) and (■) DPPC-d_{62}/DPPG (70:30) with 15% (w/w) SP-C.

of area per lipid and obtained a phase diagram for peptide-DPPC-d_{62} mixtures. Their results show the occurrence of a limiting peptide concentration beyond which two-phase coexistence may not be observed. As the peptide concentration approaches this threshold concentration, the phase transition is progressively replaced by a continuous phase change.

The first spectral moment, M_1, for both lipid compositions with and without 15% (w/w) SP-C are shown in figure 4.6. In the gel phase of the lipid mixture, SP-C appears

to have a larger effect on M_1 for the sample containing DPPG-d_{62} than for the sample containing DPPC-d_{62}. In the liquid crystalline phase, SP-C seems to have a slight ordering effect on DPPC-d_{62} but not on DPPG-d_{62} in the mixture. A similar result was obtained when this experiment was repeated with another sample prepared in the same way. As will be discussed later in this chapter, this may be due to a departure from random lateral distribution of the lipid components due to interaction with the protein.

4.4 Effect of Calcium on SP-C-mixed bilayer

The studies of SP-B-bilayer interaction described in chapter 3 and the studies of SP-C in mixed bilayers presented in the previous sections were carried out using a buffer containing no Ca^{2+}. This section describes how Ca^{2+} modifies the effect of SP-C on chain order and slow motions in PC/PG bilayers. At a pH of 7.0, SP-C carries a net positive charge and DPPG is negatively charged. The presence of Ca^{2+} in the pulmonary aqueous phase might thus influence the way in which SP-C interacts with a mixture of PC and PG in the lamellar bodies of pulmonary surfactant. To examine this possibility, the effects of SP-C on lipid order and dynamics in DPPC/DPPG-d_{62} (70:30) bilayers in the presence and absence of 5 mM Ca^{2+} are compared.

4.4.1 Effect of SP-C on mixed bilayer chain order in the presence of Ca^{2+}

Figure 4.7 shows ^{2}H-NMR spectra at selected temperatures for DPPC/DPPG-d_{62} (70:30) in the presence of 5 mM Ca^{2+} without SP-C and with 10% (w/w) SP-C. Comparison with the spectra shown in figure 4.4 indicates that the presence of Ca^{2+} shifts the transition temperature by about 6°C. For the same SP-C concentration, the temperature range

over which the gel and liquid crystal phase coexist is not significantly altered by the presence of Ca^{2+}. Figure 4.8 shows the temperature dependence of M_1 corresponding to the spectra in figure 4.7. The perturbation of DPPG-d_{62} by SP-C in the gel phase of DPPC/DPPG-d_{62} (70:30), as seen in figure 4.6(a), is largely removed in the presence of Ca^{2+}. The implication of this result is discussed in section 4.5 below.

4.4.2 Effect of SP-C on bilayer motions in the presence of Ca^{2+}

In the absence of Ca^{2+}, the presence of SP-C is found to have a significant effect on quadrupole echo decay rates in mixed DPPC/DPPG bilayers. Figure 4.9(a) shows the temperature dependence of T_{2e} for DPPC/DPPG-d_{62} and DPPC/DPPG-d_{62} plus 10% (w/w) SP-C in the absence of Ca^{2+}. As was found for SP-B, SP-C reduces transverse relaxation time in both gel and liquid crystalline phases. The T_{2e} data shown in figure 4.9(a) indicates that the influence of SP-C on the deuteron transverse relaxation rates in the lipid bilayer is similar to that of SP-B. This effect on T_{2e} seems to be common to proteins. Studies on other model systems [50, 90, 91] also show that proteins and polypeptides reduce T_{2e} in both the liquid crystal and gel phases. The addition of SP-C to bilayers of DMPC-d_{54} resulted in a similar effect on the transverse relaxation time [50]. This has also been observed when synthetic amphiphilic polypeptide is incorporated into specifically labeled phospholipid [91]. Branched-chain amphiphiles have been reported to similarly affect T_{2e} in the gel phase [92]. These and the present results suggest that the motions responsible for quadrupole echo decay display similar sensitivity to the presence of proteins, regardless of bilayer composition.

Figure 4.9(b) shows quadrupole echo decay times for DPPC/DPPG-d_{62} bilayers with and without SP-C and with Ca^{2+} present in the aqueous phase. In the absence of SP-C, the addition of 5 mM Ca^{2+} has a small effect on deuteron transverse relaxation in

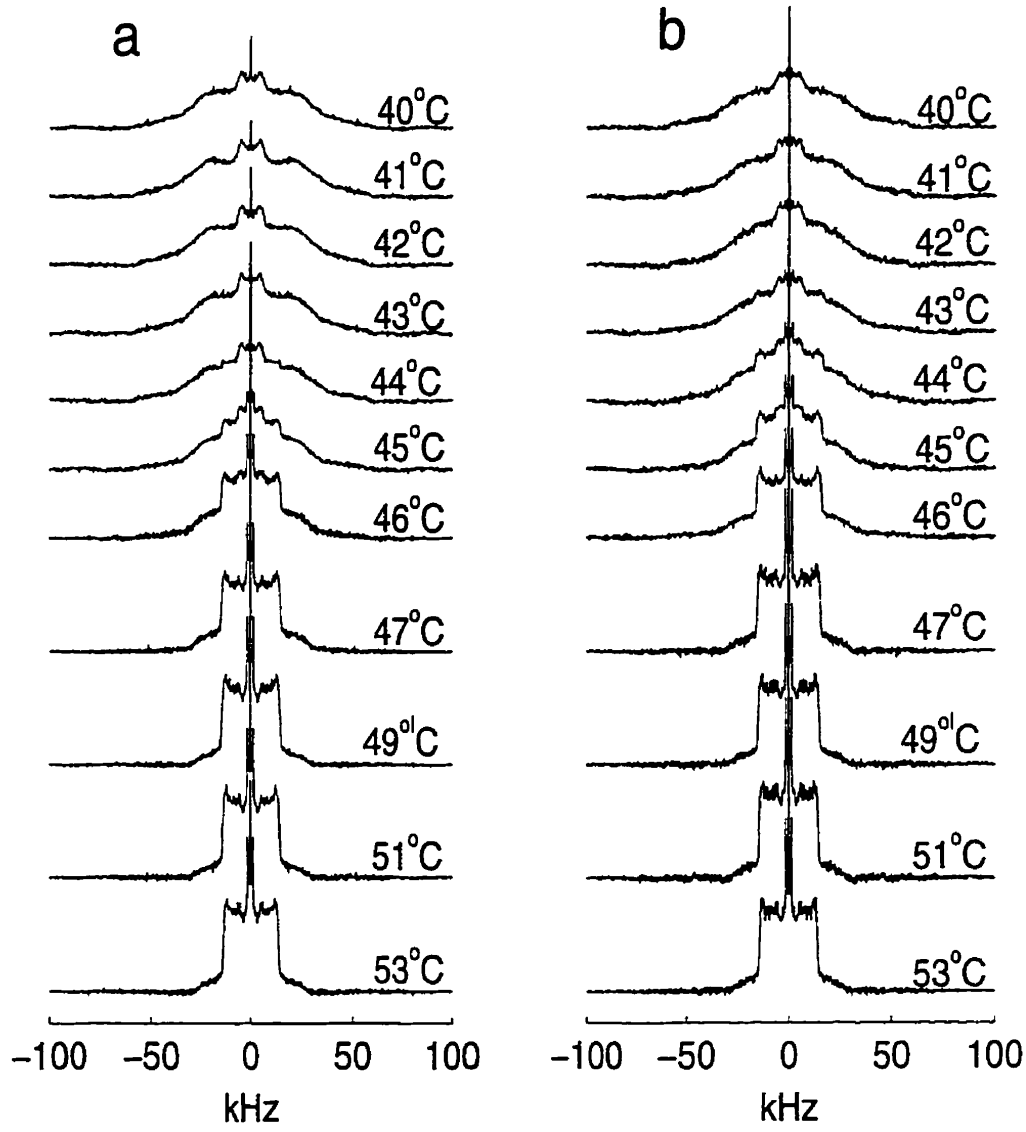

Figure 4.7: ^{2}H-NMR spectra at selected temperatures for (a) DPPC/DPPG-d_{62} (70:30) in the presence of 5 mM Ca^{2+} and (b) DPPC/DPPG-d_{62} with 10% (w/w) SP-C in the presence of 5 mM Ca^{2+}.

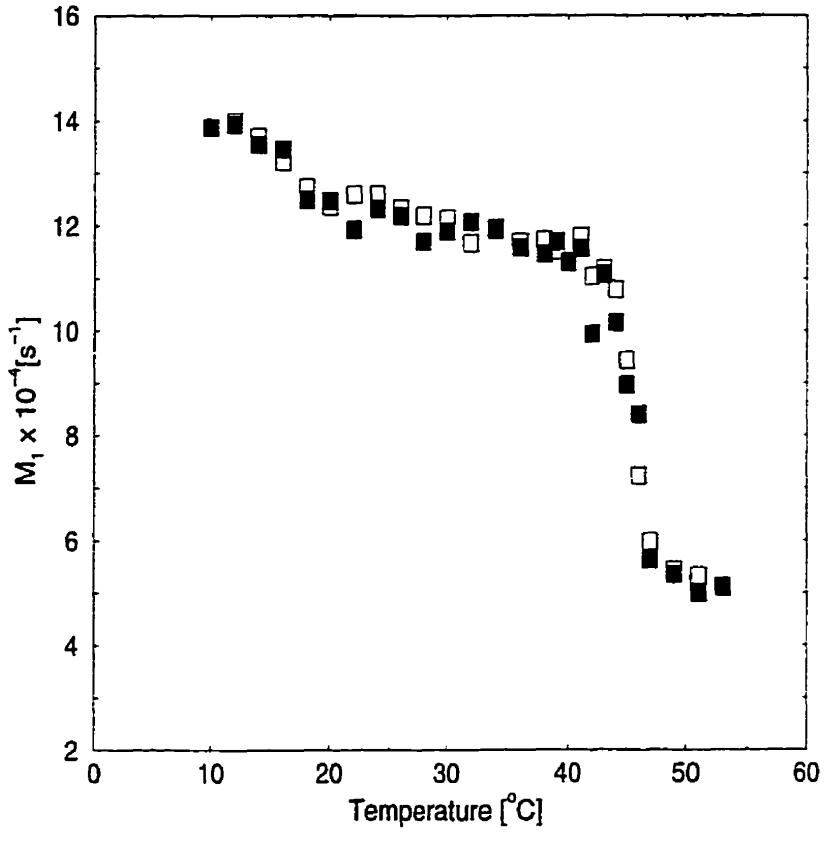

Figure 4.8: Temperature dependence of ^{2}H-NMR first spectral moments for (□) DPPC/DPPG-d_{62} (70:30) in the presence of 5 mM Ca^{2+} and (■) DPPC/DPPG-d_{62} (70:30) with 10% (w/w) SP-C in the presence of 5 mM Ca^{2+}.

the mixed lipid bilayer, but the qualitative picture is not altered. The samples with and without 5 mM Ca^{2+} both display T_{2c} values that start above 400 μs in the liquid crystalline phase and drop as temperature is lowered toward the transition. For both samples without SP-C, T_{2e} passes through a minimum at or just below the transition and then rises toward a maximum as the temperature is lowered into the gel phase region. Ca^{2+} seems to cause the gel phase bilayer motions to freeze-out faster as indicated by the rapid increase and decrease in T_{2e} with decreasing temperature below the main phase transition.

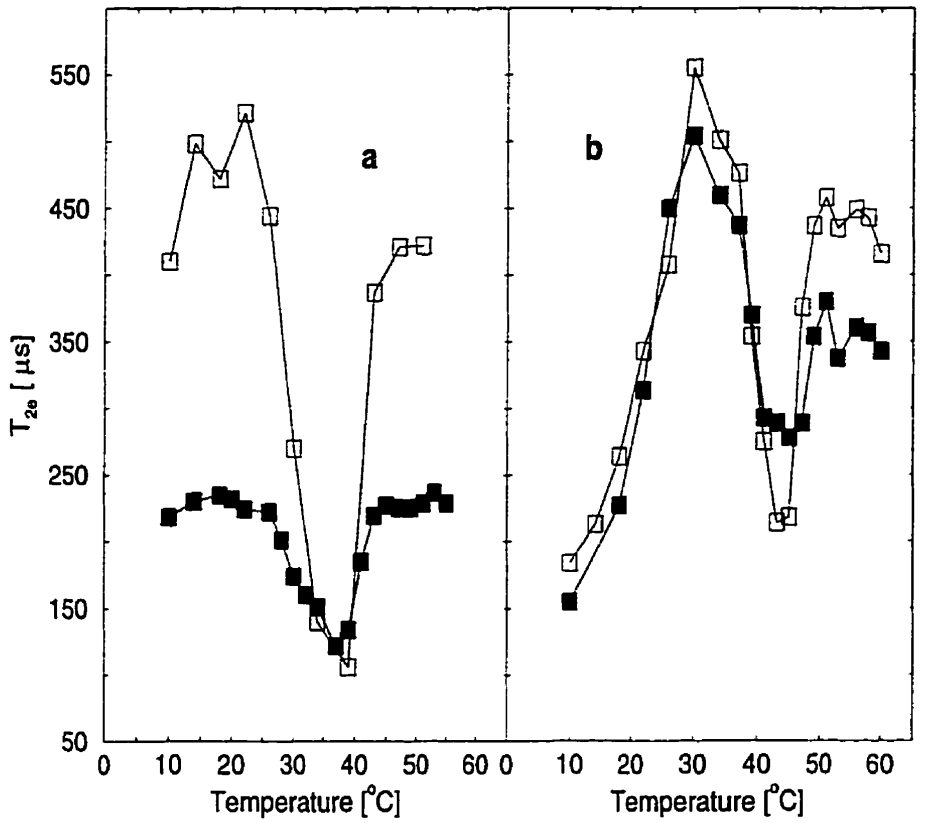

Figure 4.9: (a) Temperature dependence of T_{2e} for (□) DPPC/DPPG-d_{62} (70:30) and (■) DPPC/DPPG-d_{62} (70:30) with 10% (w/w) SP-C. (b)Temperature dependence of T_{2e} for (□) DPPC/DPPG-d_{62} (70:30) and (■) DPPC/DPPG-d_{62} (70:30) with 10% (w/w) SP-C in the presence of 5 mM Ca^{2+} in the aqueous phase.

For bilayers containing SP-C, the effect of SP-C on transverse relaxation depends strongly on whether Ca^{2+} is present or not. The presence of 5 mM Ca^{2+} in the aqueous phase substantially alters the way in which SP-C influences the motions responsible for transverse relaxation. By comparison of figures 4.9(a) and 4.9(b), in both the liquid crystal and gel phases, the presence of Ca^{2+} reduces the extent to which SP-C lowers T_{2e}. In the gel phase, Ca^{2+} appears to fully remove the ability of SP-C to influence transverse relaxation. The same result was obtained when the experiment was repeated

on another sample to check for the reproducibility of this result. The variation of the gel phase transverse relaxation rate with temperature proceeds as if there is no SP-C in the bilayer. It was discussed in the previous chapter that intermolecular (such as chain fluctuation and molecular rotations) and intra-molecular (such as trans-gauche isomerization) motions constitute the dominant relaxation process in the gel phase. The removal of the effect of SP-C on gel phase transverse relaxation may thus indicate that these motions are not affected by SP-C in the presence of Ca^{2+}.

The removal of the effect of SP-C on gel phase quadrupole echo decay may indicate the exclusion of SP-C from gel-phase domains and formation of SP-C aggregates in the presence of Ca^{2+}. The ability of SP-C to aggregate in the presence of gel-phase lipids was previously studied using fluorescence energy transfer [44]. It was found that the degree of SP-C self-association is high in the presence of gel-phase lipids and low when all lipids are in the liquid crystalline phase.

4.5 Summary and Discussion

Porcine pulmonary surfactant-associated protein SP-C has been found to have similar effects on the chain order and phase behaviour of DPPC-d_{62} and DPPG-d_{62} in bilayers containing a single lipid component. In both cases, SP-C broadened the transition slightly, but had little effect on chain order in the liquid crystalline phase. This broadening effect of SP-C has also been observed by other studies [40, 50].

In DPPC/DPPG (70:30) mixed bilayers with one or the other component deuterated, SP-C was found to have a stronger effect, in the gel phase, on DPPG than on DPPC. This may indicate that, in a mixture of PC and PG, it is possible for SP-C to associate preferentially with one or the other component and thus promote a nonrandom lateral distribution in the bilayer. The behaviour observed in the gel phase suggests a

significantly stronger perturbation of DPPG-d_{62} and thus, presumably, a higher effective concentration of SP-C in the neighborhood of DPPG molecules. The observed difference in the liquid crystalline phase is smaller and may not represent a significant preferential interaction of SP-C with liquid crystal phase DPPC. Another study using specific phospholipid spin probes in a liquid crystal DPPC matrix [53] also shows little selectivity of interaction between SP-C and various lipids, including PC and PG.

In mixed DPPC/DPPG bilayers, 10% (w/w) SP-C is found to induce two-phase coexistence near the main transition. For 15% (w/w) SP-C, however, the phase change was continuous and no two phase coexistence was observed. This suggests the presence of a threshold protein concentration beyond which two phase coexistence may not be observed.

SP-C was found to influence bilayer motions in both liquid crystalline and gel phases. The observed effect of this protein on the transverse relaxation rates is very similar to that observed for SP-B. Both proteins reduced the value of T_{2e} in the liquid crystalline phase. This suggested that both proteins decreased the correlation time of slow bilayer motions such as bilayer undulation, lateral diffusion and collective bilayer modes by shortening the wavelength of the undulation or increasing the bilayer curvature. In the gel phase, the reduction in T_{2e} indicates that these proteins interfere with the freezing out of motions that contribute to transverse relaxation in this phase.

In the presence of 5 mM Ca^{2+} in the buffer, SP-C was found to have no effect on the transverse relaxation and the first spectral moment in the gel phase of DPPC/DPPG (70:30) mixed bilayers. This removal of the effect of SP-C on bilayer properties by Ca^{2+} was again obtained when this experiment was repeated with another sample prepared in the same way. This is particularly surprising in light of the observation that Ca^{2+} does not significantly alter the properties of the bilayer in the absence of SP-C, except for a shift in the transition temperature. One possible explanation is that the interaction with

Ca^{2+}, which shifts the bilayer transition temperature, may also make it more difficult for SP-C to be accommodated in the mixed bilayer gel phase. Removal of the effect of SP-C on gel phase transverse relaxation and first spectral moment might thus reflect a Ca^{2+}-induced partial separation of bilayer components at the phase transition. It is interesting to note that the presence of Ca^{2+} in the aqueous phase has been observed to weaken the interaction between DPPG and SP-C in spread monolayers [33]. It is important to note that the concentration of Ca^{2+} in the water surrounding the bilayers changes as surfactant material moves from the type II cells into the aqueous environment in the alveoli. The observations reported here may thus be relevant to structural changes which occur in this process.

The observation that there is some selectivity of interaction between SP-C and PG in the gel phase may have consequences for bilayer rearrangement and the bilayer-to-monolayer transition in pulmonary surfactant *in situ*. It is a possibility that, during dynamic compression of the lung, SP-C might interact differently with PG and PG-like surfactant components in the pulmonary surfactant system and contribute to the removal of non-DPPC lipids from the monolayer.

Chapter 5

Results and Discussion III: SP-B Effect on DPPC Head group

5.1 Introduction

Chapters 3 and 4 discussed the effects of pulmonary surfactant proteins SP-B and SP-C on the hydrocarbon region of pure and mixed DPPC and DPPG bilayers. The focus of this chapter is on the interaction of SP-B with the DPPC head group region. ^{2}H-NMR of head group deuterated phosphatidylcholine (PC) has proved to be useful for studying the influence of external perturbations, such as electric charges, on the head group orientation. Surface charges appear to induce a conformational change in the PC head group, which is then reflected in the ^{2}H-NMR spectrum [93]. The phosphocholine P^--N^+ dipole is approximately parallel to the bilayer surface for a pure DPPC bilayer. The interaction between the P^--N^+ dipole and external perturbing surface charges causes the head group to tilt towards or away from the bilayer normal depending on the sign of the net surface charge. The head group tilts towards the water phase (towards the bilayer normal) in the presence of positive surface charges. In the presence of negative surface charges, the head group tilts towards the bilayer interior (away from bilayer

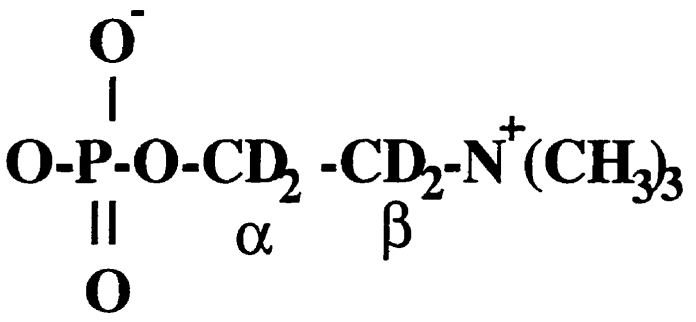

Figure 5.1: Structure of Phosphatidylcholine head group. D denotes deuterium.

normal). A tilt towards the water phase (towards the bilayer normal) causes the α-splitting to decrease and the β-splitting to increase, while a tilt towards the bilayer interior (away from the bilayer normal) results in opposite effects on α- and β-splittings. The α and β refer to the choline methylene groups nearest and next-nearest, respectively, to the phosphate group as shown in figure 5.1. Information about changes in head group orientation is thus obtained by studying changes in quadrupole splittings of α- and β-deuteron resonances. This has been used by many researchers to study the effect of cations and anions [93, 94, 95, 96], charged amphiphiles [97, 98, 99] and charged polypeptides and proteins [100, 101, 102] on lipid headgroup orientation.

The effect of SP-C on the DPPC head group was investigated previously in our laboratory [55]. It was demonstrated that the interaction of SP-C with the DPPC head group is primarily electrostatic in nature. At physiological pH, porcine SP-C has three positively charged side chains. The response of head group conformation to SP-C concentration was consistent with an interaction between the lipid head group dipole and the net positive surface charge associated with the protein.

Porcine SP-B has 9 positively charged and two negatively charged side chains at physiological pH. In this chapter, the interaction of this protein with dipalmitoylphosphatidylcholine deuterated at the α and β positions of the choline head group (DPPC-d_4) is discussed. The effect of high concentration of SP-B on chain perdeuterated DPPC

(DPPC-d_{62}) is also addressed. Sample preparation protocol and experimental conditions are as described in section 3.2 of chapter 3. The head group labeled DPPC was purchased from Avanti Polar lipids (Pelham, AL). The pulse spacing used to obtain the spectra is 55 μs. Pulse separation was varied from 55 μs to 400 μs for transverse relaxation measurements. Typical spectra were obtained by averaging 30,000 transients.

5.2 Interaction of SP-B with DPPC head group

Figure 5.2 shows ^{2}H NMR spectra for DPPC-d_4 without and with 5.7%, 8.6% and 17.3% SP-B (w/w) at selected temperatures. These concentrations of SP-B correspond, respectively, to about 399, 255, and 113 DPPC molecules per SP-B molecule. For DPPC-d_4 without and with 5.7% (w/w) SP-B, all spectra above 41°C, in the liquid crystalline phase, are a superposition of axially symmetric powder patterns. For SP-B concentration of 8.6% (w/w), the α-splittings are less sharp while the β-splittings can still be seen. This may indicate that the α-deuterons are more motionally restricted than β-deuterons at this SP-B concentration. Figure 5.2 shows that when the protein concentration is increased to 17.3% (w/w), the typical axially symmetric liquid crystalline phase powder patterns are not seen. The spectra indicate that the α and β C-^{2}H bonds do not undergo axially symmetric motion at this protein concentration.

In figure 5.3, the liquid crystalline spectra of figure 5.2 are expanded to show the variation of α- and β-splittings with temperature. The α-splittings were unaffected, while β-splittings decreased with increasing temperature for DPPC-d_4 without and with 5.7% (w/w) SP-B. For 8.6% (w/w) SP-B, the β-splittings are still observable and decrease with increasing temperature. For 17.3% (w/w) SP-B, the splittings are washed out showing the motional restriction at the α and β sites. In a recent study of DPPC-d_4 and DMPC-d_4 [103], the choline β-splitting was also observed to decrease with temperature, while

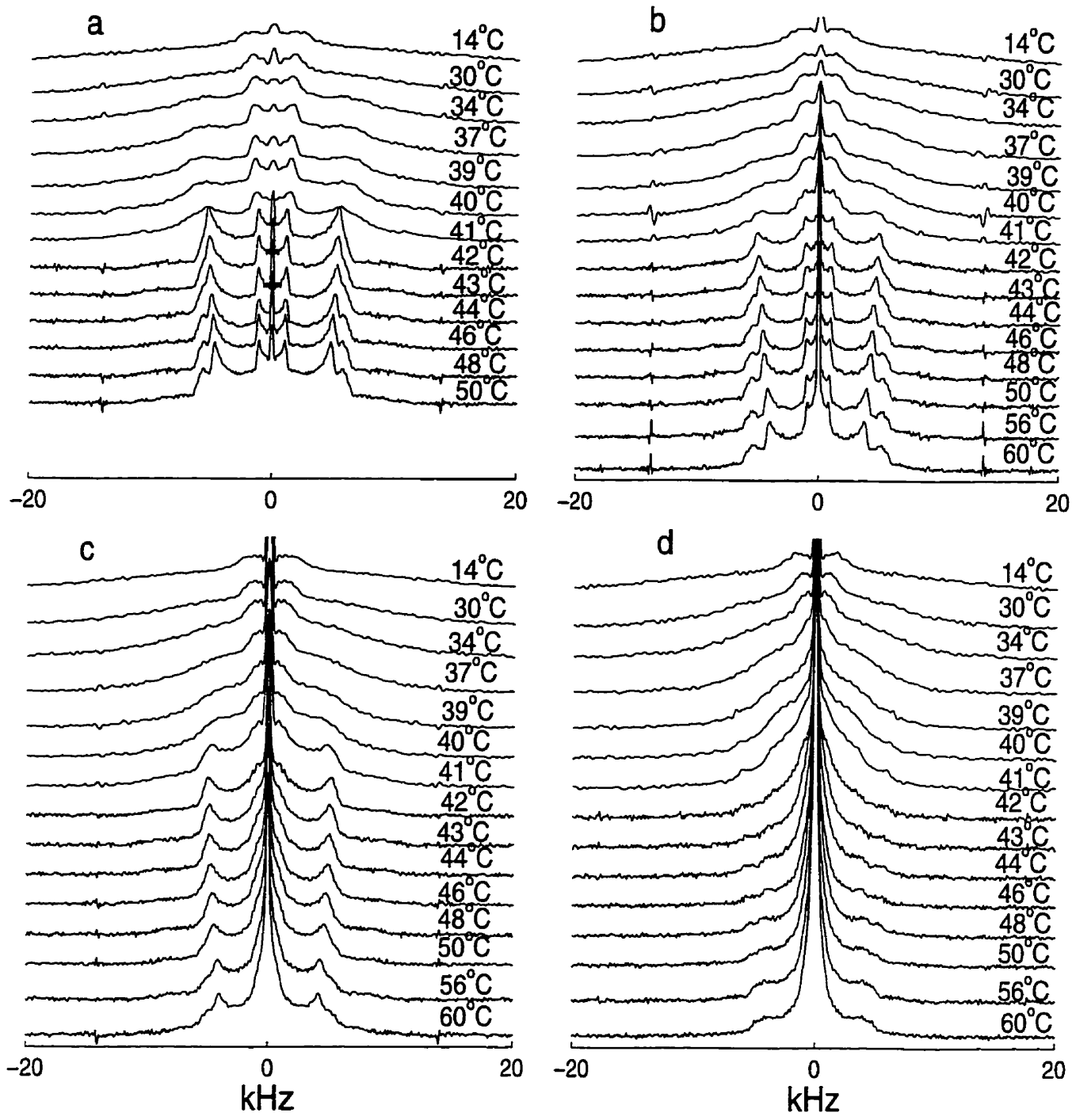

Figure 5.2: ^{2}H NMR spectra for DPPC-d_4 bilayer with (a) 0% SP-B (b) 5.7% SP-B, (c) 8.6% SP-B and (d) 17.3% SP-B.

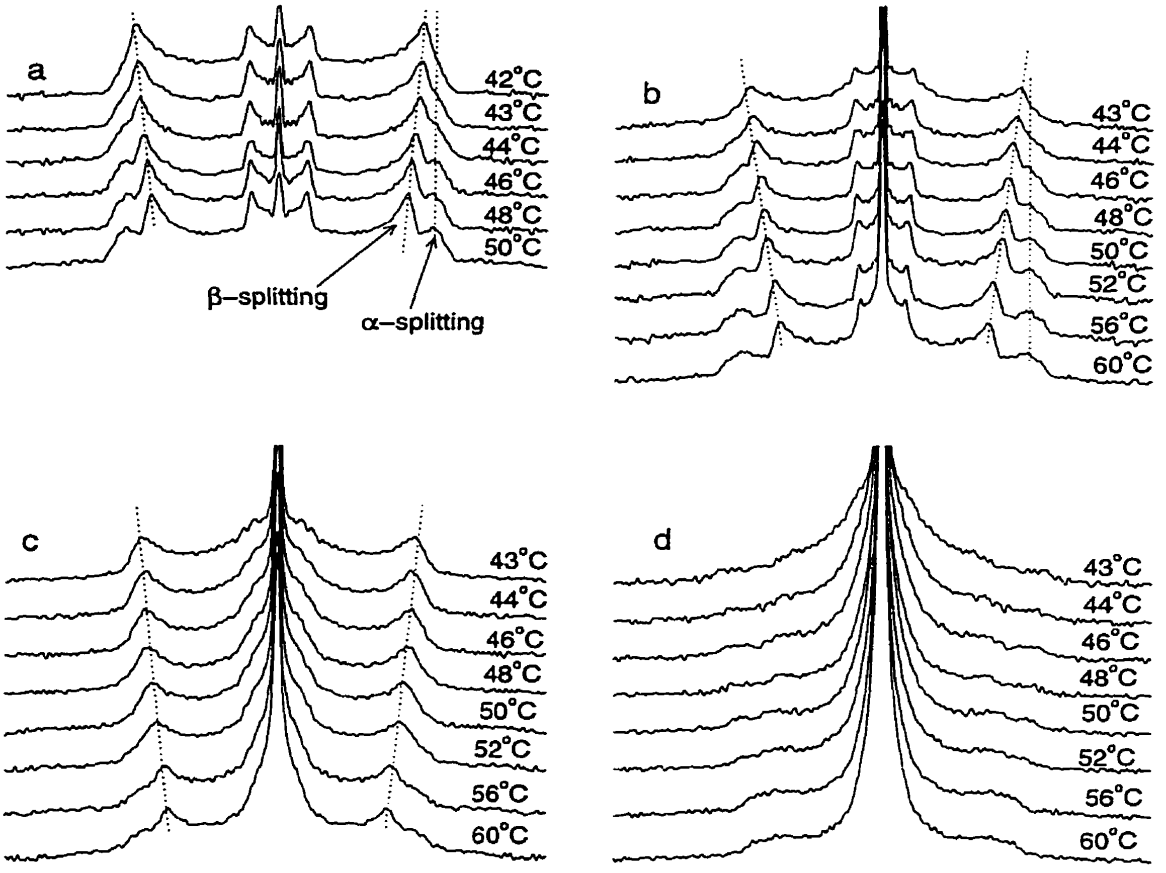

Figure 5.3: Expanded liquid crystalline ^{2}H NMR spectra showing α- and β-splittings for DPPC-d_4 with (a) 0% SP-B, (b) 5.7% SP-B (w/w), (c) 8.6% SP-B (w/w), and (d) 17.3% SP-B (w/w). The central doublet is assumed to arise from a partial deuteration of the choline methyl groups. The dashed lines are guides for the eye.

the α-splitting was unaffected. This difference in the response of α- and β-splittings to temperature is due to a combined effect of temperature induced changes in orientational order and area per lipid on head group orientation. An increase in temperature may result in an increase in area per lipid and a decrease in orientational order. A tilt of the head group towards the bilayer due to increased area per lipid would increase the α-splitting and decrease the β-splitting, while a decrease in orientational order would reduce both α- and β-splittings. For α deuterons, these two combined effects cancel each

other and the observed splittings were unaffected, while these effects are additive for β-splittings.

Figure 5.4 shows expanded ^{2}H NMR spectra and the corresponding dePaked spectra for DPPC-d_4 without and with 5.7%, 8.6% and 17.3% (w/w) SP-B. As protein concentration is increased, a reduction in α- and β-splittings is observed. The lines get broader as the concentration increases and disappear for 17.3% SP-B. As discussed above, β-splitting increases with increasing positive surface charge and decreases with increasing negative surface charge, while the α-splitting should show the opposite behaviour. According to this, assuming that the positive charges of SP-B are close to the bilayer surface, with increasing SP-B concentration (increasing net positive surface charges), the β-splitting is expected to increase. Figure 5.4 shows, however, a slight decrease in β-splitting instead. This suggests that the protein decreases the orientational order slightly which would reduce both α- and β-splittings. The presence of this disordering effect can also be seen from the first spectral moment data shown in figure 5.5. The effect of the orientational disorder at the β site on the splittings must dominate that of the charge interaction. The two effects are additive for α deuterons resulting in the observed decrease in the α-splitting.

Although the first spectral moment data shown in figure 5.5 can not be analyzed in detail for specific head group deuterons due to tilting effects, it reflects the decrease in mean quadrupole splitting with increasing SP-B concentration. Figure 5.6 shows ^{2}H transverse relaxation times for a pure DPPC-d_4 bilayer and for bilayers of DPPC-d_4 with different concentrations of SP-B. The α and β deuteron quadrupole echo decay rates are observed to increase with increasing SP-B concentration in both liquid crystalline and gel phases. The effect seems to be larger in the gel phase. Motions believed to be responsible for deuteron transverse relaxation in lipid bilayers are discussed in chapter 3. In the liquid crystalline phase, the effect of SP-B on the head group, like its effect

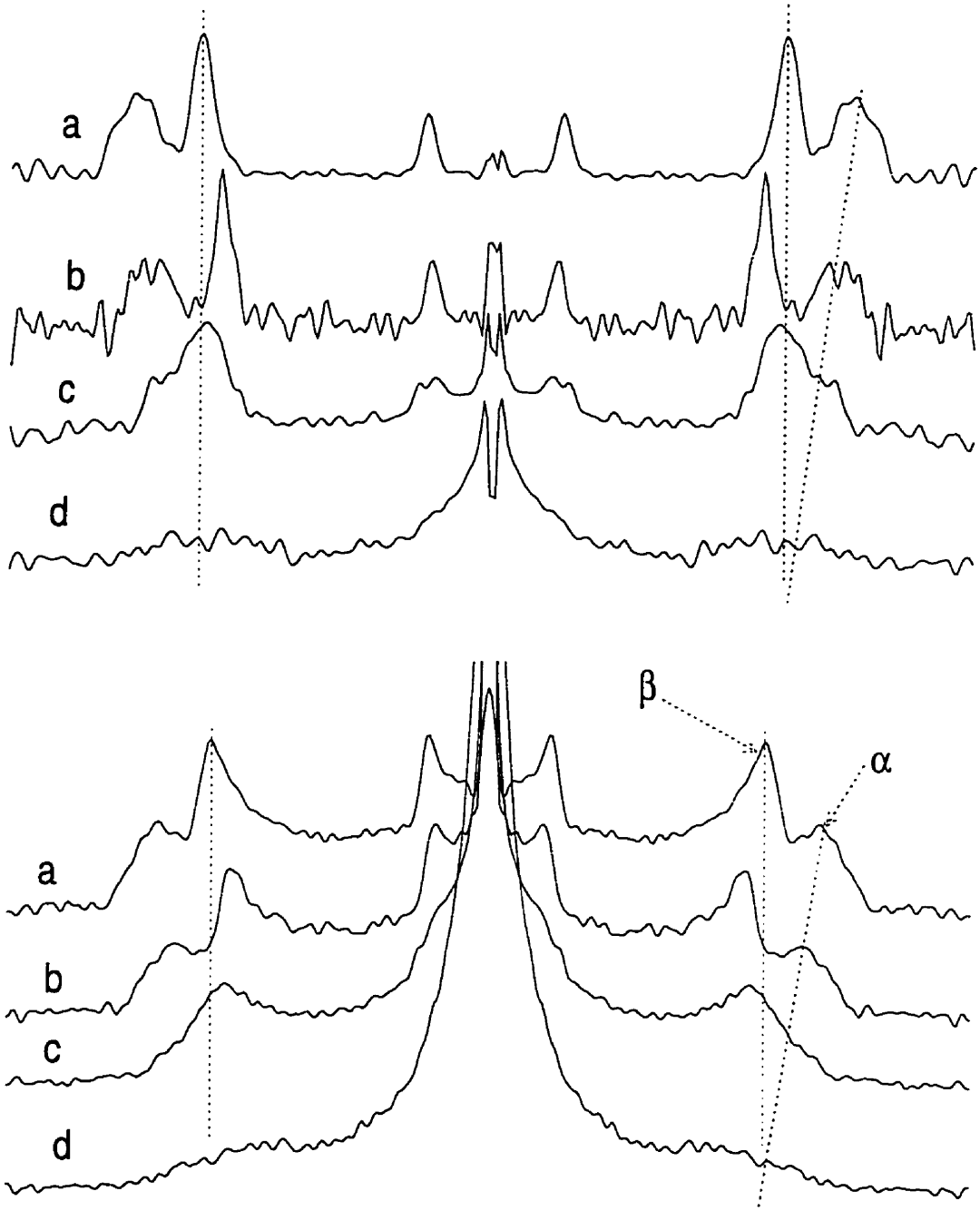

Figure 5.4: ^{2}H NMR expanded spectra (bottom) and same but dePaked spectra (top) at 50°C for DPPC-d_4 bilayer with (a) 0% SP-B (b) 5.7% SP-B, (c) 8.6% SP-B and (d) 17.3% SP-B. These spectra show the variation of α- and β-splittings with SP-B concentration. DePaking is done according to the method developed by Sternin *et al.* [81]. The dashed lines are guides for the eye.

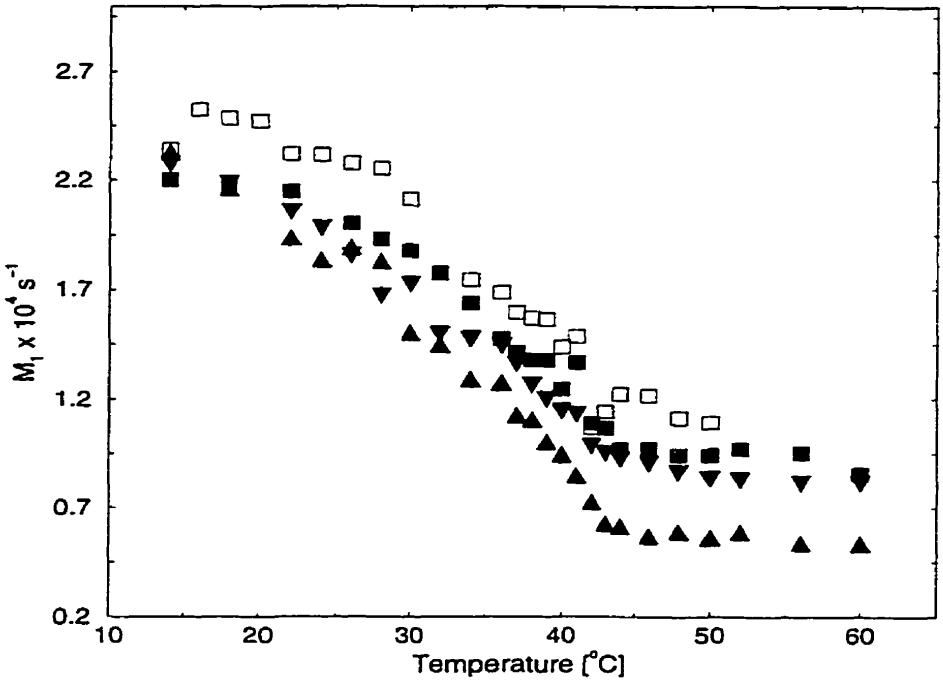

Figure 5.5: ^{2}H NMR first spectral moment (M_1) for DPPC-d_4 bilayer with 0% SP-B (□), 5.7% SP-B (■), 8.6% SP-B (▼), and 17.3% SP-B (▲)

on the hydrocarbon region, is to shorten the correlation times of slow bilayer motions. In the gel phase, SP-B interferes with the freezing-out of slow motions as discussed in chapter 3. Figure 5.6 also shows that as concentration increases, T_{2e} decreases for a given temperature indicating the effect of the protein concentration on the head group slow motions. It is interesting to note that the phase transition in DPPC-d_4 plus 17.3% (w/w) SP-B, even though not obvious from the spectra, can be seen in T_{2e} data.

The spectra shown in figure 5.2(d) for DPPC-d_4 plus 17.3% (w/w) SP-B show qualitatively the extent to which the axial symmetry of motion in the head group region is removed. In order to determine whether the protein-induced motional asymmetry observed for this SP-B concentration was specific to the head group region or common to both the head group and hydrocarbon regions, 15% (w/w) SP-B (about 142 DPPC

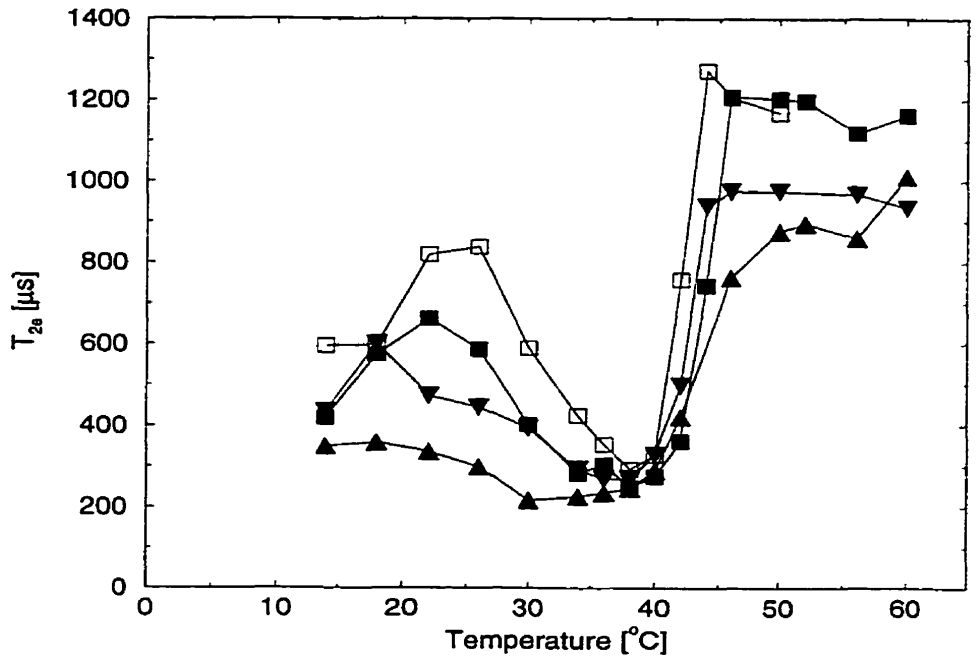

Figure 5.6: Effective transverse relaxation time (T_{2e}) for DPPC-d_4 bilayer with 0% SP-B (□), 5.7% SP-B (■), 8.6% SP-B (▼), and 17.3% SP-B (▲)

molecules per SP-B molecule) was incorporated into chain perdeuterated DPPC (DPPC-d_{62}). The ^{2}H-NMR spectra for this experiment are shown in figure 5.7. The spectra at higher temperatures in the liquid crystalline phase are not the axially symmetric powder patterns normally observed for chain perdeuterated DPPC-d_{62} in the liquid crystalline phase. Axial asymmetry is generally the case in the gel phase but is unusual in the liquid crystalline phase. This indicates a strong removal of axial symmetry of motion but not a strong change in amplitude since the splittings remain small. It is clear that the interaction of SP-B at high concentration with DPPC-d_4 is significantly different from that observed for transmembrane proteins such as SP-C. At a concentration of 30% (w/w), the transmembrane protein SP-C didn't cause much change in spectral features of DPPC-d_4 [55]. This difference may be due to the larger number of positively charged

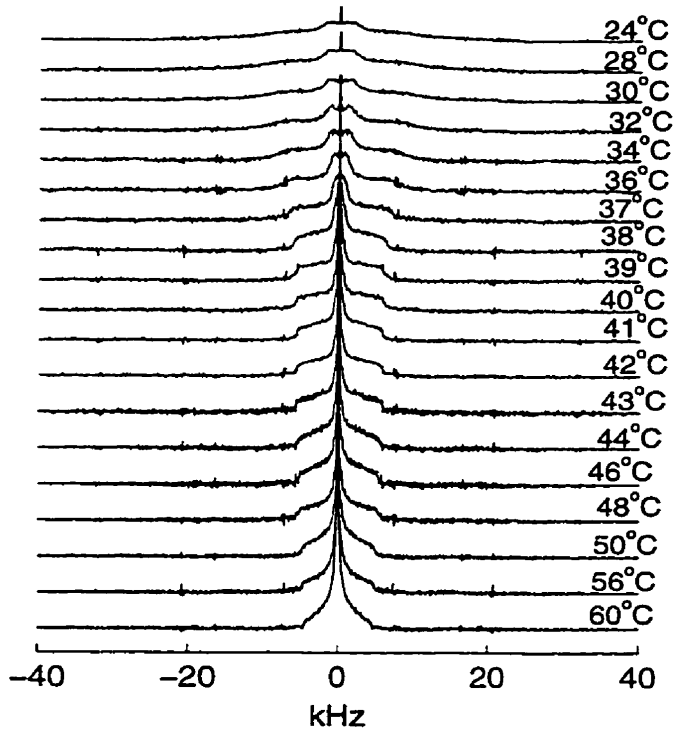

Figure 5.7: ^{2}H NMR spectra at selected temperatures for DPPC-d_{62} with 15% (w/w) SP-B.

residues of SP-B or due to the way these proteins are accommodated into the bilayer. It is clear however that SP-B is closely associated with the bilayer.

SP-B is not a transmembrane protein and yet it has a large effect on the acyl chains at this concentration. The explanation for this is not obvious, but the observed effect could be due to one or both of the following reasons. The surface charge interaction with the lipid head group dipoles may cause a restriction in reorientation of the lipid molecules. The second possibility could be that at large concentration the hydrophobic parts of SP-B may be somehow pushed into the acyl chain region of the bilayer and

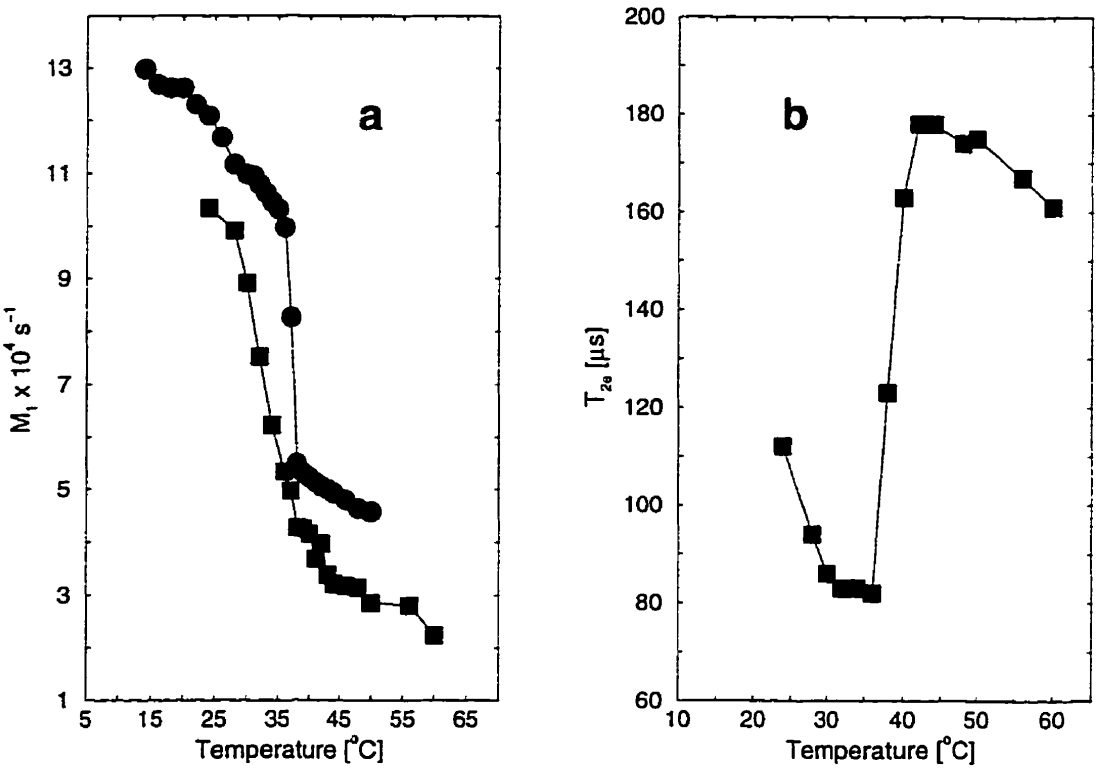

Figure 5.8: (a) ^{2}H NMR first spectral moment (M_1) for DPPC-d_{62} without (●) and with (■) 15% (w/w) SP-B. (b) Deuteron transverse relaxation time (T_{2e}) for DPPC-d_{62} plus 15% (w/w) SP-B.

interact with the lipid hydrophobic parts to induce the observed motional restriction. These observations suggest that SP-B may interact with the bilayer in two ways. This would be particularly interesting if influences other than concentration could also control the way in which SP-B interacts with the bilayer.

First spectral moment (M_1) values for pure DPPC-d_{62} and for DPPC-d_{62} plus 15% (w/w) SP-B are compared in figure 5.8(a). The liquid crystalline to gel phase transition temperature is slightly broadened by 15% (w/w) SP-B. At this SP-B concentration, the orientational order of the acyl chains of DPPC-d_{62} is reduced in both liquid crystal and

gel phases. In another study [54], the addition of 11% (w/w) SP-B did not have a large effect on orientational order in either the gel or liquid crystalline phases of DPPC-d_{62}. In this work, the effect of SP-B on chain order at 15% (w/w) concentration is thus larger than would be expected from extrapolation of results at lower SP-B concentration. Figure 5.8(b) shows T_{2e} data for DPPC-d_{62} plus 15% (w/w) SP-B. T_{2e} values for this sample are of the same order of magnitude as those observed for mixed DPPC-d_{62}/DPPG bilayer shown in figure 3.9 of chapter 3.

5.3 Summary

The effect of pulmonary surfactant SP-B on the DPPC head group is found to be concentration dependent. For pure DPPC-d_4 and DPPC-d_4 plus 5.7% (w/w) SP-B, the spectra in the liquid crystalline phase were superpositions of axially symmetric powder patterns indicating that, at this protein concentration, the motions in the liquid crystalline phase are axially symmetric. At this low concentration of SP-B, the β-splitting was observed to decrease with increasing temperature, while the α-splitting was unaffected. This indicates the presence of counter-acting effects which tend to influence the α- and β-splittings in such a way that changes cancel for α-splitting and are reinforced for β-splitting. These temperature induced effects are a tilt in head group (due to increased area per lipid) and a decrease in methylene orientational order.

Decreases in α- and β-splittings were observed with increasing SP-B concentration. Considering that SP-B introduces net positive charge to the bilayer surface, if the protein interaction with the head group is purely electrostatic, the β-splitting is expected to increase. The decrease in β-splitting with increasing SP-B concentration (increasing positive charge) thus indicates the presence of other interaction which affects the β-splitting in opposite sense to the charge interaction. This interaction might be hydrophobic in

nature and occurs in the bilayer interior.

As SP-B concentration is increased, spectral features in the liquid crystalline phase show more asymmetry. Highly asymmetric spectra were observed at 17.3% (w/w) SP-B, showing the large motional restriction induced by SP-B at the head group region. This effect was not observed by the presence of 30% (w/w) SP-C in DPPC-d_4 bilayer [54]. This may suggest that SP-B has a larger influence than SP-C on the physical properties of the head group for these concentrations.

The effect of 17.3% (w/w) SP-B is not only in the head group region. At 15% (w/w) concentration SP-B also induced motional asymmetry in the acyl chains region as indicated by the asymmetric ^{2}H-NMR spectra observed for chain perdeuterated DPPC (DPPC-d_{62}) plus 15% (w/w) SP-B. This indicates that SP-B at higher concentration affects both the head group and acyl chain regions and suggests that SP-B may interact with the bilayer in two ways. The presence of charges on SP-B near the bilayer surface may result in an interaction which restricts molecular reorientation. At the same time, due to its hydrophobicity and higher concentration, SP-B at this concentration may interfere with the acyl chains reorientation causing motional asymmetry in the interior of the bilayer.

Chapter 6

Summary and Concluding Remarks

Interactions of the two important hydrophobic pulmonary surfactant proteins SP-B and SP-C with model membranes were studied by using ^{2}H-NMR spectroscopy. These model membranes include multilamellar vesicles of DPPC-d_{62}, DPPG-d_{62}, mixed DPPC-d_{62}/DPPG (70:30 w/w), mixed DPPC/DPPG-d_{62} (70:30 w/w) and DPPC-d_4.

When incorporated into pure DPPC-d_{62} or pure DPPG-d_{62} bilayer, both SP-B and SP-C were found to broaden the main phase transition without significant effect on acyl chain order in both the liquid crystalline and gel phases. SP-B slightly increased the main phase transition temperature, while SP-C lowered it.

The investigation of the effect of SP-B on DPPC/DPPG mixed bilayers showed no evidence of specific interaction with DPPC or DPPG in the mixed bilayer. SP-C was found to affect lipid acyl chain order in the gel phase of mixed DPPC/DPPG-d_{62} (70:30 w/w) bilayer, suggesting a preferential selectivity of this protein to the anionic lipid DPPG in the mixed lipid bilayer.

Two-phase coexistence at the transition was observed in the presence of 11% (w/w) SP-B in the mixed DPPC/DPPG bilayer. No two-phase coexistence was seen for 15% SP-B. This suggests the occurrence of a threshold SP-B concentration beyond which two-phase coexistence may not be observed. A similar effect was observed for 10% and 15% (w/w) SP-C. 10% SP-C induced two-phase coexistence, while for 15% SP-C the

transition proceeded continuously without showing two-phase coexistence.

Dynamics in the pure DPPG and mixed DPPC/DPPG bilayers were studied by quadrupole echo decay time measurements. The effects of SP-B and SP-C on the dynamics of these bilayers were also investigated. For lipid bilayers without SP-B or SP-C, the deuteron transverse relaxation time was found to display a minimum just below the main phase transition and a maximum in the gel phase as the temperature was varied. Both SP-B and SP-C were found to affect the quadrupole echo decay rates in both liquid crystalline and gel phases of pure DPPG and mixed DPPC/DPPG (70:30 w/w) bilayers. This indicated that these proteins have a large influence on the slow bilayer motions which modulate the quadrupole interaction and result in echo decay. These motions include bilayer surface undulations, collective lipid motions, diffusion along a curved bilayer surface, molecular rotations, chain fluctuations and *trans-gauche* isomerization motions. The surface undulation, collective motions and diffusion are largely responsible for the quadrupole echo decay in the liquid crystalline phase, while the remaining motions influence the echo decay in the gel phase. At the phase transition all motions may coexist and have maximum effect on the echo amplitude as indicated by the minimum (maximum) transverse relaxation time (rate) observed near the main phase transition. The effect of SP-B or SP-C is thus to shorten the correlation times of the slow motions in the liquid crystalline phase and to interfere with the freezing-out of the motions in the gel phase.

Since the pulmonary surfactant system contains lipid and protein mixtures in a calcium containing environment, the interaction of SP-C with mixed DPPC/DPPG bilayer in the presence of 5 mM $CaCl_2$ in the aqueous phase was examined. In the presence of Ca^{2+}, SP-C was found to have no effect on acyl chain order and deuteron transverse relaxation rates in the gel phase. The removal of the effect of SP-C by Ca^{2+} may indicate a Ca^{2+}-induced partial separation of bilayer components at the phase transition.

SP-B is a hydrophobic protein with many positively charged side chain residues. The

observation that SP-B has little or no effect on acyl chain order may suggest that the interaction of this protein with the bilayer is mainly in the head group region at least for low SP-B concentration. This was studied by investigating the interaction of SP-B with the head group deuterated DPPC (DPPC-d_4). The effect of SP-B on the head group physical properties was found to be concentration dependent. At a concentration of 17.3% (w/w), SP-B was found to induce motional asymmetry in the head group region as indicated by asymmetric liquid crystalline ^{2}H-NMR spectra observed for DPPC-d_4 plus 17.3% (w/w) SP-B. This effect is not specific to the head group region of the bilayer. When 15% (w/w) SP-B was incorporated into chain perdeuterated DPPC (DPPC-d_{62}), unusual asymmetric liquid crystalline phase ^{2}H-NMR spectra were observed. This effect of SP-B is not fully understood and requires further studies. The results, however, suggest that SP-B may interact with the bilayer in two different ways. One mode of interaction is primarily at the head group region while the other affects motions of the whole molecule and is seen in our experiments only at high SP-B concentration.

The α and β-splittings were found to decrease with increasing SP-B concentration. Normally, β-splitting increases with increasing positive surface charge which causes the head group to tilt away from the bilayer surface. This observation that the β-splitting reduced with increasing SP-B concentration (increasing positive surface charges) thus suggests the interaction is not purely electrostatic in nature. This result and the observation that SP-B induced motional asymmetry in both head group and hydrocarbon regions indicate the importance of the hydrophobic interaction in these systems at high concentrations of SP-B.

The results described in this work may give some insight into how the surfactant proteins might be accommodated in the bilayer. The secondary structure of SP-B in lipid bilayers is not yet fully elucidated. The results of this work argue against the models in which the amphipathic helical segments intercalate substantially into the bilayer head

group region at low concentration, while it may be more consistent with a model in which SP-B molecules form boundaries around discs of relatively unperturbed lipid molecules. The results obtained for SP-C are consistent with the α-helical bilayer-spanning property of the protein. The observation that SP-C shows some selectivity in interaction in DPPG/DPPC in the gel phase may have consequences for bilayer rearrangement and bilayer-to-monolayer transformation in pulmonary surfactant system *in situ*. The observations that calcium modifies the way SP-C interacts with mixed lipid bilayer may also have a consequence in pulmonary surfactant system *in situ*. This and the results discussed above may be relevant to structural changes that take place during surfactant transformations from type II cells to the air-water interface at the alveolar surface.

The effect of the interaction of both SP-B and SP-C, when they coexist in the mixed lipid bilayers, was not addressed in this work. It would be interesting to study how the observations described in this work might be modified when the two proteins coexist in the mixed lipid bilayer. A future systematic study of these systems is required in order to fully understand some of the physical properties of pulmonary surfactant system. The natural pulmonary surfactant is a very complex system consisting of both saturated and unsaturated lipids, cholesterol, hydrophilic proteins and highly hydrophobic proteins. This work provides a contribution towards the eventual understanding of this complex system and gives information of how the hydrophobic proteins might interact with lipid bilayers of tubular myelin *in situ*. This work, thus, lays the foundation for future studies of the pulmonary surfactant system using ^{2}H-NMR techniques.

Bibliography

[1] L. Marin, in *Pulmonary Surfactant: Biochemical, Functional, Regulatory and Clinical Concepts*, (J. R. Bourbon, Eds.), CRC Press, Boca Raton, (1991) pp 15-36.

[2] M. Dehan, J. Francoual, M. C. Imbert, and B. Denizot, in *Pulmonary Surfactant: Biochemical, Functional, Regulatory and Clinical Concepts*, (J. R. Bourbon, Eds.), CRC Press, Boca Raton, (1991) pp 333-358.

[3] K. M. W. Keough, in *Pulmonary Surfactant, from molecular biology to clinical practice*, (B. Robertson, L. M. G. Van Golde, and J. J. Batenburg, Eds.), Elsevier, Amsterdam, (1992) pp 109-163.

[4] J. M. Synder, J. M. Johanson, and C. R. Mendelson, *Cell Tissue Res.*, **220**, 17 (1981)

[5] J. R. Bourbon, in *Pulmonary Surfactant: Biochemical, Functional, Regulatory and Clinical Concepts*, (J. R. Bourbon, Eds.), CRC Press, Boca Raton, (1991) pp 143-183.

[6] M. C. Williams, *J. Cell Biol.* , **72**, 260 (1977).

[7] M. C. Williams, *Exp. Lung Res.*, **4**, 37 (1982).

[8] T. Akino, in *Pulmonary Surfactant: from Molecular Biology to Clinical Practice* (B. Robertson, L. M. G. Van Golde, and J. J. Batenburg, Eds.), Elsevier, Amsterdam, (1992) pp 19-31.

[9] F. Possmayer, *Am. Res. Respir. Dis.* , **138**, 990-998 (1988).

[10] J. A. Whitsett and T. E. Weaver, in *Pulmonary Surfactant: Biochemical, Functional, Regulatory and Clinical Concepts*, (J. R. Bourbon, Eds.), CRC Press, Boca Raton, (1991) pp 77-104.

[11] J. M. Synder, in *Pulmonary Surfactant: Biochemical, Functional, Regulatory and Clinical Concepts*, (J. R. Bourbon, Eds.), CRC Press, Boca Raton, (1991) pp 105-126.

[12] T. E. Weaver, and J. A. Whitsett, *Biochem. J.*, **273**, 249-264 (1991).

[13] T. Voss, H. Eistetter, K. P. Shafer, J. Engel, *J. Mol. Biol.* **201**, 219 (1988)

[14] A. Persson, D. Chang, and E. Crouch, *J. Biol. Chem.*, **265**, 5755 (1990)

[15] J. Johansson, T. Curstedt, and B. Robertson, *Eur. Respir. J.*, **7**, 372-391 (1994).

[16] T. Curstedt, J. Johansson, and J. B Soderling, *Eur. J. Biochem.* , **172**, 521-525 (1988).

[17] J. Johansson, T. Curstedt, and H. Jonvall, *Biochemistry*, **30**, 6917-6921 (1991).

[18] T. Curstedt, J. Johansson, P. Persson, A. Eklund, B. Robertson, B. Lowenadler, and H. Jornvall, *Biochemistry*, **87**, 2985-2989 (1990).

[19] B. Pastrana, A. J. Mautone, and R. Mendelsohn, *Biochemistry* , **30**, 10058-10064 (1991).

[20] G. Vandenbussche, A. Clercx, T. Curstedt, J. Johansson, H. Jornvall, and J. M. Ruysschaert, *Eur. J. Biochem.* , **203**, 201-209 (1992).

[21] G. Vandenbussche, A. Clercx, M. Clercx, *et. al.*, *Biochemistry* , **31** , 9169-9176 (1992).

[22] J. E. Baatz, K. L. Smyth, J. A. Whitsett, C. Baxter, and D. R. Absolom, *Chem. Phys. Lipids* , **63**, 91-104 (1992).

[23] J. A. Clements, *Am. Rev. Respir. Dis* , **115**, 67-71 (1977).

[24] J. F. Van Iwaarder, H. Shimizu, P. M. H Van Golde, D. R. Voelker, L. M. G. Van Golde , *Biochem. J.* , **286**, 5-8 (1992).

[25] T. Curstedt, H. Jornvall, B. Robertson, T. Bergman, and P. Berggren, *Eur. J. Biochem.* , **168**, 255-262 (1987).

[26] S. H. Yu, and F. Possmayer, *Biochim. Biophys. Acta* , **1046**, 233-241 (1990).

[27] R. H. Notter, in *Pulmonary Surfactant,* (B. Robertsen, L. M. G. Van Golde, and J. J. Batenburg eds.) Elsevier, Amsterdam, (1984) pp 17-65.

[28] S. G. Taneva and K. M. W. Keough, *Biochemistry,* **33**, 14660-14670 (1994).

[29] J. Pérez-Gil, J. Tacker, G. Simatos and K. M. W. Keough, *Biochm. Cell Biol.*,**70**, 332-338 (1992).

[30] Z. Wang, S. B. Hall, and R. H. Notter, *J. of Lipid Research*, **36**, 1283-1292 (1995).

[31] M. A. Oosterlaken-Dijksterhuis, H. P. Haagsmann, L. M. G. Van Golde and R. A. Demel, *Biochemistry*, **30**, 10965-10971 (1991)

[32] M. A. Oosterlaken-Dijksterhuis, H. P. Haagsmann, L. M. G. Van Golde, and R. A. Demel, *Biochemist ry*, **30**, 8276-8281 (1991).

[33] S. G. Taneva and K. M. W. Keough, *Biochim. Biophys. Acta,* **1236**, 185-195 (1995).

[34] R. H. Hotter, in *Pulmonary Surfactant* , (B. Robertson, L. M. G. Van Golde, and J. J. Batenburg, Eds.) Elsevier, Amsterdam, (1984) pp 17-65.

[35] Nag K, and K. M. W. Keough, *Biophys. J.* **65** 1019-1026 (1993)

[36] Nag K, N. H. Rich, C. Boland and K. M. W. Keough, *Rev. Sci. Instrum.*, **61**, 3425-3430 (1 990)

[37] Nag K, N. H. Rich, C. Boland and K. M. W. Keough, *Biochim. Biophys. Acta,* **1068**, 157-160 (1991).

[38] B. Pastrana, S. Taneva, K.M.W. Keough, A. J. Mautone and R. Mendelsohn, *Biophys. J.*, **69**, 2531-2540 (1995).

[39] R. A. Dluhy, K. E. Reilly, R. D. Hunt, M. L. Mitchell, A. J. Mautone, and R. Mendelsohn, *Biophys. J.*, **56**, 1173-1181 (1989).

[40] A. D. Horowitz, B. Elledge, J. A. Whitsett and J. E. Baatz, *Biochim. Biophys. Acta,***1107**, 44-54 (1992).

[41] J. E. Baatz, B. Elledge, and J. A. Whitsett, *Biochemistry,* **29**, 6714-6720 (1990).

[42] J. E. Baatz, V. Sarin,D. Absolom, C. Baxter, and J. A. Whitsett, *Chem. Phys. of lipids,* **60**, 163-178 (1991).

[43] F. R. Poulain, L. Allen, M. C. Williams, R. L. Hamilton, and S. Hawgood, *Am. J. Physiol.*, **262**, L730-L739 (1992).

[44] A. D. Horowitz, J. E. Baatz and J. A. Whitsett, *Biochemistry,* **32**, 9513-9523 (1993).

[45] M. A. Oosterlaken-Dijksterhuis, M. Van Eijk and L. M. G. Van Golde, *Biochim. Biophys. Acta,* **1110**, 45-50 (1992).

[46] J. S. Vincent, S. D. Revak, C. G. Cochrane and I. W. Levin, *Biochemistry,***32**, 8228-8238 (1993).

[47] J. S. Vincent, S. D. Revak, C. G. Cochrane, and I. W. Levin, *Biochemistry* , **30**, 8395-84 01 (1991).

[48] S. Krill and S. L. Gupta, *J. of Pharmaceutical Sci.,***83**, 539-541 (1994).

[49] K. Shiffer, S. Hawgood, H. P. Haagsmann, B. Benson, J. A. Clements, and J. Goerke, *Biochemistry,* **32**, 590-597 (1993).

[50] G. A. Simatos, K. B. Forward, M. R. Morrow, and K. M. W. Keough, *Biochemistry,***29**, 5807-5814 (1990).

[51] M. C. Williams, S. Hawgood, and R. L. Hamilton, *Am. J. Respir. Cell Biol.*, **5**, 41-50 (19 91).

[52] J. Pérez-Gil, C. Casals, and D. Marsh, in *NATO ASI Series, Biological Membranes: Structure, Biogenesis and Dynamics*, (Jos A. F. Op den Kamp, Eds.) Springer-Verlag, Berlin Heidelberg, (1994) Vol. **H 82**, pp 93-100.

[53] J. Pérez-Gil, C. Casals and D. Marsh, *Biochemistry,* **34**, 3964-3971 (1995)

[54] M. R. Morrow, J. Pérez-Gil, G. Simatos, C. Boland, J. Stewart, D. Absolom, V. Sarin, and K. M. W. Keough, *Biochemistry,* **32**, 4397-4402 (1993).

[55] M. R. Morrow, S. Taneva, G. A. Simatos, L. A. Allwood and K. M. W. Keough, *Biochemistry,* **32** 11338-11344 (1993).

[56] J. Johansson, T. Szyperski, T. Curstedt and K. Wuthrich, *Biochemistry*, **33**, 6015-6023 (1994).

[57] M. Mehring, *Principles of High Resolution NMR in Solids.* Springer-Verlag, Berlin Heidelberg (1983).

[58] J. H. Davis, *in Isotopes in the Physical and Biological Science*, (E. Buncel and J.R. Jones, Eds.) Elsevier, Amsterdam (1991) Vol.**2** pp 99.

[59] R. Y. Dong, *Nuclear Magnetic Resonance of Liquid Crystals.* Spring-Verlag, Berlin Heidelberg (1994).

[60] C. P. Slichter, *Principles of Magnetic Resonance,* (P. Fulde, Ed.) Springer-Verlag, Berlin Heidelberg (1990).

[61] J. J. Sakurai, *Modern Quantum Mechanics* , (San Fu Tuan, Ed.) Addison-Wesley, New York (1994).

[62] J. H. Davis, *Biochim. Biophys. Acta*, **737**, 117-171 (1983)

[63] J. Seelig, *Quarterly Review of Biophysics* **10**, 3, 353-418 (1977)

[64] J. Seelig and A. Seelig, *Quarterly Review of Biophysics* **13**, 1, 19-61 (1980)

[65] J. H. Davis, K. R. Jeffrey, M. Bloom, M. I. Valic, and T. P. Higgs, *Chem. Phys. lett.*, **4 2**, 390-394 (1976).

[66] Abragam, *The Principles of Nuclear Magnetism,* Clarendon Press, Oxford (1985).

[67] M. Bloom, C. Morrison, E. Sternin, and J. L. Thewalt, *in Pulsed Magnetic Resonance: NMR, ESR, and Optics,* (D. M. S. Bagguley, Ed.) Clarendon Press, Oxford (1992) pp 274-316.

[68] M. Bloom and E. Sternin, *Biochemistry,* **26**, 2101-2105 (1987).

[69] M. Bloom and E. Evans, in *Biologically Inspired Physics,* (Peliti, L., Ed.) Plenum Press, New York, (1991) pp 137-147.

[70] J. Stohrer, G. Gröbner, D. Reimer, K. Weisz, C. Mayer and G. Kothe, *J. Chem Phys.* , **95**, 672-678 (1991).

[71] P. Meier, E. Ohmes and G. Kothe, *J. Chem. Phys.,* **85**, 3598-3614 (1986).

[72] J. H. Davis, M. Auger, and R. Hodges, *Biophys. J.,* **69**, 1917-1932 (1995).

[73] M. R. Paddy, F. W. Dahlquist, J. H. Davis and M. Bloom, *Biochemistry,* **20**, 3152-3162 (1981).

[74] K. P. Pauls, A. L. MacKay, O. Soderman and M. Bloom, *Eur. Biophys. J.*,**12**, 1-11 (1985).

[75] M. Bloom, E. Evans, and O. G. Mouritsen, *Quarterly Review of Biophysics,* **24**, 293-397 (1991).

[76] E. Sternin, PhD Thesis: *Some Mechanisims of Transverse Nuclear Relaxation in Model Membranes*, University of British Colombia, (1988).

[77] A. J. Vega, *J. of Magn. Res.,* **65**, 252-267 (1985).

[78] G. Vandenbussche, A. Clercx, M. Clercx, T. Crustedt, J. Johanson, H. Jornvall, and J. Ruysschaert, *Biochemistry,* **32**, 9169-9176 (1992).

[79] U. K. Laemmli, *Nature,* **227**, 680-685 (1970).

[80] S. S. Undenfriend, P. B. Stein, W. W. Dairman, W. Loimgrukes, and M. Weigele, *Science,* **178**, 871-872 (1972).

[81] E. Sternin , M. Bloom, and A. L. MacKay, *J. Magn. Res.* , **55**, 274-282 (1983)

[82] M. Bloom, J. H. Davis, and A. L. MacKay, *Chem. Phys. Lett.***80**, 198-202 (1981).

[83] M. R. Morrow, and D. Lu, *Chem. Phys. Lett.*, **182**, 435-439 (1991).

[84] A. Jonas, K. E. Kezdy and J. H. Wald, *J. Biol. Chem.* , **264**, 4818-4824 (1989).

[85] D. W. Nielson, *Pediatr. Res.*, **17**, *386A (1983).*

[86] S. Taneva, T. McEachren, J. Stewart, and K. M. W. Keough, Biochemistry, **34**, 10279-10289 (1995).

[87] O. G. Mouritsen, and M. Bloom, *Biophys. J.*,**46**, 141-153 (1984).

[88] R. B. Gennis, *Biomembranes: Molecular Structure and Function*, (C. R. Cantor, Ed.) Springer-Verlag New York (1989).

[89] M. R. Morrow, and J. P. Whitehead, *Biochim. Biophys. Acta*, **941**, 271-277 (1988).

[90] M. R. Morrow, *Biochim. Biophys. Acta*, **1023**, 197-205 (1990).

[91] R. S. Prosser, J. H. Davis, C. M. Mayer, K. Weisz, and G. Kothe, *Biochemistry,* **31**, 9355-9363 (1992).

[92] J. Yue, J. L Thewalt, and R. J. Cushley, *Chem. Phys. Lipids*, **49**, 205-213 (1988).

[93] P. M. Macdonald and J. Seelig, *Biochemistry*, **27**, 6769-6775 (1988).

[94] M. Roux and M. Bloom, *Biophys. J.*, **60**, 38-44 (1991).

[95] H. Akutsu and T. Nagamori, *Biochemistry*, **30**, 4510-4516 (1991).

[96] J. R. Rydall and P. M. Macdonald, *Biochim. Biophys. Acta*, **1111**, 211-220 (1992).

[97] P. G. Scherer and J. Seelig, *Biochemistry*, **28**, 7720-7728 (1989).

[98] P. M. Macdonald, J. Leisen, and F. M. Marassi, *Biochemistry,* **30**, 3558-3566 (1991).

[99] F. M. Marassi and P. M. Macdonald, *Biochemistry,* **31**, 10031-10036 (1992).

[100] E. Kuchinka and J. Seelig, *Biochemistry,* **28**, 4216-4221 (1989).

[101] M. Roux, J. M. Neumann, R. S. Hodges, P. F. Devaux, and M. Bloom, *Biochemistry,* **28**, 2313-2321 (1989).

[102] C. Dempsey, M. Bitbol, and A. Watts, *Biochemistry,* **28**, 6590-6596 (1989).

[103] B. B. Bonev and M. R. Morrow, *Biophys. J.,* **69**, 518-523 (1995).

IMAGE EVALUATION
TEST TARGET (QA–3)

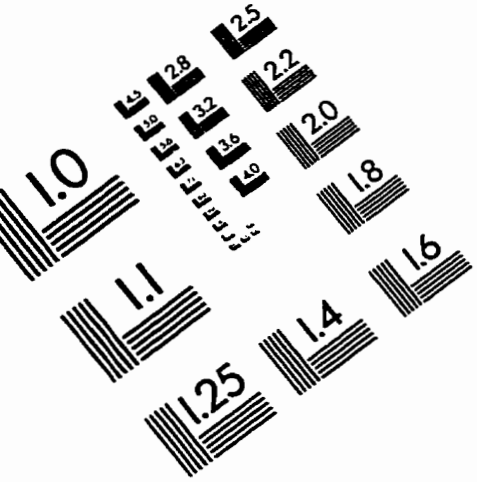

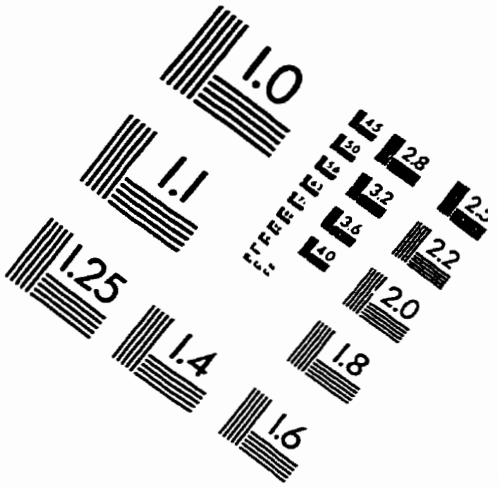

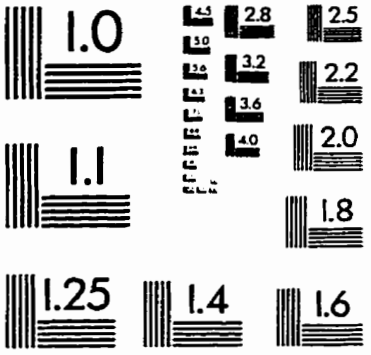

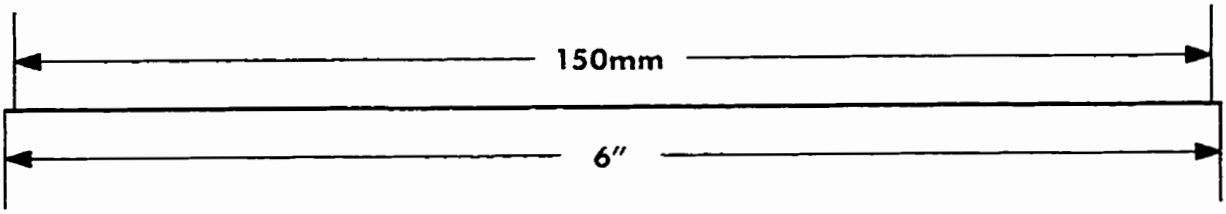

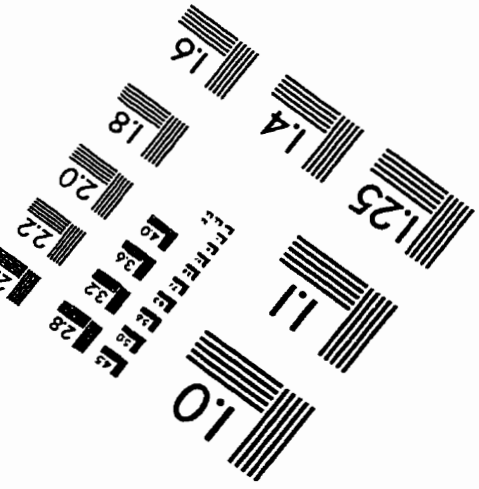

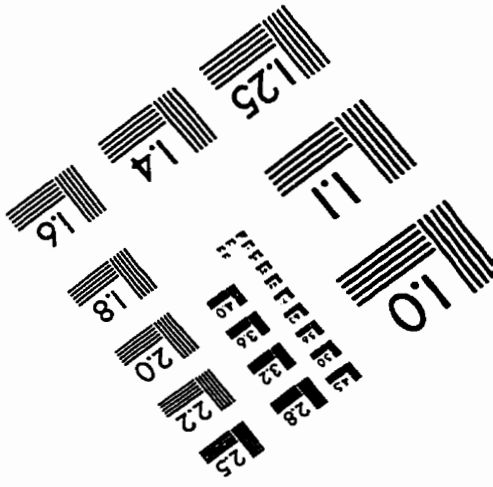

APPLIED IMAGE, Inc
1653 East Main Street
Rochester, NY 14609 USA
Phone: 716/482-0300
Fax: 716/288-5989